NUMERICAL STUDY OF THE DYNAMICAL CASIMIR EFFECT AND ITS CLASSICAL ANALOGUE IN A DOUBLE CAVITY

NUMERICAL STUDY OF THE DYNAMICAL CASIMIR EFFECT AND ITS CLASSICAL ANALOGUE IN A DOUBLE CAVITY

By

FAIYAZ HASAN, B.Sc.

A Thesis
Submitted to the School of Graduate Studies
in Partial Fulfilment of the Requirements
for the Degree
Doctor of Philosophy

McMaster University

DOCTOR OF PHILOSOPHY (2016) McMaster University
(Physics) Hamilton, Ontario

TITLE:	Numerical Study of The Dynamical Casimir Effect and its Classical Analogue in a Double Cavity
AUTHOR:	Faiyaz Hasan, B.Sc., University of Toronto (2009)
THESIS ADVISER:	Duncan H. J. O'Dell
NUMER OF PAGES:	xx , 152

Abstract

We study the time evolution of light fields inside a double cavity which is comprised of two perfect end mirrors and a parametrically driven, partially transmissive central mirror in both a classical and a quantum mechanical framework. It is common practise in the field of optomechanics to take a Hamiltonian approach [1] ignoring non-linear coupling terms between the light field and the moving mechanical element. By contrast, we start from the Maxwell wave equation which is second order in time and find that a first order in time Schrödinger-type wave equation (equivalent to neglecting the non-linear coupling) is a valid approximation for low enough mirror reflectivity and speed and for large light frequencies. We also study adiabatic dynamics for the Maxwell wave equation and find it differs from the more familiar adiabaticity in the Schrödinger equation.

Next, we numerically simulate the dynamical Casimir effect (DCE) in the double cavity with a sinusoidally driven central mirror following earlier numerical work on the perfect single cavity [2, 3, 4]. Because our central mirror is partially transmissive it is physically more realistic and circumvents fundamental problems associated with having perfectly reflecting moving mirrors [5, 6]. The corresponding photon creation rates are drastically lower when compared to the perfectly reflective mirror case. Furthermore, if we make one of the cavities much longer than the other we can simulate the DCE for a single open cavity coupled to an environment without having to make the Markov approximation. The resultant asymmetric double cavity (ADC) model is valid for times short enough that only a negligible number of the photons that has leaked out of the open cavity has sloshed back in again. As for the symmetric case, one advantage of the ADC is that driven mirror is partially transmissive rather than perfectly reflecting.

Acknowledgements

First and foremost, I wholeheartedly would like to thank my supervisor Dr. Duncan O'Dell for the patient and supportive guidance he has provided throughout my Phd. I find his ability to remain positive and productive under all circumstances truly inspiring and working with him has been a joyful experience. Secondly, I consider myself extremely lucky to have an incredible supervisory committee and would like to thank Dr. Harold Haugen and Dr. An-Chang Shi for their guidance. I would like to thank my middle school teacher, Dr. Shehab Ul Alam, under whose tutelage my love for math and physics first began. He also instilled the mentality in me that learning is one of the most fun things you can do. I would especially like to thank Dr. Daniel James for the extremely energetic and beautifully delivered Quantum Mechanics I lectures and working with him has been a pleasure. I am indebted to Dr. Hua Wu for the incredible tech support he has provided over the years. I have thoroughly enjoyed the many long hikes on the trails of Hamilton with David Bazak and Jesse Mumford that most of the time ended up at Taylor's Tea Room. I thank Braden for the amazing roast beef dinners and Andrea for being a wonderful hostess and providing such a warm and enjoyable atmosphere. I would also like to thank Chad Gu and Baran Sarejelahi for their enduring friendship. Furthermore, I thank Ali Kinross, Matt Williams, Vicki Walasyzk, Ryan Baley, Tmo, Robin Tunley, Dan Irvine, Joey Sham, Mingxuan Fu and Jared Telegdi for all the fun times we've had during my stay at Hamilton.

Lastly, I would like to thank my family for their love and unwavering support over all of these years.

Contents

List of Figures

Chapter 1

Overview

The thriving field of optomechanics studies systems with interacting optical and mechanical degrees of freedom [1]. Optomechanical systems have many physically realizable implementations with one of them being the membrane-in-middle setup [7, 8] which is the focus of this thesis. Theoreticallly, both cooling effects [8] and photon shuttling amongst the cavity halves [9] have been studied in this system. In this thesis, we theoretically study the double cavity with a parametrically driven central mirror and perfectly reflecting end mirrors which is an idealization of the membrane-in-middle setups.

In chapter 2, we study the properties of the static double cavity such as the allowed eigenfrequencies and corresponding electric field eigenmodes for arbitrary central mirror position and reflectivity. We treat the partially transmissive central mirror using a δ-function model [10] due to mathematical convenience. In practise, the central mirror has a non-zero width and finite index of refraction [11]. We show that as long as the light frequency is not resonant inside the central mirror, i.e. the light field in the cavity is not localized in the central mirror, then the δ-function model is a good approximation. The

classical dynamics for the optical degree of freedom can be described using the Maxwell wave equation for time dependent boundary conditions [12, 13, 14]. The resulting equations of motion are non-unitary and second order in time with an exact first order in time reduction possible only for a cavity with static boundary conditions. Neverthless, in the literature [8, 9], a unitary and first order in time dynamics approximation is used even for cavities with moving boundaries since it is an adequate approximation in the parameter regimes of the corresponding experiments. In chapter 3, we study the validity of such an approximation in relation to the mirror velocity, reflectivity and light frequency in the double cavity. Furthermore, the light field inside the cavity exerts a radiation pressure on the central mirror. In order for the central cavity to be driven at a constant speed which is the scenario we study in chapter 3, the external source pushing the mirror has to do work to overcome the radiation pressure. This results in energy being pumped into/out of the light field. We find the validity condition of the first order in time dynamics to be intimately related to the extent of this energy non-conservation. In chapter 4, we confirm that the change of energy in the light field generated from the Maxwell wave equation is equivalent to the work done by the external source to counteract the radiation pressure on the mirror derived using the Maxwell stress tensor. The last topic of our classical study is the adiabatic theorem in the context of the Maxwell wave equation for the double cavity with the parametric mirror in Sec. 4.4. The adiabatic theorem for the Schrödinger equation (non-relativistic quantum mechanics) states that if a physical system starts out in an initial eigenstate of the Hamiltonian and the system is changed slowly enough and there is a gap between the eigenvalue and the rest of the Hamiltonian's spectrum, then the system will continue to remain in an instantaneous eigenstate

of the Hamiltonian [15]. We find that in the context of the double cavity, moving the central mirror slowly enough ensures that the system will continue to remain in an instantaneous eigenstate, but in contrast to the Schrödinger case the amplitude of the eigenmode experiences a finite change while the changes in all the others vanish (the sum of the squares of all the amplitudes is not conserved). The external driving source counteracting the radiation pressure of the light field on the mirror necessarily has to do work on the light field and this manifests itself in a lack of conservation in the latter sum over squares of the amplitude. The eigenstate amplitudes of the Schrödinger equation field variable, on the other hand, are conserved because they represent probability.

Quantized Hamiltonians for the double cavity type setups have been written down in references [16, 17] which contain both photon scattering terms along with photon number non-conserving terms. These terms contribute to the dynamical Casimir effect (DCE). The static Casimir effect was first proposed by Hendrik B. G. Casimir [18] leading to a force due to the vacuum modes in the presence of boundaries creating an imbalance in the density of modes. Despite the vanishing of the average electric and magnetic fields of the vacuum state, the quadratic powers of the field variables are finite and leads to a non-zero radiation pressure. Later on, G. T. Moore studied the dynamical equivalent of the static Casimir effect, where photons are created in a single perfect cavity due to the motion of one boundary starting out with the light field in the vacuum state [5] and this work was later expanded on in reference [19]. Since then, numerous theoretical investigations have been conducted in the field of DCE [20, 21, 22, 23, 24, 6, 25, 26, 27, 28, 29, 30, 31]. In particular, analytical results for short enough times in the perfect single cavity with a sinusoidally driven end mirror have been derived in references [22, 28, 30]

and were checked numerically in references [3, 2]. Even though the DCE was initially described for moving mirrors, the smallness of the effect combined with the requirement of very large mirror speeds has made it difficult to detect [32]. Experimental detection in the context of semiconductor slabs with rapidly changing conductivity to mimic moving metallic mirrors was suggested in references [33, 34]. Since then, the DCE has been observed experimentally in a superconducting circuit [35] with the resultant radiated photons exhibiting two mode squeezing which is a signature of the quantum nature of the generated photons [23]. In chapter 5, we review the reformulation due to reference [24] of the Heisenberg equations of motion for light in the presence of boundaries. The reformulated equations of motion used in references [3, 2, 4] are a very convenient form for numerical simulation of the dynamical propagator. Furthermore, motivated by the latter numerical study of the DCE in a perfect single cavity, we study the DCE in a double cavity in chapter 6. There is an important qualitative difference in our numerical simulations since we are dealing with a partially transmissive central mirror instead of all mirrors being perfect. We find that this can drastically alter the photon growth rate inside the cavity as suspected by the authors in references [5, 6]. Moreover, this forms an intermediate step to studying an open cavity coupled to an infinite environment. Theoretical work on the DCE in a parametrically driven open cavity has been conducted [36] using the master equation approach [37, 38], scattering approach [25, 39, 40] and in reference [26] using cavity quasi-modes. Furthermore, open cavity DCE treating the mirror as a dynamical variable has been tackled in reference [41]. Defining a single semi-open cavity to be a cavity with one perfect and one partially transmissive mirror, the double cavity can be thought of as two semi-open cavities coupled to one another. We can model

a semi-open cavity coupled to an infinite environment by using a highly asymmetric double cavity where one cavity length is much longer than the other and is used to mimic the environment. Modelling the infinite environment by a finite but large cavity ensures that the eigenmode structure is discrete and it is much easier to deal with a discrete set of modes than a continuum. This amounts to a modes of the universe approach to describing the finite transmission of one of the end mirrors employed in references [10, 42, 43, 44]. The beauty of our numerical approach is that it is not reliant on simplifying assumptions other than treating the environment as being finite which is a very good approximation for short enough times. In chapter 7, we summarize the main results of our thesis and future directions for this work.

Chapter 2

Properties of the Stationary Double Cavity

2.1 Introduction

In this chapter, we study the properties of light inside a static double cavity as shown in Fig. 2.1. The end mirrors of the double cavity are taken to be perfectly reflective and we assume that there is no pumping/decay of light into/outside the cavity. For a partially transmissive central mirror fixed at an arbitrary position, we investigate the allowed wavenumbers of light inside the cavity and the corresponding eigenmodes. Our starting point is the Maxwell wave equation with stationary boundary conditions and in Sec. 2.2 we derive the corresponding Sturm-Liouville problem. In Sec. 2.3 we derive the eigenvalue equation for the allowed wavenumbers inside the double cavity for arbitrary positions of the partially transmissive central mirror. We find that the wavenumber structure is composed of a net of avoided crossings and present analytical approximations near an avoided crossing valid in the regime

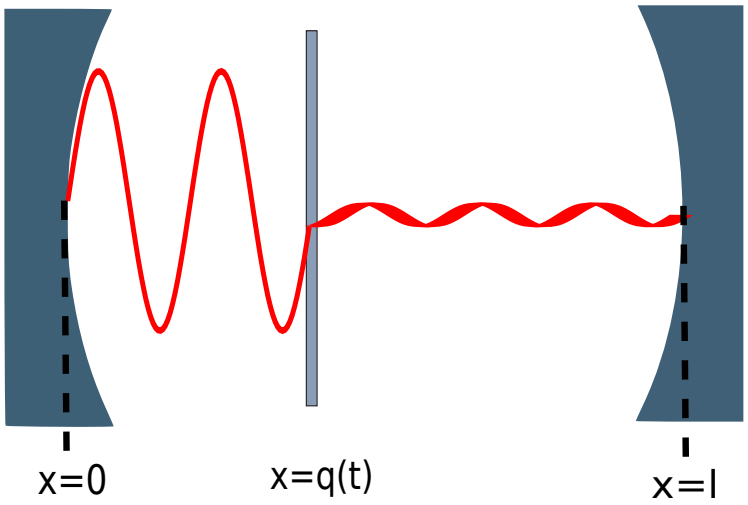

Figure 2.1: Schematic of amplitude of light in a double cavity with perfectly reflective end mirrors and a partially transmissive, moveable central mirror.

of highy reflective central mirror and large wavenumbers. In Sec. 2.4, we study the form of the eigenmodes corresponding to the wavenumbers. For a perfectly centered mirror, the eigenmodes are equally localized in both cavity halves. However, as the mirror is displaced, the light field becomes localized in the left and right sides of the cavity. An understanding of such properties provides intuition into the dynamics of light transfer amongst cavity halves for an adiabatically moving central mirror and could potentially be useful in devices requiring on demand photon transfer with high fidelity in quantum networks [45, 46, 47, 48]. In this thesis, we model the central mirror using a δ-function, i.e. having zero width and infinite index of refraction due to the mathematical and numerical tractablity this model offers. In Sec. 2.5, we compare the validity of this model to a more realistic model of the mirror with a non-zero width and finite index of refraction.

2.2 Maxwell Equations, Boundary Conditions and Sturm-Liouville Problem

In this section, starting from the Maxwell wave equation for a static double cavity, i.e. with time independent boundary conditions, we derive the eigenvalue equation for allowed wavenumbers of the light field inside the cavity. We consider the convention where the cavity mirrors are situated parallel to the y-z plane and move along the x axis. Furthermore, we assume that the electric field is polarized along the z axis and the magnetic field along the y axis, i.e. $\vec{A} = A(x,t)\vec{e}_z$, $\vec{E} = -\partial_t A\vec{e}_z$, and $\vec{B} = -\partial_x A\vec{e}_y$. The dielectric function of the double cavity is given by

$$\epsilon(x, \Delta L) = \begin{cases} \epsilon_0[1 + \alpha\delta(x)], & -L_1 < x < L_2 \\ \infty, & x > L_2,\ x < -L_1 \end{cases}, \tag{2.1}$$

where

$$L_{1/2} = \frac{L \pm \Delta L}{2}. \tag{2.2}$$

In the absence of a central mirror, $\alpha = 0$. Hence, the δ function term is used to model the partially transmissive central mirror following the approach in reference [10]. This is an idealization and in Sec. 2.5 we discuss a more realistic model with a non-zero mirror width and finite index of refraction. We note that in the case of the static double cavity, changing the central mirror position and keeping the end mirrors fixed is mathematically equivalent to keeping the central mirror fixed and changing the end mirror positions. Physically, we assume that it is the central mirror that moves in order to avoid issues that reference [5] shows are associated with driving a perfect mirror as opposed to

a partially transmissive one. For the sake of convenience, we opt for the latter convention. The central mirror is placed at the origin, while the end mirrors are placed at positions $x = -L_1$ and L_2. The total length of the double cavity is fixed and given by $L = L_1 + L_2$ and the displacement of the moveable mirror from the center is given by $\Delta L/2$, where, $\Delta L = L_1 - L_2$. For a stationary mirror, the Maxwell wave equation is given by

$$\frac{\partial^2 E(x,t)}{\partial x^2} - \mu_0 \epsilon(x, \Delta L) \frac{\partial^2 E(x,t)}{\partial t^2} = 0. \tag{2.3}$$

Eqn. (2.3) is a second order in time differential equation that has a first order in time reduction. We separate the temporal and spatial variables of the electric field by letting

$$E(x,t) = e^{-i\omega_m(\Delta L)t} U_m(x, \Delta L) \tag{2.4}$$

where the frequencies ω_m and mode functions U_m depend on ΔL. Substituting this ansatz into Eqn. (2.3) we find the Helmholtz equation

$$\frac{\partial^2 U_m(x, \Delta L)}{\partial x^2} + k_m^2(\Delta L) \frac{\epsilon(x, \Delta L)}{\epsilon_0} U_m(x, \Delta L) = 0, \tag{2.5}$$

where $k_m(\Delta L) = \omega_m(\Delta L)/c$. Since the end mirrors are perfect, we have the boundary condition $U_m(x = -L_1, \Delta L) = U_m(x = L_2, \Delta L) = 0$. This implies that the light eigenmodes inside the cavity take the form

$$U_m(x, \Delta L) = \begin{cases} A_m(\Delta L) \sin[k_m(\Delta L)(x + L_1(\Delta L))], & -L_1 \leq x \leq 0 \\ B_m(\Delta L) \sin[k_m(\Delta L)(x - L_2(\Delta L))], & 0 \leq x \leq L_2 \end{cases}, \tag{2.6}$$

where A_m and B_m are the amplitudes of the electric field eigenmodes corresponding to the left and right halves of the double cavity. There exists a unique set of eigenmodes and eigenfrequencies to Eqn. (2.3) for each fixed mirror position. To clearly show this dependence, we have expressed U_m and k_m as functions of ΔL. From here onwards we refer to these stationary cavity eigenmodes as the adiabatic modes. For a double cavity with a moving central mirror, we can imagine for each fixed time, that the mirrors are all instantaneously at rest. Corresponding to each arbitrary central mirror position, we have a set of instantaneous eigenmodes parametrized by ΔL. These instantaneous eigenmodes form a complete basis that is very natural for describing the light dynamics and also intuitively explains light transfer amongst cavity halves for adiabatic mirror motion. For the sake of convenience in future analysis and numerical simulations, we impose the normalization condition

$$\frac{1}{\epsilon_0}\int_{-L_1}^{L_2}\epsilon(x,\Delta L)U_l(x,\Delta L)U_m(x,\Delta L)\mathrm{dx}=\delta_{lm}. \tag{2.7}$$

Furthermore, by integrating Eqn. (2.5) in a small region surrounding the central mirror and taking the limit of the integration range to approach 0, we find another boundary condition given by

$$U'_m(x=0^+,\Delta L)-U'_m(x=0^-,\Delta L)=-\alpha k_m^2(\Delta L)U_m(x=0,\Delta L). \tag{2.8}$$

Here, $'$ denotes spatial derivative and the boundary condition expresses the fact that despite the continuity of the adiabatic modes, the first spatial derivative is discontinuous at the central mirror. Substituting Eqn. (2.6) into the two

boundary conditions and combining them, we find the eigenvalue equation

$$\cos(2k_m\Delta L) - \cos(k_m L) = 2\frac{\sin(k_m L)}{\alpha k_m}. \tag{2.9}$$

2.3 Eigenvalue Structure and Analytical Approximations

In this section we numerically generate the allowed wavenumbers of the light field inside a double cavity from the eigenvalue equation in Eqn. (2.9) and compare them to analytical approximations derived in reference [12]. To gain an intuitive understanding of the double cavity eigenvalue structure, let us imagine dialing the reflectivity of the central mirror up to 100%. In this perfect central mirror limit, the double cavity is comprised of two perfectly reflective single cavities. When the central mirror is equidistant from the two end mirrors, the allowed wavenumbers are given by $k_n = 2\pi n/L$, where $n \in \mathbb{N}$. In general, for an arbitrary mirror position, the wavenumber pairs in the two perfect cavities are given by

$$k_n(\Delta L) = 2n\pi/(L \pm \Delta L). \tag{2.10}$$

From here onwards, we denote these wavenumbers as the diabatic wavenumbers. These network of wavenumbers which correspond to the diabatic light modes, i.e. modes localized in the left or right cavity halves, criss cross each other as can be seen in Fig. 2.2. Wherever the set of eigenvalues intersect, we have a degeneracy in the wavenumber structure corresponding to the uncoupled double cavity. In analogy with perturbation theory in quantum mechan-

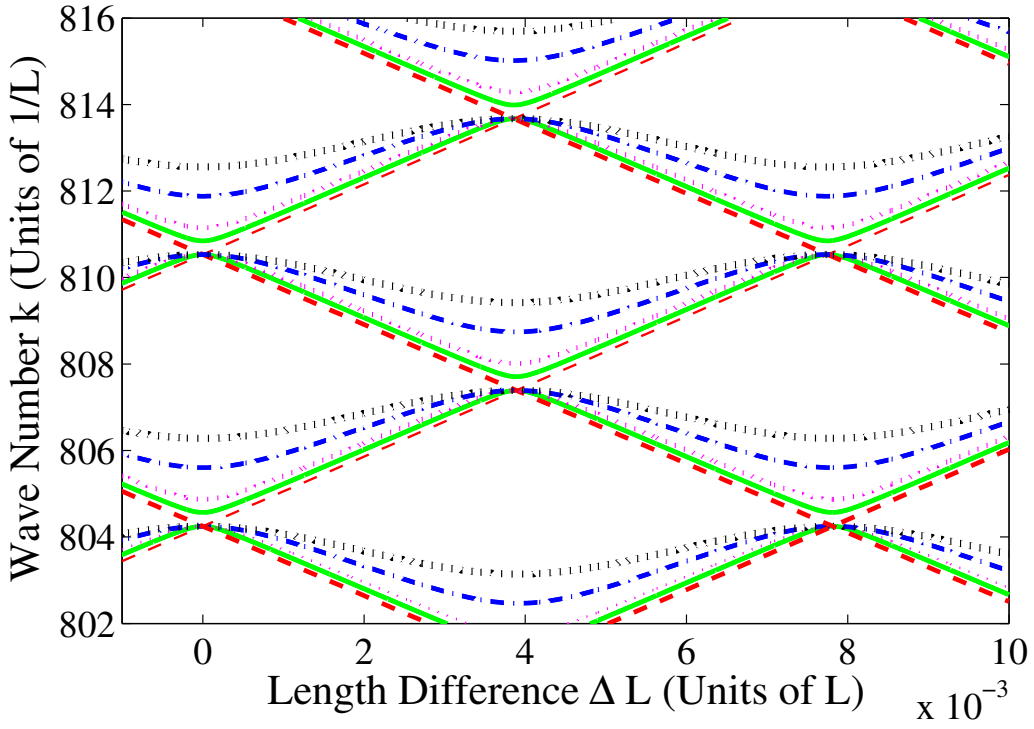

Figure 2.2: The wave numbers allowed inside the double cavity as a function of the mirror displacement from the center forms a network of avoided crossings. The red, dashed lines correspond to a perfectly reflective central mirror. The green, solid lines correspond to a mirror of reflectivity 98% , the magenta, small dotted lines correspond to a mirror reflectivity of 91%, the blue, dashed dotted lines correspond to 61% and the larger, black dotted lines correspond to a mirror reflectivity of 28%. All curves except the red curve have avoided crossings. The size of the avoided crossing (2Δ) goes down as the reflectivity is increased. The wavenumbers were generated using Eqn. (2.9).

ics, the wavenumber degeneracy will be broken as the two single cavities are coupled by making the central mirror partially transmissive. The splitting of the wavenumbers give us an avoided crossing structure shown in Fig. 2.2. Taking inspiration from the avoided crossing structure in the quantum mechanical two level system Hamiltonian with an off-diagonal perturbation, we write the wavenumbers near an avoided crossing in the form

$$k_{2/1}(\Delta L) = k_{\text{av}} \pm \frac{1}{c}\sqrt{\Delta^2 + \Gamma(\Delta L)^2} \tag{2.11}$$

and the corresponding frequencies are then given by

$$\omega_{2/1}(\Delta L) = \omega_{\text{av}} \pm \sqrt{\Delta^2 + \Gamma(\Delta L)^2} \tag{2.12}$$

where Δ/c is half the separation of the wavenumbers at the center of the avoided crossing as in Fig. 2.2 and k_{av} is the average wavenumber. Here, the mode corresponding to the the lower branch of the avoided crossing has subscript 1, while the mode corresponding to the higher eigenmode has subscript 2. Near an avoided crossing, we can apply a multidimensional Taylor expansion to Eqn. (2.9) around the diabatic modes ($k_n = 2n\pi/L$) for the centered mirror and for small central mirror displacements ($\Delta L/2$) and solve to find analytic approximations for the wavenumbers

$$\begin{aligned} k_1(\Delta L) &= \frac{2\pi n}{L} + \frac{\Delta}{c} - \frac{1}{c}\sqrt{\Delta^2 + \gamma\Delta L^2} \\ k_2(\Delta L) &= \frac{2\pi n}{L} + \frac{\Delta}{c} + \frac{1}{c}\sqrt{\Delta^2 + \gamma\Delta L^2}, \end{aligned} \tag{2.13}$$

where

$$\begin{aligned} \gamma &= 2\Delta c \frac{2\pi^3 n^3 \alpha}{L^4} \\ \Delta &= \frac{c}{L} \frac{n\pi}{1 + n^2\pi^2\alpha/L}. \end{aligned} \tag{2.14}$$

In Fig. 2.3, we compare the approximate analytic wavenumber formulae in Eqn. (2.13) to the numerically generated wavenumbers from Eqn. (2.9). Moreover, we plot the diabatic wavenumbers corresponding to the localized left/right case of a perfectly reflective central mirror. We find that the analytic wavenumber formulae is a good approximation close to the avoided crossing. We can see in Fig. 2.3 that the diabatic wavenumbers when the central mirror is symmetrically placed intersects with the lower adiabatic wavenumber curve. The corresponding adiabatic eigenmode is an odd function vanishing at the mirror and hence does not "see" the coupling strength of the cavity halves. This leads to an agreement in the diabatic and lower adiabatic wavenumber values when the mirror is centered. Let us note in the context of the double cavity that in general the eigenfunctions corresponding to the lower (upper) wavenumber branch at the center of the avoided crossing is an odd (even) function. In the symmetric double-well potential case in quantum mechanics, the situation is reversed and the eigenmode corresponding to the lower eigenvalue branch is an even (symmetric) function. This difference occurs because the mirror dielectric function corresponds to a dip potential in the "equivalent" Schrödinger equation.

The reflectivity of the delta mirror is given by

$$R = \frac{\alpha^2 k^2}{4 + \alpha^2 k^2}. \tag{2.15}$$

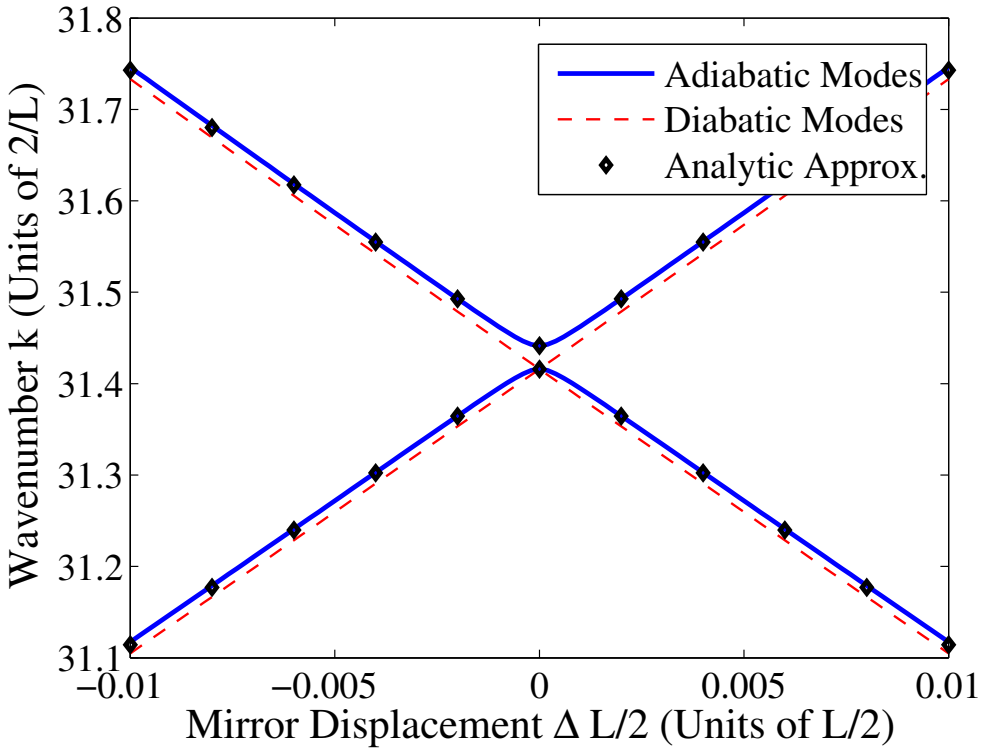

Figure 2.3: Wavenumber structure versus mirror displacement from the center near an avoided crossing. In this plot we look at the avoided crossing close to the wavenumbers corresponding to $n = 10$, $\alpha = 2.5$ m. We can see that the analytic formulae in Eqn. (2.13) are a good approximation to the numerically generated wavenumbers from Eqn. (2.9). The two sets of curves will be called Analytic Approximation and Adiabatic Modes respectively. We have also plotted the diabatic modes, i.e. wavenumbers when the two cavity halves are completely uncoupled due to a perfectly reflective central mirror. For a perfectly centered mirror, the diabatic modes cross and hence the wavenumbers are degenerate. Coupling the left and right halves of the cavity via a partially transmissive mirror, the degeneracy of the allowed wavenumbers (Adiabatic modes) is broken as one of the wavenumbers moves upwards from the diabatic wavenumber. The lower (odd) adiabatic mode vanishes at the mirror when it is perfectly centered and therefore does not "see" the mirror. As a result, the odd adiabatic eigenmode is also a diabatic eigenmode of the cavity when the mirror is perfectly centered leading to an intersection between the lower adiabatic and the diabatic wavenumber structure. The diabatic wavenumbers were generated using Eqn. (2.10).

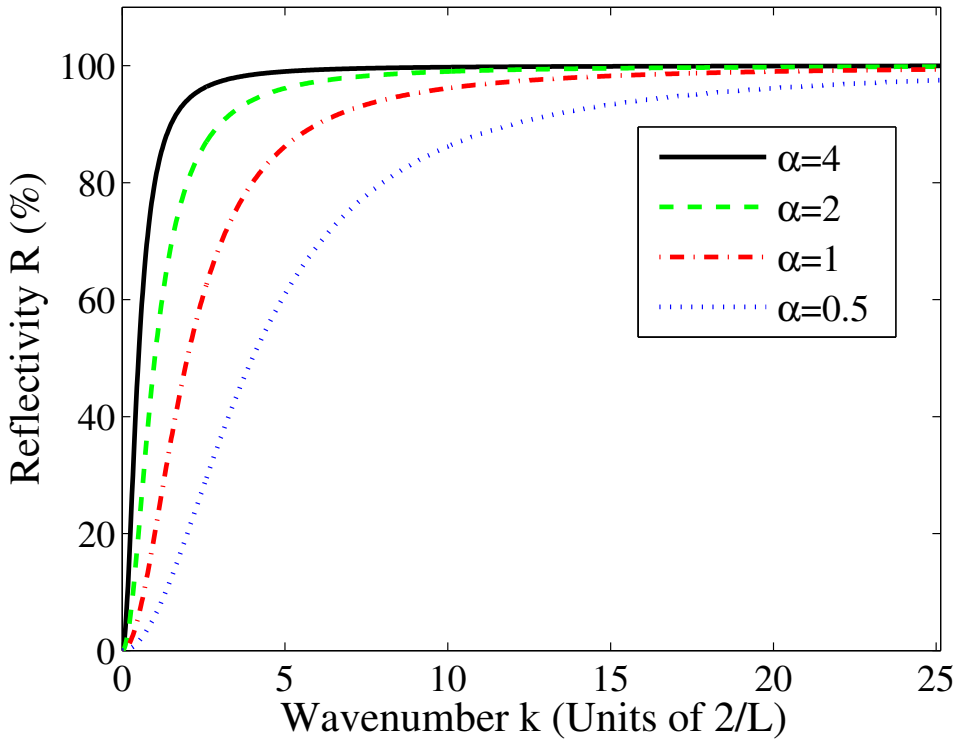

Figure 2.4: Mirror reflectivity curves versus light wavenumber. For a fixed wavenumer, increasing the reflectivity paramater, α (as in Eqn. (2.1)), leads to increasing central mirror reflectivity. The reflectivity curves were generated using Eqn. (2.15).

As $\alpha \to \infty$, the reflectivity $R \to 100\%$. Fig. 2.4 shows a set of reflection curves. Since $\Delta \to 0$ as $\alpha \to \infty$, we can conclude that for increasing reflectivity, the gap at the avoided crossing becomes smaller. This can be seen in Fig. 2.2.

2.4 Adiabatic versus Diabatic Modes

Let us begin with a review of our definition of adiabatic and diabatic modes. Consider a double cavity with a stationary, partially transmissive mirror. The adiabatic state refers to the eigenstate of the light mode corresponding to the allowed wavenumbers in the static cavity. As we will see later, the adiabatic

state is in general finite on both sides of the cavity. In fact, when the mirror is perfectly centered, the adiabatic states are symmetric or anti-symmetric in nature and hence have equal amplitude in both halves of the cavity. The usefulness of the diabatic modes lies both in the perfectly reflective case and the fact that the Landau-Zener formulation is in terms of them (See Sec. 3.4). For a perfectly reflective central mirror, the double cavity becomes two uncoupled single cavities. The eigenmodes of these single cavities, which are localized either in the left or right half of the double cavity, form the diabatic basis. This begs the question, whether analogous modes exist for a partially transmissive central mirror and how could they be defined. The adiabatic and the diabatic modes are related to each other via a linear change of basis. Consider the similarity transform between the two matrices

$$M_{\text{adiab}} = \begin{pmatrix} \omega_2(\Delta L) & 0 \\ 0 & \omega_1(\Delta L) \end{pmatrix} \tag{2.16}$$

and

$$M_{\text{diab}} = \begin{pmatrix} \omega_{\text{av}} + \Gamma(\Delta L) & \Delta \\ \Delta & \omega_{\text{av}} - \Gamma(\Delta L) \end{pmatrix} \tag{2.17}$$

written as $M_{\text{adiab}} = S^{-1} M_{\text{diab}} S$. The diagonal terms of M_{diab} give the diabatic energies for the perfect central mirror case while the off diagonal terms give the coupling between the two halves of the double cavity. Then, writing S in the form

$$S = \begin{pmatrix} \cos\theta & \sin\theta \\ -\sin\theta & \cos\theta \end{pmatrix} \tag{2.18}$$

we find that

$$\sin\theta = \sqrt{\frac{1}{2} - \frac{\Gamma(\Delta L)}{2\sqrt{\Delta^2 + \Gamma(\Delta L)^2}}} \tag{2.19}$$

and

$$\cos\theta = \sqrt{\frac{1}{2} + \frac{\Gamma(\Delta L)}{2\sqrt{\Delta^2 + \Gamma(\Delta L)^2}}}. \tag{2.20}$$

Since the adiabatic modes are given to use by solving Eqn. (2.5), we can now define the diabatic modes $\{\phi_L, \phi_R\}$ by

$$\begin{aligned} \phi_L(x, \Delta L) &= U_2(x, \Delta L)\cos\theta + U_1(x, \Delta L)\sin\theta \\ \phi_R(x, \Delta L) &= -U_2(x, \Delta L)\sin\theta + U_1(x, \Delta L)\cos\theta \end{aligned} . \tag{2.21}$$

In Fig. 2.5, we plot the eigenmodes corresponding to the parameters and wavenumber curves in Fig. 2.3. From the middle row in Fig. 2.5, we can see that the modes are either symmetric or anti-symmetric when the mirror is perfectly centered. The anti-symmetric mode corresponds to the lower wavenumber curve, while the symmetric mode corresponds to the higher wavenumber curve of the avoided crossing in Fig. 2.3. As the mirror is displaced to the left and the right, in the first, second, fourth and fifth row of Fig. 2.5, we see that the adiabatic modes become strongly localized in the left and right halves of the cavity. The amplitudes for the mode functions are derived using

$$\frac{A_n(\Delta L)}{B_n(\Delta L)} = -\frac{\sin\left[k_n(\Delta L)L_2(\Delta L)\right]}{\sin\left[k_n(\Delta L)L_1(\Delta L)\right]} \tag{2.22}$$

for the "even" mode and

$$\frac{A_n(\Delta L)}{B_n(\Delta L)} = \frac{\cos\left[k_n(\Delta L)L_2(\Delta L)\right]}{\cos\left[k_n(\Delta L)L_1(\Delta L)\right] - \alpha k_n(\Delta L)} \tag{2.23}$$

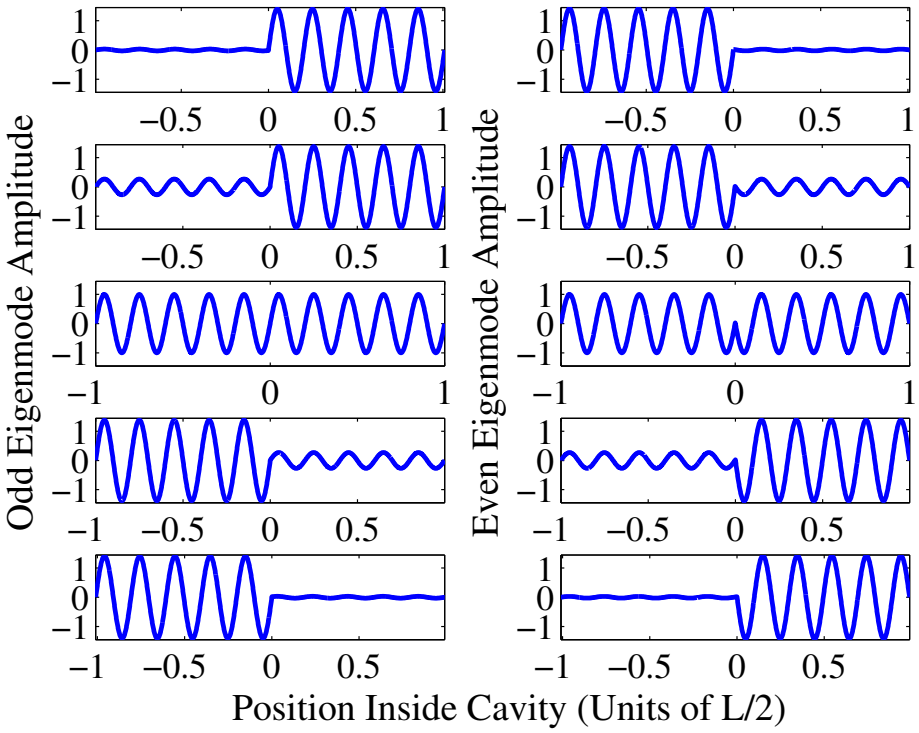

Figure 2.5: Electric field eigenmode structure and its dependence on mirror position. First row corresponds to mirror displacement of -0.01, second row -0.001, third row when the mirror is centered and $\Delta L/2 = 0$, fourth row 0.001 and fifth row 0.01. $\alpha = 2.5$. $n = 10$. Corresponding wavenumber structure is plotted in Fig. 2.3. The even amplitudes are generated using Eqns. (2.24) and (2.22). Meanwhile, the odd amplitudes are generated using Eqns. (2.24) and Eqn. (2.23). The spatial variations of the mode function are generated using Eqn. (2.6).

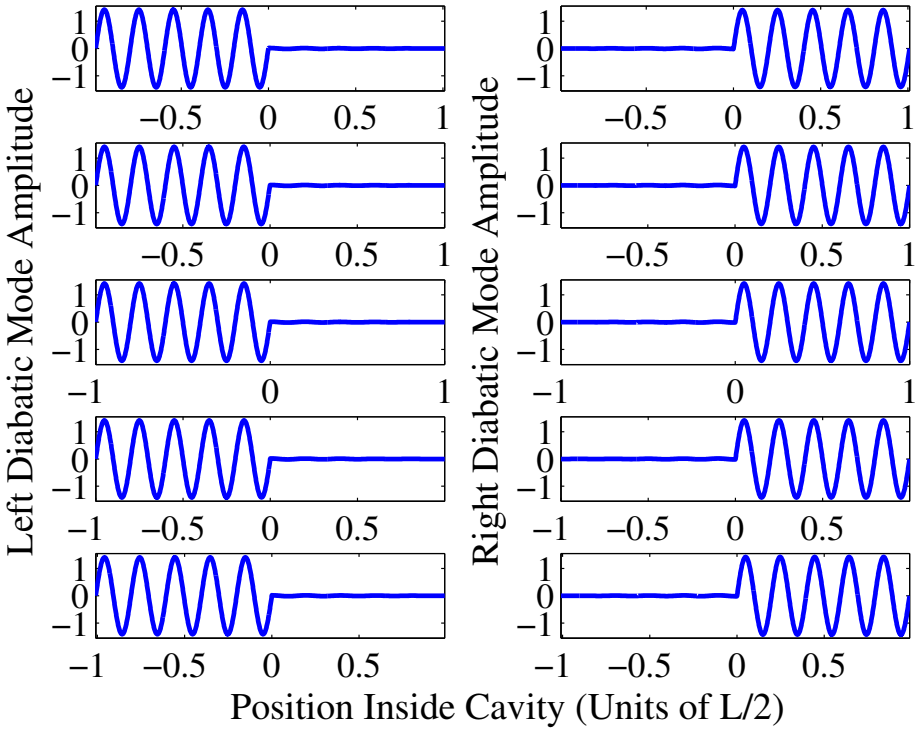

Figure 2.6: Diabatic mode structure and its dependence on mirror position. First row corresponds to mirror displacement of -0.01, second row -0.001, third row when the mirror is centered and $\Delta L/2 = 0$, fourth row 0.001 and fifth row 0.01. $\alpha = 2.5$ m. $n = 10$. Corresponding wavenumber structure is plotted in Fig. 2.3. The localized diabatic left/right modes were generated using Eqn. (2.21).

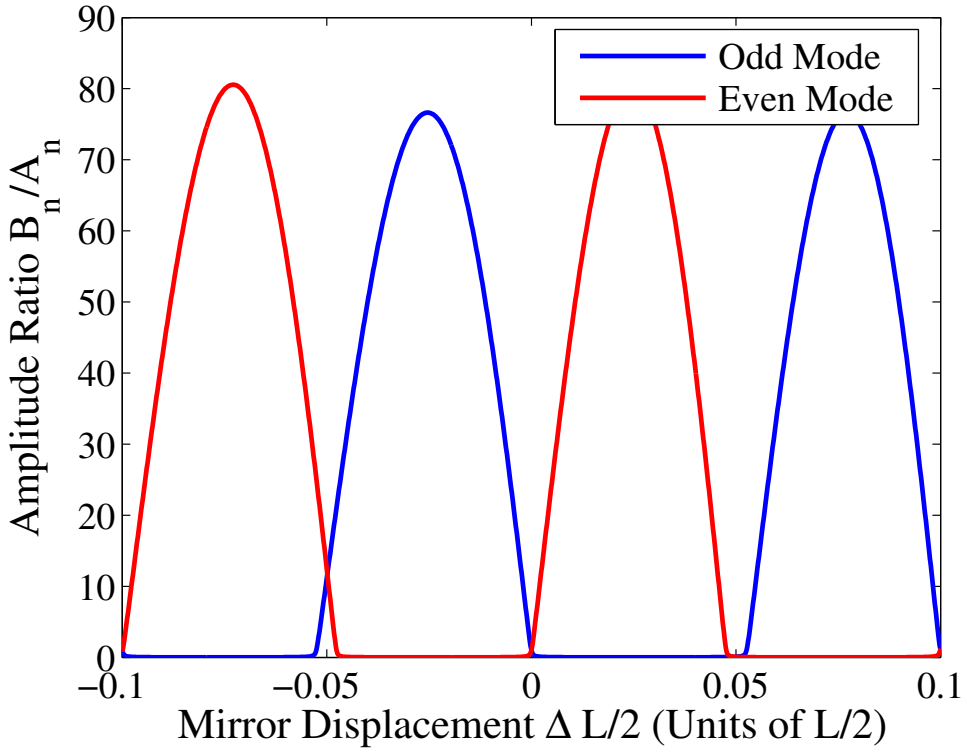

Figure 2.7: Electric field mode localization and its dependence on mirror position. This figure shows the ratio B_n/A_n for the adiabatic wavenumbers pairs near 10π corresponding to Fig. 2.3 where $\alpha = 2.5$ m. When mirror is displaced to the left side, the odd adiabatic mode becomes localized in the right side of the cavity, i.e. $A_n/B_n \ll 1$. Meanwhile, when the mirror is displaced to the left side of the cavity, the even adiabatic mode becomes localized in the left side of the cavity, i.e. $A_n/B_n \gg 1$. The wavelength corresponding to the wavenumber is $\lambda_n = 2\pi/k_n = 0.2$ in units of $2/L$. Hence, in this plot we see that we need displace the central mirror a fraction of the wavelength to achieve light transfer. The mode amplitude ratios are derived using Eqns. (2.22) and (2.23). We also see that the localization of the adiabatic modes alternates between the two cavity halves as the mirror is being displaced.

for the "odd" mode, which come from substituting Eqn. (2.6) into the boundary conditions of the adiabatic mode at the mirror. The adiabatic modes are labelled "even"/"odd" based on the property satisfied when the mirror is centered. For arbitrary mirror positions, i.e. when symmetry is lacking, the states are not even or odd. Furthermore, from the normalization condition we find the relation

$$\frac{A_n^2}{4k_n}\left[-\sin\left(2k_nL_1\right)+2k_nL_1\right]+\frac{B_n^2}{4k_n}\left[-\sin\left(2k_nL_2\right)+2k_nL_2\right]+\alpha B_n^2\sin^2\left(k_nL_2\right)=1 \tag{2.24}$$

which is also satisfied by the mode functions. In Fig. 2.7, we can see that as the central mirror is displaced, the mode alternates between which half of the cavity it is localized in.

Meanwhile, Fig. 2.6 depicts the diabatic local modes derived from Eqn. (2.21), corresponding to the adiabatic modes shown in Fig. 2.5. We can see that the diabatic modes remain localized for all mirror displacements. This localization is not perfect but still quite good even for modest values of reflectivity and improves as the central mirror reflectivity is increased. Since the change in the diabatic modes is very small, as we will see in Chapter 2, writing the light field in this basis allows us to ignore the time dependence of the diabatic mode functions and consider only the time dependence of their amplitudes, greatly simplifying the dynamical equations. We also have that

$$\frac{1}{\epsilon_0}\int_{-L_1}^{L_2}\epsilon(x,\Delta L)\phi_L(x,\Delta L)\phi_R(x,\Delta L)\mathrm{dx}=\delta_{LR} \tag{2.25}$$

implying that the diabatic basis derived from the superposition of the orthonormal adiabatic basis is also an orthonormal basis.

2.5 Delta versus Finite Barrier Mirror

Previously, we modelled the partially transmissive central mirror in the double cavity by a δ function. This is an idealization of a real mirror which has a finite index of refraction and non-zero width. In this section we model such a mirror, physically realized as a 50nm thick SiN membranes in references [11, 8], by a uniform slab of dielectric and characterized by the dielectric function

$$\epsilon(x, \Delta L) = \begin{cases} \epsilon_0 n_r^2 & -M \leq x \leq M \\ \epsilon_0 & -L_1 < x < -M \text{ and } M < x < L_2 \\ \infty & \text{elsewhere} \end{cases} \tag{2.26}$$

where $2M$ is the mirror width and n_r is the index of refraction of the central mirror. We refer to this as the Finite Barrier (FB) mirror model. We wish to compare the validity of the δ mirror model by comparing the wavenumber structures to those of the more realistic FB mirror model. Due to the perfect end mirrors, the FB model adiabatic modes satisfy $U_n(x = -L_1, \Delta L) = U_n(x = L_2, \Delta L) = 0$ and the eigenmodes can then be written as

$$U_m(x, \Delta L) = \begin{cases} A_m(\Delta L) \sin\left[k_m(\Delta L)(x + L_1)\right] & -L_1 < x < -M \\ B_m(\Delta L) \sin\left[n_r k_m(\Delta L) x + \phi_1\right] & -M < x < M \\ C_m(\Delta L) \sin\left[k_m(\Delta L)(x - L_2)\right] & M < x < L_2 \end{cases} . \tag{2.27}$$

In addition, we have the boundary conditions that the FB adiabatic modes and their first derivatives are continuous at the dielectric interfaces, which

gives us the eigenvalue equation

$$-n_r^2 \sin(2n_r kM) \sin\left[k\left(\frac{L}{2} - M + \frac{\Delta L}{2}\right)\right] \sin\left[k\left(\frac{L}{2} - M - \frac{\Delta L}{2}\right)\right] + n_r \cos(2n_r kM) \sin[k(L-2M)] + \sin(2n_r kM) \cos\left[k\left(\frac{L}{2} - M + \frac{\Delta L}{2}\right)\right] \cos\left[k\left(\frac{L}{2} - M - \frac{\Delta L}{2}\right)\right] = 0. \quad (2.28)$$

This equation would be the same as the δ mirror eigenvalue equation given by Eqn. (2.9) if it weren't for the terms due to the resonance of light in the central mirror given by the wavenumbers $k_{\text{resonance}} = l\pi/2Mn_r$ for $l \in \mathbb{N}$. In order to find the condition for the convergence of the two models, we briefly look at the transmission functions respective to the δ and FB mirror given by

$$T_\delta = \frac{1}{1 + k^2\alpha^2/4} \quad (2.29)$$

and

$$T_{FB} = \frac{1}{1 + \frac{(n_r^2-1)^2}{4n_r^2} \sin^2(2Mkn_r)}. \quad (2.30)$$

We find, as shown in Fig. 2.8, away from the resonance condition inside the central mirror, letting $M \to 0$ and $n_r \to \infty$ while satisfying, $2Mn_r^2 = \alpha$, the finite mirror transmission function approaches the delta mirror transmission function. Using this as a clue, if we take a similar limit in the FB eigenvalue equation given by Eqn. (2.28), we get back the δ mirror eigenvalue equation. In Fig. 2.9, we see the set of wavenumbers in the FB model converging to the δ model wavenumbers showing the validity of the δ mirror model away from the resonance condition for thin enough mirrors. In Fig. 2.8, we see that $M = 1e{-}2$ and $M = 5e - 3$ are resonant near the wavenumbers generated. Meanwhile,

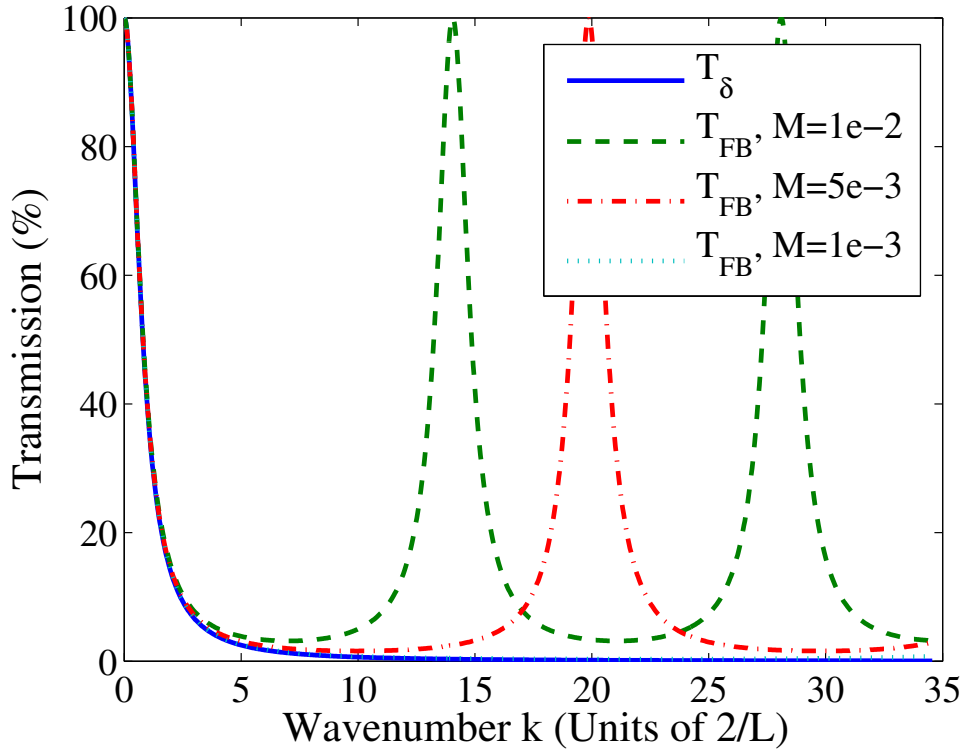

Figure 2.8: Comparison of mirror transmission functions for the δ and FB model of the mirror. In this figure we compare the transmission function of light for the δ mirror model given by Eqn. (2.29) and the finite barrier model given by Eqn. (2.28). We find that the finite mirror model has extra features not present in the δ mirror model due to the non-zero width of the central mirror which has resonances associated with the mirror width ($2M$). At the central mirror resonant wavenumbers, the transmission function exhibits Lorentzian type peaks. Decreasing the mirror width while increasing the mirror index of refraction while $2Mn_r^2 = \alpha$ leads to the resonant wavenumbers moving out further and a convergence of T_{FB} to T_δ. Here, the reflectivity parameter $\alpha = 2.5$ m.

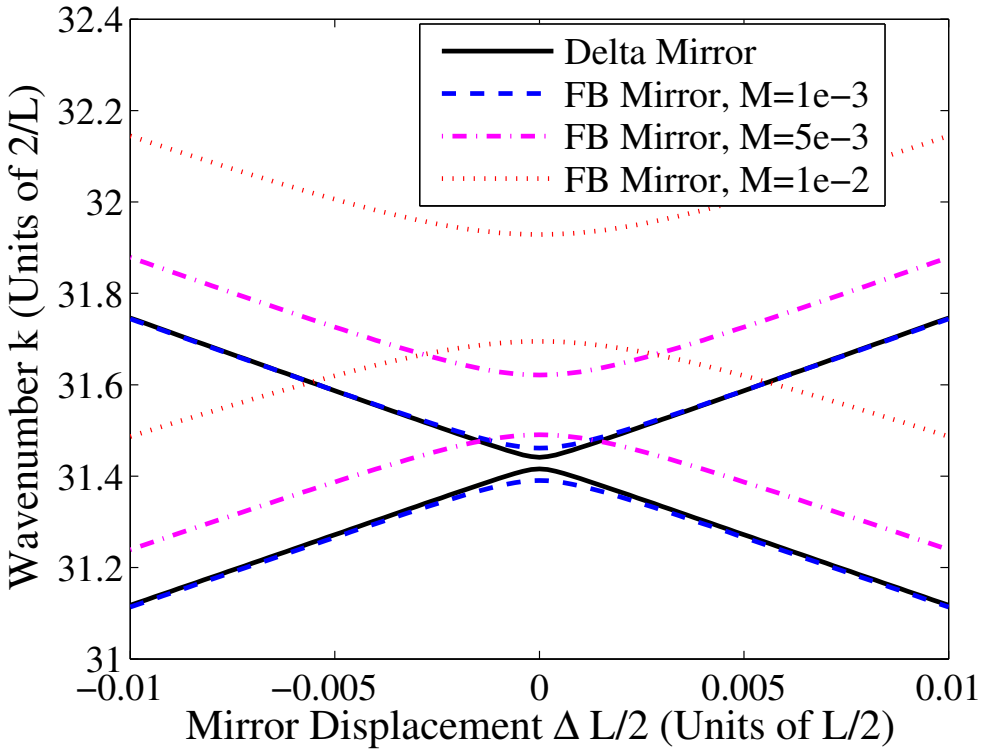

Figure 2.9: Comparison of wavenumber structures for the δ and FB model of the mirror. We compare the avoided crossing structure of wavenumber pairs around 10π numerically generated using Eqn. (2.28) to the corresponding δ model wavenumber structure with $\alpha = 2.5$ m. For wavenumbers away from the central mirror resonance condition, the FB eigenvalue structure converges to the δ model eigenvalues.

from the $M = 1e-3$ transmission plot we see that the wavenumber curves generated in Fig. 2.9 are away from any central mirror resonance. Therefore, we see a close agreement to the δ mirror wavenumbers for the corresponding mirror thickness. And as the mirror thickness is reduced, this agreement would get better. Therefore, we can model the central mirror as a δ-function if we are dealing with wavenumbers away from the resonance condition of a thin central mirror.

Chapter 3

Classical Dynamics of Light in the Non-Stationary Double Cavity

3.1 Introduction

In Chapter 2, we studied the properties of the light field inside the double cavity with a stationary, partially transmissive central mirror at an arbitrary position. We found that the allowed wavenumber structure of the light field inside the cavity forms a net of avoided crossings. Moreover, we defined an orthonormal basis in terms of the eigenmodes corresponding to each fixed central mirror position ($\{U_m(x, \Delta L)\}$). Knowledge of the wavenumber structure and the corresponding orthonormal basis completely determines how the light field will evolve in time inside a stationary double cavity. The initial optical electric field can be written as a superposition of the orthornomal basis. Replacing each $U_m(x, \Delta L)$ term by $U_m(x, \Delta L) \exp\{-i\omega_m(\Delta L)(t - t_0)\}$, we can determine the electric field at later times.

In this chapter, we study the time evolution of a light field for a double

cavity with a central mirror driven at a constant speed, or in other words, with time dependent boundary conditions. It is important to emphasize that in this thesis the time dependence is due to the parametric driven central mirror whose dynamics is therefore a prescribed function of time [49] as opposed to a time dependence of the mirror caused by a combination of the radiation pressure plus the mirror being coupled to some conservative potential like a spring, as in the case of optomechanics [50]. The time dependence of the boundary conditions make the dynamics of the light field much more complex and no general analytical results exist. The Maxwell wave equation, which once again forms the starting point of our investigation of the light field dynamics in Sec. 3.2 is second order in time. An exact first order in time reduction of the dynamics exists only for stationary cavities. We show in Sec. 3.4 that in the case of the double cavity with a linearly moving mirror, an *approximate* reduction of the second order dynamics to a first order in time Landau-Zener (L-Z) dynamics exists. We will find that the diabatic modes we defined earlier in analogy with the L-Z problem plays a central role in the approximation scheme. This approximate L-Z dynamical treatment in optomechanical systems has been in use in the literature [8] and has exact solutions. Experimentally, both L-Z [51, 52] and Landau-Zener-Stueckelberg [9] dynamics has been studied in the context of photon shuttling. Moreover, cooling of the central membrane in a double cavity via radiation pressure due to the light field using a first order in time description has also been studied [8]. Furthermore, the Landau-Zener formula gives us the condition required for adiabatic dynamics. We provide a more refined understanding of the parameter regimes when such an approximation is valid. A key point is that first order time dynamics conserves energy while second order in time dynamics does not. Hence, the validity of the first

order approximation is connected to the issue of energy non-conservation in the double cavity with the driven central mirror. We will study the connection between the energy of the light field and the work done by the parametrically moving mirror on it in greater detail in Chapter 4. In chapters 3 and 4, for all numerical simulations, we set the total cavity length to be $L = 100$ μm and consider wavenumber pairs corresponding to the avoided crossing near 8.0425×10^{-6} m^{-1} as the electromagnetic field inside the cavity. We consider central mirror speeds as high as 2×10^4 ms^{-1} which can be realized by modulating the refractive indices of a double cavity filled with some background dielectric material via the electro-opto effect and discussed in Appendix A.2 [53, 12].

3.2 Maxwell Wave Equation with Time-Dependent Boundary Conditions

We derive the equations of motion describing the time evolution of light in a double cavity starting from the Maxwell wave equation. We write the electric field in the adiabatic basis and find a differential equation that is second order in time for the corresponding amplitudes. These equations of motion are exact and from here onwards will be referred to as the adiabatic second order equations (ASOE). They provide us with the most accurate description of light dynamics in this chapter. ASOE are also the equations of motion by which we compare validity of all approximate dynamics in Chapters 2 and 3.

In the previous chapter, we considered the case where the central mirror inside the double cavity was stationary. Under such circumstances, the evolu-

tion of light was described by Eqn. (2.3). As the speed of the central mirror is slowly increased, we can expect that relativistic corrections will become relevant to the Maxwell wave equation. The Maxwell wave equation in free space is relativistically invariant, but inside a medium there are additional relativistic corrections that need to be considered if the medium is moving very fast [54]. In Appendix A.1, we find that the order of magnitude of relativistic corrections to Eqn. (3.1) corresponding to relavant experimental parameters are negligible. The electric field inside the cavity for a mirror moving at non-relativistic speed is described by

$$\frac{\partial^2 E(x,t)}{\partial x^2} - \mu_0 \epsilon(x,t) \frac{\partial^2 E(x,t)}{\partial t^2} = 0. \tag{3.1}$$

Eqn. (3.1) describes the dynamics of light regardless of whether the central mirror is being moved parametrically or is part of a dynamical system due to being coupled to a spring potential. Since we consider the electromagnetic field to be linearly polarized, the vector Maxwell wave equation reduces to a scalar Maxwell wave equation. The adiabatic modes form a complete basis and we can write the electric field as (the real part of)

$$E(x,t) = \sum_n c_n(t) \exp\left\{-i \int_{t_0}^{t} \omega_n(t')\mathrm{dt}'\right\} U_n(x,t) \tag{3.2}$$

where $U_n(x,t)$ is described in Eq. (2.6). Substituting equation (3.2) into (3.1),

one finds [42]

$$\sum_n \Bigg[\underbrace{-2i\omega_n \frac{\partial}{\partial t}(c_n(t)U_n(x,t))}_{1} + \underbrace{\frac{\partial^2}{\partial t^2}(c_n(t)U_n(x,t))}_{2} \underbrace{-i\frac{\partial \omega_n(t)}{\partial t} c_n(t)U_n(x,t)}_{3} \Bigg] \times \exp\left[-i\int_{t_0}^{t} \omega_n(t')\mathrm{dt}'\right] = 0. \quad (3.3)$$

In Eq. (3.3), term 1 is by far the most dominant term due to the very large optical frequency prefactor. In the slow mirror limit, term 2 is small while term 3 is much smaller still because the adiabatic mode can change more significantly in comparison to the rate of change of the optical frequency near an avoided crossing. At the center of the avoided crossing, the frequencies are at a maximum or minimum and hence, the rate of change of frequencies is strictly zero at that point. The relative magnitude of all these terms is analyzed in greater detail in reference [42]. For faster mirror speeds, terms 2 and 3 can start interacting on an equal footing. From Eqn. (3.3), we find that the amplitudes corresponding to the adiabatic basis satisfy

$$\ddot{c}_m(t) - i\dot{\omega}_m(t)c_m(t) - 2i\omega_m(t)\dot{c}_m(t) + \sum_n \{[2\dot{c}_n(t) - 2i\omega_n(t)c_n(t)]P_{mn}(t) + c_n(t)Q_{mn}(t)\} = 0 \quad (3.4)$$

where

$$\theta_{mn}(t) = \int_{t_0}^{t} [\omega_m(t') - \omega_n(t')]\,\mathrm{dt}' \quad (3.5)$$

$$P_{mn}(t) = \frac{1}{\epsilon_0}\int_{-L_1}^{L_2} \epsilon(x,t)U_m(x,t)\frac{\partial U_n(x,t)}{\partial t} e^{i\theta_{mn}(t)}\,\mathrm{dx} \quad (3.6)$$

and

$$Q_{mn}(t) = \frac{1}{\epsilon_0}\int_{-L_1}^{L_2} \epsilon(x,t)U_m(x,t)\frac{\partial^2 U_n(x,t)}{\partial t^2}e^{i\theta_{mn}(t)}\,\mathrm{dx}. \tag{3.7}$$

In order to solve the differential equations, we need to specify the initial conditions. Since Eqn. (3.4) is a set of second order in time differential equations, we need to specify both $c_m(t_0)$ and $\dot{c}_m(t_0)$. However, the initial conditions are not independent and we find that once $c_m(t_0)$ has been specified that $\dot{c}_m(t_0) = -\sum_n P_{mn}(t_0)c_n(t_0)$. Despite this, we still have two independent initial conditions since the real parts as well as the complex parts of $c_m(t_0)$ need to be specified. The terms $P_{mn}(t)$ and $Q_{mn}(t)$ depend on the motion of the mirror. If the mirror is stationary, then the dielectric function, $\epsilon(x,t)$, is constant in time and the adiabatic modes $U_n(x,t)$ are constant in time. The terms P_{mn} and Q_{mn}, which depend on the rates of change of the adiabatic modes, then become zero. Hence, the essence of mirror motion which leads to time dependent boundary conditions are captured in the terms, $P_{mn}(t)$ and $Q_{mn}(t)$. We simulate the dynamics of light in this chapter using three different equations of motion: adiabatic second order equations (ASOE), diabatic second order equations (DSOE) and diabatic first order equations (DFOE). The most accurate of these, ASOE, uses Eqn. (3.4) and as shown in Appendix A.1 can be a good approximation even for mirror speeds as high as $20,000\ \mathrm{ms}^{-1}$ in a cavity containing light with wavenumber $8.0425 \times 10^6 \mathrm{m}^{-1}$. Furthermore, the mirror reflectivites used in the simulations in chapters 3 and 4 of $R = 28\%,\ 61\%,\ 91\%,\ 98\%$ are given by $\alpha = 1.5 \times 10^{-7},\ 3.1 \times 10^{-7},\ 7.7 \times 10^{-7},\ 1.5 \times 10^{-6}$ m.

3.3 Energy of Light Field in The Cavity

We briefly derive the expression for the energy inside the cavity since it is relavant to the results in the next section. The energy of the light field inside the cavity is given by

$$\begin{aligned} \mathcal{E} &= \frac{1}{2}\int_{\mathcal{V}} \left[\epsilon(x)|E(x,t)|^2 + \mu_0|H(x,t)|^2\right] \mathrm{dV} \\ &= \frac{\mathcal{A}}{2}\int \left[\epsilon(x)|E(x,t)|^2 + \mu_0|H(x,t)|^2\right] \mathrm{dx} \end{aligned} \tag{3.8}$$

where $H(x,t)$ is the magnetizing field related to the magnetic field by $H = B/\mu_0$ and $\mathcal{A}$ is he transverse area of the mirror. For a dichromatic wave inside a cavity, comprised of frequencies $\omega_{1/2}$, i.e. two neighbouring adiabatic modes, the electric field can be written as (the real part of)

$$E(x,t) = a_1(t)\exp[-i\theta_1(t)]U_1(x,t) + a_2(t)\exp[-i\theta_2(t)]U_2(x,t) \tag{3.9}$$

where $U_m(x,t)$ is defined in Eqn. (2.6) and

$$\theta_m(t) = \int_{t_0}^{t} \omega_m(t')\mathrm{dt}'.$$

Hence, the energy per unit area becomes

$$\frac{\mathcal{E}}{\mathcal{A}} = \frac{\epsilon_0}{2}\left\{|a_1(t)|^2 + |a_2(t)|^2\right\} + \frac{\mu_0}{2}\int_{-L_1}^{L_2} |H(x,t)|^2 \mathrm{dx}.$$

In the stationary central mirror limit, the magnetic field term in the integrand gives a contribution equal to that of the electric field term. However, a non-stationary mirror implies corrections to the energy and force formula via

additional terms in the magnetizing field. Considering that we work in the non-relativistic central mirror speed regime, we ignore the additional corrections. The energy is then given by

$$\frac{\mathcal{E}}{\mathcal{A}} = \epsilon_0 \left\{ |a_1(t)|^2 + |a_2(t)|^2 \right\} \tag{3.10}$$

i.e. the instantaneous stationary cavity energy.

3.4 Approximate Dynamics of Light

In Zener's paper [55], he points out that the time dependence of the diabatic modes should be small compared to the time dependence of the corresponding amplitudes. In Sec. 3.2, we derived the dynamics of light in the double cavity by writing the electric field in the adiabatic basis. We mentioned in that section that close to the avoided crossing, the adiabatic modes change drastically compared to the corresponding amplitudes as can be seen in Fig. 2.5. In this section, we derive the dynamics of light by writing the electric field in terms of the diabatic mode basis. Contrary to the adiabatic basis, the diabatic modes change insignificantly compared to their amplitudes near an avoided crossing as can be seen in Fig. 2.6. This allows us to ignore the time dependence of the diabatic mode functions ultimately leading us to deriving the DSOE and the analytically more convenient DFOE as in reference [12]. Assuming that the mirror motion is restricted near an avoided crossing of wavenumbers, we can employ the two level approximation and write

$$E(x,t) = a_L(t)\phi_L(x,t) + a_R(t)\phi_R(x,t). \tag{3.11}$$

From $E'' = \mu_0 \epsilon(x,t)\ddot{E}$, ignoring $\dot{\phi}_{L/R}$ and $\ddot{\phi}_{L/R}$ we find that

$$a_L(t)\phi_L'' + a_R(t)\phi_R'' = \mu_0 \epsilon(x,t)[\ddot{a}_L(t)\phi_L + \ddot{a}_R(t)\phi_R]. \tag{3.12}$$

As the mirror is swept through the avoided crossing, the left and right amplitudes swap populations as shown in Fig. 3.1 and light is transferred from one side of the double cavity to the other. Even for a stationary mirror, the light initially localized on one side would oscillate between the left and right modes with frequency $\sqrt{\Delta^2 + \Gamma(\Delta L)^2}/2$ (see Eqn. (2.12)) exactly like Rabi oscillation in a two level atom interacting with a single mode field. The combined effect of light sloshing back and forth and the moving mirror transferring light population leads to an even larger rate of change of the diabatic amplitudes compared to the corresponding modes. One of the goals of this section is to numerically check that ignoring the time dependence of the mode functions is justified. The other goal is to check numerically that the first order in time reduction of the second order dynamics is valid.

3.4.1 Diabatic Equations of Motion Ignoring Time Dependence of Local Mode Functions

To find the spatial second derivatives of the diabatic modes for Eqn. (3.12), we write each diabatic mode in the adiabatic basis, whose second derivatives we know in terms of the Sturm-Liouville relationship in Eqn. (2.5), $\partial_x^2 U_m(x,\Delta L) = -k_m^2 \left(\epsilon(x,\Delta L)/\epsilon_0\right) U_m(x,\Delta L)$, and then convert back to the

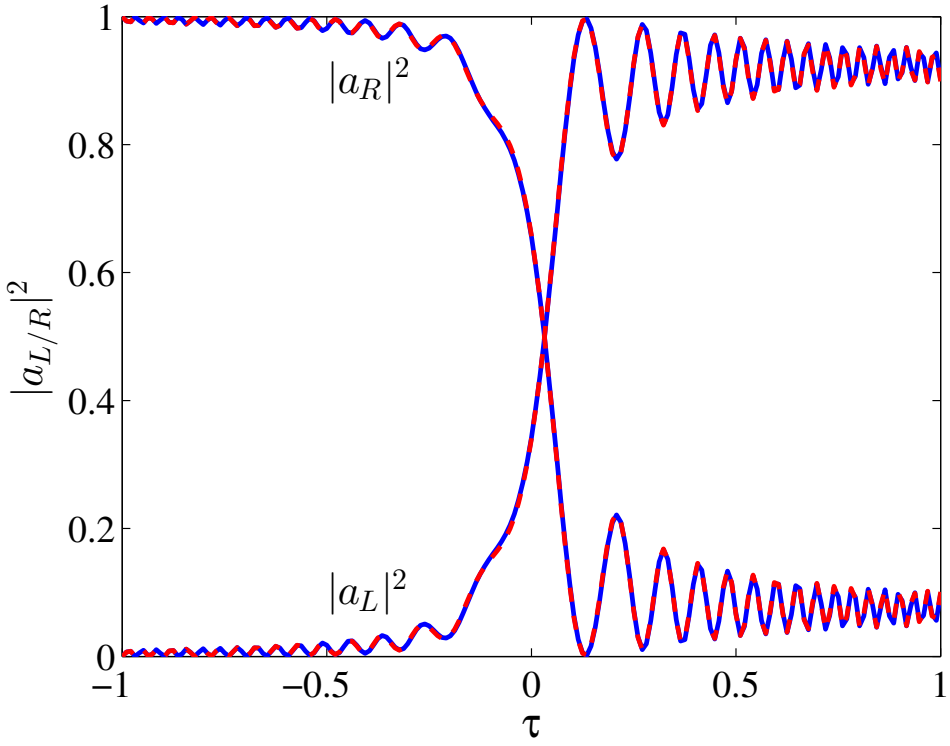

Figure 3.1: Comparison of the adiabatic and diabatic second order equations. Here, we plot the time evolution of the left and right diabatic amplitudes due to the ASOE from Eqn. (3.4) and DSOE from Eqn. (3.14). In this parameter regime, (reflectivity 98%, mirror speed 5000 ms^{-1} and mirror displacement of 1×10^{-3} L, where L is the total length of the double cavity) the two curves lie on top of each other showing that any differences are very small effects. In order to see the subtle variations between the two sets of equations, we turn to Figs. 3.2 and 3.3.

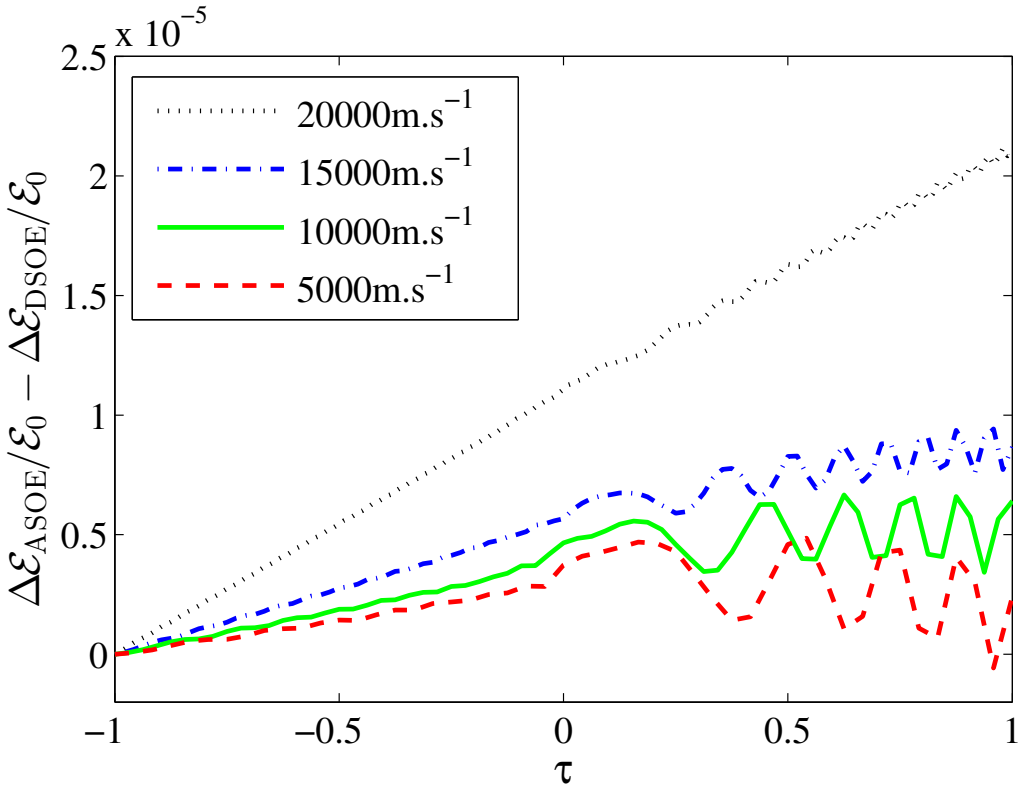

Figure 3.2: Comparison of adiabatic and diabatic second order equations. Here, we plot the difference of fractional change in energy due to the ASOE from Eqn. (3.4) and DSOE from Eqn. (3.14) versus a rescaled time co-ordinate. $\mathcal{E}_0$ denotes the initial energy of the light field. In this figure, each curve corresponds to a different mirror speed while the reflectivity is held constant at 98%. We see that the order of magnitude of difference between ASOE and DSOE, quantified by the fractional change of energy, is about 1×10^{-5}. This result validates the approximation of ignoring the time dependence of the diabatic modes in going from Eqn. (3.4) to Eqn. (3.14).

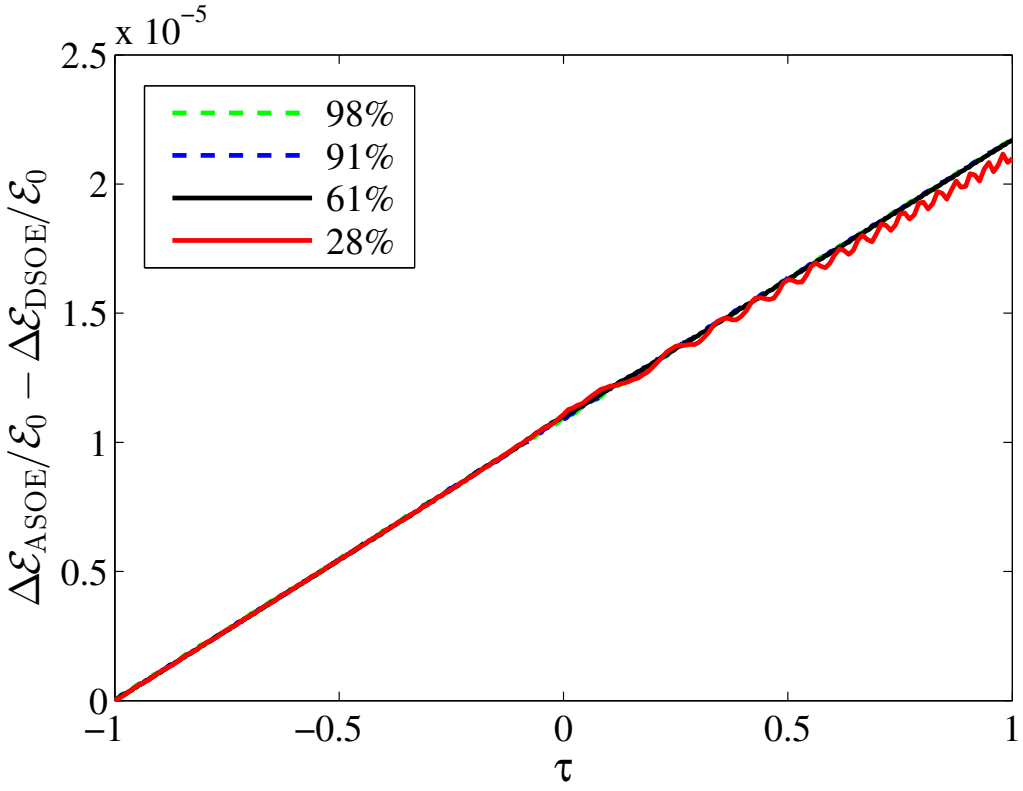

Figure 3.3: Comparison of adiabatic and diabatic second order equations. Here, we plot the difference of fractional change in energy due to the ASOE from Eqn. (3.4) and DSOE from Eqn. (3.14) versus a rescaled time co-ordinate. In this figure, each curve corresponds to a different mirror reflectivity while the velocity is held constant at 5000 ms^{-1}. We see that the order of magnitude of difference between ASOE and DSOE, quantified by the fractional change of energy, is about 1×10^{-5}. The conclusion is the same as in Fig. 3.2.

diabatic mode basis using Eqn. (2.21). In matrix form, we then write

$$-\begin{pmatrix} \ddot{a}_L \\ \ddot{a}_R \end{pmatrix} = \begin{pmatrix} \cos^2\theta\omega_2^2 + \sin^2\theta\omega_1^2 & \cos\theta\sin\theta(\omega_1^2 - \omega_2^2) \\ \cos\theta\sin\theta(\omega_1^2 - \omega_2^2) & \cos^2\theta\omega_1^2 + \sin^2\theta\omega_2^2 \end{pmatrix} \begin{pmatrix} a_L \\ a_R \end{pmatrix} \quad (3.13)$$

or

$$-\begin{pmatrix} \ddot{a}_L \\ \ddot{a}_R \end{pmatrix} = \begin{pmatrix} [\omega_{\rm av} + \Gamma(t)]^2 + \Delta^2 & 2\Delta\omega_{\rm av} \\ 2\Delta\omega_{\rm av} & [\omega_{\rm av} - \Gamma(t)]^2 + \Delta^2 \end{pmatrix} \begin{pmatrix} a_L \\ a_R \end{pmatrix}. \quad (3.14)$$

From here onwards, we refer to Eqn. (3.14) as the diabatic second order equations (DSOE).

3.4.2 Approximate First Order in Time Equations of Motion

In the next stage, we see how to approximate this second order in time dynamics via the first order in time Landau-Zener type dynamics. We transform the left/right mode variables as

$$a_{L/R} = \tilde{a}_{L/R} \exp\left\{-i\int_{t_0}^{t} \beta_{L/R}(t')dt'\right\} \quad (3.15)$$

where

$$\beta_{L/R}(t) = \sqrt{(\Gamma(t) \pm \omega_{\rm av})^2 + \Delta^2}. \quad (3.16)$$

Then, we have

$$\ddot{a}_{L/R} = \left\{\ddot{\tilde{a}}_{L/R} - 2i\beta_{L/R}\dot{\tilde{a}}_{L/R} - i\dot{\beta}_{L/R}\tilde{a}_{L/R} - \beta_{L/R}^2\tilde{a}_{L/R}\right\} \exp\left\{-i\int_{t_0}^{t} \beta_{L/R}(t')dt'\right\}. \quad (3.17)$$

Let us ignore the first and third terms since they are much smaller than the $\beta_{L/R}^2 \approx \omega_{\rm av}^2$ term which is of the order of magnitude 10^{30} for optical frequencies. We will check the validity of these approximations later. Then, we have that

$$i\dot{\tilde{a}}_{L/R} = \frac{\omega_{\rm av}\Delta}{\beta_{L/R}}\tilde{a}_{R/L}\exp\left\{\pm i\int_{t_0}^{t}[\beta_L - \beta_R]dt'\right\}. \tag{3.18}$$

Assuming $\omega_{\rm av}$ is very large, and using the binomial expansion, we find that

$$\beta_{L/R}(t) \approx \omega_{\rm av}\left\{1 \pm \frac{\Gamma(t)}{\omega_{\rm av}} + \frac{1}{2}\frac{\Delta^2}{\omega_{\rm av}^2}\right\}. \tag{3.19}$$

Hence, $\beta_L - \beta_R \approx 2\Gamma$ and $\omega_{\rm av}/\beta_{L/R} \approx 1$, giving us

$$i\dot{\tilde{a}}_{L/R} = \Delta\tilde{a}_{R/L}\exp\left\{\pm 2i\int_{t_0}^{t}\Gamma(t')dt'\right\}. \tag{3.20}$$

Changing the variables back to $a_{L/R}$, assuming that the mirror is moving at a constant speed so that $\Gamma(t)$ is linear in time, we indeed get Landau-Zener dynamics

$$i\begin{pmatrix}\dot{a}_L\\ \dot{a}_R\end{pmatrix} = \begin{pmatrix}\omega_{\rm av}+\Gamma(t) & \Delta\\ \Delta & \omega_{\rm av}-\Gamma(t)\end{pmatrix}\begin{pmatrix}a_L\\ a_R\end{pmatrix} \tag{3.21}$$

with linearly varying diagonal elements and constant off-diagonal elements. Mathematically, this equation resembles the Schrödinger equation with the Landau-Zener Hamiltonian, but here the role of the quantum probability amplitudes are played by the amplitudes of the classical electric fields (hence, the absence of $\hbar$). An important property of the Schrödinger equation is conservation of probability (unitary dynamics) which is thus imposed on the electric field amplitudes as $|a_L|^2 + |a_R|^2 = 1$. This is artificial since in classical electromagnetism this is an energy (Eqn. (3.10)) which is not conserved for a

parametric driven mirror. From here onwards, we refer to Eqn. (3.21) as diabatic first order equations (DFOE). Hence, we have the following hierarchy: the ASOE in Eqn. (3.4) are the Maxwell wave equation with time dependent boundary conditions written in terms of the adiabatic basis. The DSOE in Eqn. (3.14) are the two-level approximation near an avoided crossing of the ASOE, while neglecting the time dependence of the diabatic mode functions. Lastly, the DFOE in Eqn. (3.21) are an approximation to the DSOE by neglecting fast oscillating terms, i.e. the first and third terms of the right hand side of Eqn.(3.17). Furthermore, for linearly varying diagonal elements (setting $\Gamma(t) = \vartheta t/2$), which occurs for a central mirror being driven at a constant speed we can determine the adiabatic condition for adiabatic transfer of light amongst the cavity halves. If the two level system is prepared in one of the diabatic modes at time $t = -\infty$, then the probability of transition to the other mode at time $t = \infty$ is given by $P_{\mathrm{LZ}} = \mathrm{e}^{-2\pi\Delta^2/\vartheta}$ [56, 55]. Hence, the adiabatic transfer of light can be achieved for $2\pi\Delta^2/\vartheta \gg 1$. In this section, we simulate the dynamics for light initially located in the right side of the cavity and moving the mirror from the left to the right using the ASOE and DSOE. The dynamics in the two sets of equations are described in two different basis, i.e. adiabatic modes for Eqn. (3.4) and diabatic modes for Eqn. (3.14) and therefore the calculations are quite different. We can change between the two bases using Eqn. (2.21). Comparing the dynamics of the two sets of equations will show if it is valid to ignore the time dependence of the diabatic mode functions or not. In Fig. 3.1, we see that the left/right amplitudes from the ASOE and DSOE lie on top of each other. We can conclude that the difference in the mode amplitudes due to the ASOE and DSOE are very small relative to the order of magnitude of the amplitudes themselves. To get a closer look

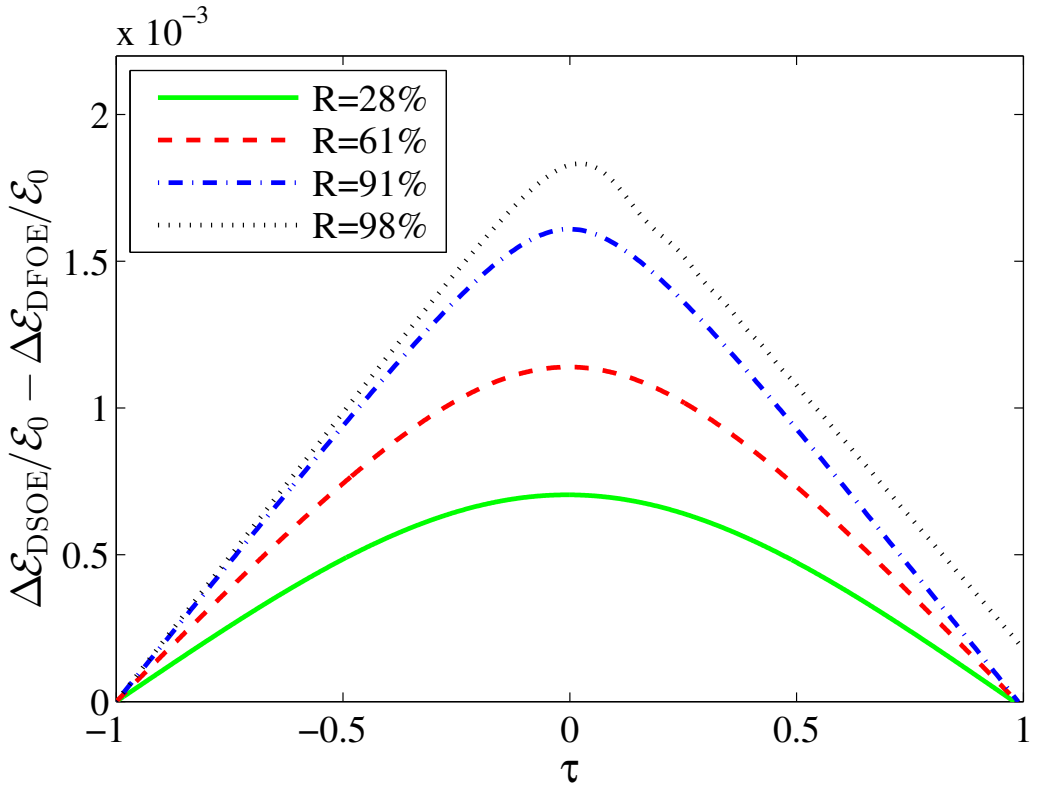

Figure 3.4: Comparison of diabatic second and first order in time equations and the role of mirror reflectivity. This figure shows the difference of fractional change in energy due to the DSOE in Eqn. (3.14) and the DFOE in Eqn. (3.21) versus a rescaled time co-ordinate. Each curve corresponds to a different mirror reflectivity, while the velocity is held fixed at 5000 ms^{-1}. For first order dynamics, $\Delta\mathcal{E}_{\mathrm{DFOE}}/\mathcal{E}_0$ has to be identically zero, while for second order it is non-zero. Hence the difference between this quantity and zero can be used to quantify the validity of the first order model to the more correct second order equations of motion. As reflectivity goes up, the first order approximation becomes less valid. However, it is still a very good approximation in the optical frequency regime.

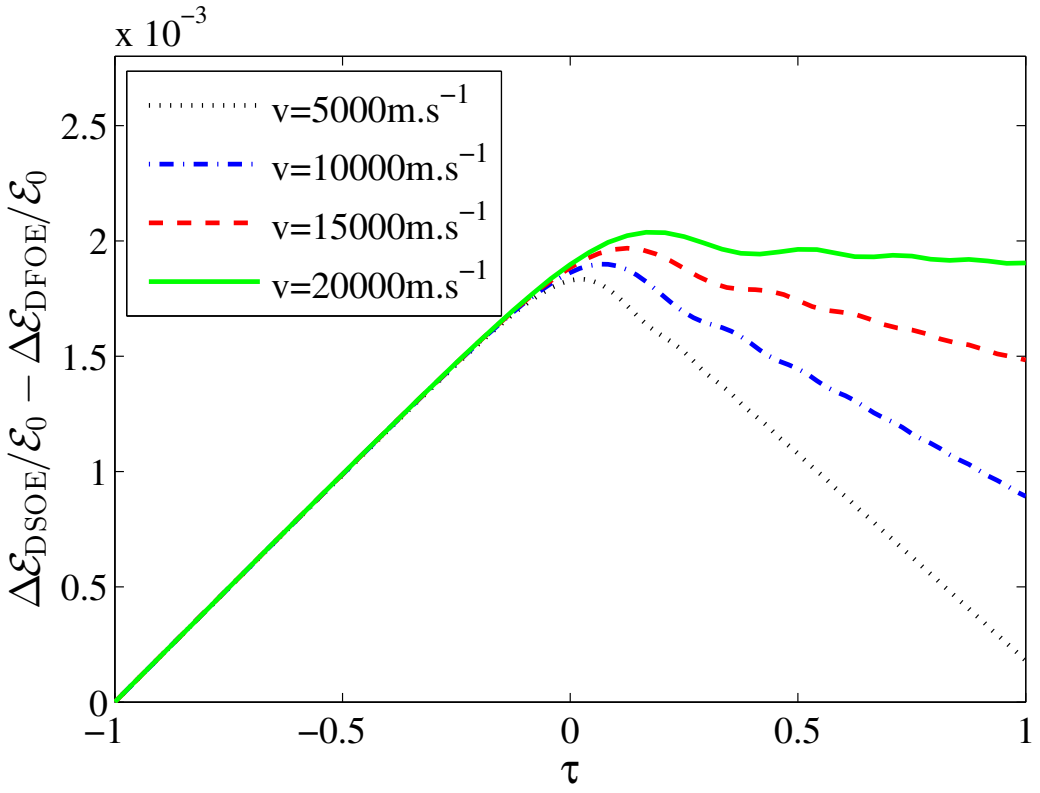

Figure 3.5: Comparison of diabatic second and first order in time equations and the role of mirror velocity. This figure shows the difference of fractional change in energy due to the DSOE in Eqn. (3.14) and the DFOE in Eqn. (3.21) versus a rescaled time co-ordinate. Each curve corresponds to a different mirror velocity, while the reflectivity is held constant at 98%. As our intuition would suggest, the first order approximation becomes less valid for higher speeds. Although a speed of 20000 ms^{-1} seems very high, such effective speeds can be achieved by changing the background index of refractions rather than physically moving the mirror as discussed in Appendix A.2.

into the order of magnitude of the effect of ignoring the time dependence of the diabatic modes, we compare $\Delta\mathcal{E}/\mathcal{E}_0$ for the two sets of equations of motion. The change in energy is proportional to the adiabatic amplitude sum as discussed in Sec. 3.3, Eqn. (4.11). From Figs. 3.2 and 3.3, we see that as long as the mirror motion is close to the avoided crossing, the difference is of the order of 10^{-5} even for mirror speeds as high as 20000 ms^{-1}.

The other objective of this section is to check how good of an approximation it is to ignore the first and the third term in Eqn. (3.17), i.e. how good of an approximation the DFOE is to the DSOE. In Figs. 3.4 and 3.5 we compare the DSOE to its first order reduction, the DFOE. Once again, the fluctuation in the amplitudes due to the second order dynamics and its approximation is much smaller than the magnitude of the modes. Hence it is easier to look at $\Delta\mathcal{E}/\mathcal{E}_0$. Due to the unitary structure of the Schrödinger equation, the first order dynamics is unitary (we have checked this numerically) and therefore, the change in energy ratio, $\Delta\mathcal{E}_{\text{DFOE}}/\mathcal{E}_0$, is identically zero. The difference between the first and second order model is directly related to the energy pumped into and out of the system. We can see that for increasing reflectivity and mirror speed, the first order approximation becomes less valid. Though, in the optical frequency regime, it is a very good approximation. The discrepancy in this parameter regime is of the order of magnitude 10^{-3}. This also shows that ignoring the time dependence of the diabatic mode functions is a much smaller effect than the first order reduction of DSOE.

3.4.3 Effect of mirror reflectivity and speed

Just above, we showed that for large optical frequencies, one can approximate the diabatic second order equations by diabatic first order equations that is exactly mappable onto the analytically solvable Landau-Zener dynamics for mirrors moving at constant speeds. However, the analysis does not clearly show us the subtler dependence on mirror reflectivity and speed and were smudged out when we ignored the first and third terms of Eqn. (3.17). We can see that they have an effect, though small, from Figs. 3.4 and 3.5. This section is dedicated to developing a criterion that allows us to evaluate when the first order approximation is good or bad depending upon the mirror reflectivity and speed.

Define the following matrix

$$M = -i \begin{pmatrix} \omega_{\text{av}} + \Gamma(t) & \Delta \\ \Delta & \omega_{\text{av}} - \Gamma(t) \end{pmatrix} \tag{3.22}$$

and let

$$\vec{a} = \begin{pmatrix} a_L \\ a_R \end{pmatrix}. \tag{3.23}$$

We are interested in the condition/parameter regime where the DFOE are a good approximation of the DSOE, which in turn we have also established to be a very good approximation to the dynamics of light from the ASOE. Then, we would like to have the condition for when the DFOE rewritten as

$$\frac{d}{dt}\vec{a} = M\vec{a} \tag{3.24}$$

is a good approximation to the DSOE rewritten as

$$\frac{d^2}{dt^2}\vec{a} = M^2\vec{a}. \tag{3.25}$$

To compare the two, we take the derivative of both sides of Eqn. (3.24), we find

$$\frac{d^2}{dt^2}\vec{a} = M^2\vec{a} + \dot{M}\vec{a} \tag{3.26}$$

where

$$\dot{M} = -i\begin{pmatrix} \dot{\Gamma} & 0 \\ 0 & -\dot{\Gamma} \end{pmatrix}. \tag{3.27}$$

Eqn. (3.27) is the same as Eqn. (3.25) apart from the $\dot{M}\vec{a}$ term. In order for the diabatic first order equations to be a valid approximation of the second order equations, we require that $r = \frac{||M^2||^2}{||\dot{M}||^2}$ be large, i.e. $||\dot{M}||$ is much smaller than $||M^2||$.

The symbol $||\cdot||$ represents the norm of the matrix given by the sum of each matrix element squared [57]. Then, the ratio describing first order approximation validity becomes

$$r = \frac{8\Delta^2\omega_{\text{av}}^2 + ([\omega_{\text{av}} + \Gamma]^2 + \Delta^2)^2 + ([\omega_{\text{av}} - \Gamma]^2 + \Delta^2)^2}{2\dot{\Gamma}^2}. \tag{3.28}$$

Note that this quantity takes account of the mirror speed ($\dot{\Gamma}$) and the reflectivity (Δ). Before, we move on, let us take a brief excursion through the structure of $\omega_{2/1}(\Delta L)$ and the analytical implications of being near an avoided crossing for central mirrors with high enough reflectivity. Detailed derivations are given in references [12]. In analogy with the Landau-Zener Hamiltonian and the avoided crossings the eigenvalues form, we fit the frequencies near the

avoided crossing in the double cavity with

$$\omega_{2/1} = \omega_{\text{av}} \pm \sqrt{\Delta^2 + \gamma \Delta L^2}. \tag{3.29}$$

Comparing this with Eq. (2.12), we see that

$$\Gamma(\Delta L) = \sqrt{\gamma} \Delta L. \tag{3.30}$$

In Fig. 2.2, one can see that as the central mirror reflectivity approaches unity, the avoided crossing curves become steeper which implies *faster* change of frequencies with change in mirror position and that second order corrections become important. As $R \to 1$, the term $\sqrt{\gamma}$ asymptotically approaches the slope of the diabatic frequency curve (red-dotted curve in Fig. 2.2). Furthermore, we have the analytic formulae [12]

$$\Delta = \frac{\omega_0}{2} \frac{1}{1 + \frac{\omega_0^2 L \alpha}{4c^2}} \tag{3.31}$$

and

$$\gamma = \frac{\omega_0^3}{2Lc^2} \Delta\alpha \tag{3.32}$$

where

$$\omega_0 = \frac{2cn\pi}{L} \tag{3.33}$$

where n denotes the n-th eigenfrequency. Then

$$r = \tag{3.34}$$

$$\frac{(\gamma^2 \Delta L^4 + \Delta^4 + \omega_{\text{av}}^4) + 6\omega_{\text{av}}^2(\Delta^2 + \gamma \Delta L^2) + 2\gamma \Delta^2 \Delta L^2}{\gamma \Delta \dot{L}^2} \tag{3.35}$$

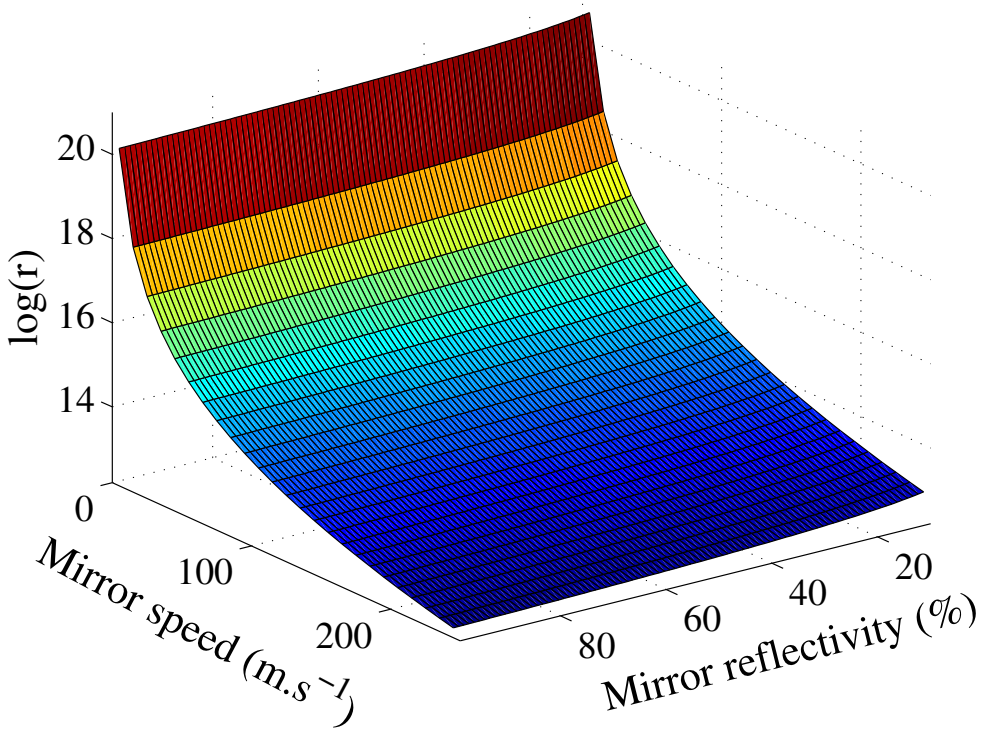

Figure 3.6: The analytical condition of first order EOM validity is given by the ratio, r in Eqn. (3.35) or log(r). Large r, means first order is a good approximation. Here, we look at the dependence of r on mirror velocity and reflectivity. It can be clearly seen that r becomes large as the mirror velocity becomes small as well as r becomes small when the mirror reflectivity increases. This supports what the numerical simulations have indicated previously as to the validity of the first order model depending on the mirror velocity and reflectivity. This figure is generated using equation (3.35).

where

$$\omega_{\rm av} = \omega_0 + \Delta. \tag{3.36}$$

For large r, first order equations of motion are a good approximation. From the form of r, the role of bare cavity eigenfrequency and mirror speed in the DFOE validity is quite clear. Increasing ω_0 and decreasing mirror speed imply that r is increasing. Intuitively, we expect that a higher reflectivity should lead to a breakdown of the first order approximation because a more reflective

mirror perturbs the field more. Since $R = \frac{1}{1+4c^2/\omega^2\alpha^2}$, as α increases, then so does reflectivity, R and the avoided crossing gap 2Δ. We need to understand the dependence of r on increasing α. Differentiating r with respect to α, we find that the derivative is always negative showing that r is a monotonically decreasing function of α. This means that r goes down as α or mirror reflectivity goes up. Hence, the first order approximation becomes worse with increasing reflectivity.

Chapter 4

Work Energy Theorem and Classical Dynamics

4.1 Introduction

In chapter 3 we saw that a first order in time reduction of the Maxwell wave equation artificially conserves energy of the light field inside the double cavity. The validity of the first order approximation (DFOE) is greater for lower work done on the light field by the external agent driving the mirror. For a stationary double cavity, where the energy is conserved, the first order reduction is exact. When the mirror begins to move, however, energy non-conservation becomes inevitable. Consider a central mirror moving at a constant speed. For the external source to continue to move the central mirror in such a fashion, it needs to apply a force equal and opposite to the radiation pressure of the light field inside the cavity on the mirror. Hence, the external source ends up doing work on the light field. In this chapter, we take a detailed look at the radiation pressure of the light field on the mirror. We compare the work done

by the external source on the light field to the change in energy and in fact find the two quantities to be in agreement as they should be. This serves as a validity check for our numerical simulations. Lastly, we look at adiabaticity for the Maxwell wave equation for time-dependent boundary conditions. We compare adiabaticity in the context of the double cavity with a moving mirror to our understanding of adiabaticity from the Schrödinger wave equation. This provides closure to our classical study of the double cavity system.

4.2 Maxwell Stress Tensor and Radiation Pressure of Light on Mirror

In this section, we connect two aspects of the double cavity: the radiation pressure of light on the central mirror and the energy of the light field in the system. Starting from the Maxwell stress tensor, we derive the radiation pressure of light in the two level approximation near an avoided crossing. We find that the radiation pressure obtained by simply adding the pressures of each adiabatic mode ($U_{1/2}(x, \Delta L)$) leads to erroneous results and is not equivalent to the radiation pressure of the net electric field. We also check that the work-energy theorem, $\Delta\mathcal{E} = \mathcal{W} = \int \mathcal{F}\mathrm{dx}$ is satisfied, which gives us a self consistency check of the numerical simulations in this thesis.

Moreover, studying the radiation pressure gives an intuitive explanation for the energy non-conservation with the ASOE and DSOE as seen in Figs. 3.4 and 3.5. Assume that initially light is localized in the right side of the cavity. Suppose we want to move the mirror from left to right at a constant speed. The radiation pressure of light localized on the right side of the cavity will push

against the mirror. Hence, to maintain a constant speed we need to apply a force equal in magnitude to the radiation pressure force, but in the direction of the mirror motion. Therefore, to maintain a constant mirror velocity, positive work has to be done by the mirror on the light field and the energy of the system will increase. One can see in Figs. 3.4 and 3.5 that the energy pumped in reaches a maximum value. This occurs at the point where the light intensity on the left and right are equal and the radiation pressure cancels to zero as will be shown in Fig. 4.3 which provides the radiation pressure corresponding to the curves in Fig. 3.4. On the other hand, if the mirror is being moved from right to left, the radiation pressure points in the same direction as the mirror motion. Hence, a force from the mirror on the light field has to be applied opposite to the mirror motion to maintain a constant speed. This implies that negative work is being done on the light field due to the mirror and energy will end up being pumped out of the light field. The force due to radiation pressure on some region of volume $\mathcal{V}$ and surface area $\mathcal{S}$ is given by [58]

$$\mathcal{F} = \int_{\mathcal{S}} \overleftrightarrow{T} \cdot \mathrm{d}\vec{\mathrm{a}} - \frac{d}{dt} \int_{\mathcal{V}} \epsilon(\vec{r}) \vec{E} \times \vec{B} \mathrm{dV} \tag{4.1}$$

where $\overleftrightarrow{T}$ is the Maxwell stress tensor defined by

$$T_{ij} \equiv \epsilon(\vec{r}) \left(E_i E_j - \frac{1}{2} \delta_{ij} E^2 \right) + \frac{1}{\mu_0} \left(B_i B_j - \frac{1}{2} \delta_{ij} B^2 \right). \tag{4.2}$$

We are interested in the force on a central mirror in a double cavity due to electromagnetic waves. $\mathcal{S}$ represents the interfaces of this mirror, while $\mathcal{V}$ is its volume. The central mirror can be described by the finite mirror or the δ function model. The latter is mathematically tractable while the

former represents a more physically realistic model. Let us set the following conventions: Electric field is polarized along the y-axis and the magnetic field is polarized along the z-axis. The cavity axis is in the $\hat{x}$ direction, i.e. $\epsilon(\vec{r}) = \epsilon(x)$. In this case, T_{xx} is the only matrix element with a non-zero projection along the surface are vector and given by

$$T_{xx} = \frac{\epsilon(x)}{2} E_y^2 + \frac{1}{2\mu_0} B_z^2. \tag{4.3}$$

Let us look at the second term of the force formula, $\frac{d}{dt} \int_{\mathcal{V}} \epsilon(\vec{r}) \vec{E} \times \vec{B} \mathrm{dV}$ (for the finite mirror model). In general, this term is non-zero. Since we are interested in a frequency regime far away from the resonance of the central mirror, the electric and magnetic field strength inside $\mathcal{V}$ is negligible and we can neglect this term. Hence, the force becomes

$$\mathcal{F}_M = \int_{\mathcal{S}} T_{xx} \mathrm{da}_x = \mathcal{A} \left\{ \frac{\epsilon_M(x)}{2} E_{y,M}^2 + \frac{1}{2\mu_0} B_{z,M}^2 \right\}_{\text{Right}}^{\text{Left}} \tag{4.4}$$

where $\mathcal{A}$ is the transverse area of the cavity and $2M$ is the width of the mirror. When we take the limit $M \to 0,\ n \to \infty$ s.t. $2Mn^2 = \alpha$ [12], and the field near the mirror is almost a node, the finite mirror approaches the δ-function model and the force becomes

$$\frac{\mathcal{F}}{\mathcal{A}} = \left\{ \frac{\epsilon(x)}{2} E_y^2 + \frac{1}{2\mu_0} B_z^2 \right\}_{\text{Right}}^{\text{Left}}. \tag{4.5}$$

We could have written down this formula without appealing to the finite mirror model. However, this shows us that there are no unwanted surprises in using the less physically realistic δ-function mirror (away from the resonance condition of the central mirror).

One last simplification can be made to the force formula. The electric field is continuous at the mirror interface while the magnetic field is discontinuous. This is due to the fact that the magnetic field is related to the spatial derivative of the electric field which happens to be discontinuous. Hence, the radiation pressure becomes

$$\begin{aligned} \mathcal{P} &= \left\{ \frac{\epsilon(x)}{2} E_y^2 + \frac{1}{2\mu_0} B_z^2 \right\}_{\text{Right}}^{\text{Left}} \\ &= \frac{1}{2\mu_0} \left\{ B_z^2 \right\}_{\text{Right}}^{\text{Left}} \end{aligned} \tag{4.6}$$

which is simply proportional to the difference of the magnetic field intensity between the left and right sides of the central mirror.

4.3 Numerical check of the Work-Energy Theorem in the Double Cavity

The electric field corresponding to frequency ω_m is

$$\vec{E}_m(x,t) = \hat{y} a_m(t) \exp[-i\theta_m(t)] U_m(x,t) \tag{4.7}$$

The coefficient $a_m(t)$ is time dependent, since we are assuming a non-stationary mirror. From

$$\nabla \times \vec{H} = \frac{\partial \vec{D}}{\partial t}$$

the magnetizing field is given by

$$-\partial_x H_z \hat{y} = \hat{y}\left\{-i\epsilon a_m(t)\omega_m(t)\exp[-i\theta_m(t)]U_m(x,t) + \epsilon\exp[-i\theta_m(t)]\frac{\partial}{\partial t}[a_m(t)U_m(x,t)]\right\} \quad (4.8)$$

where $\vec{D}$ is the displacement field related to the electric field by $D = \epsilon E$. Let us ignore the last term on the grounds that the optical frequency prefactor in the first term will dominate. Then, the solution to Eqn. (4.8) where U_m is given by Eqn. (2.6) is

$$\vec{H}_m(x,t) = -\hat{z}\epsilon_0 a_m(t)c \cdot i\exp[-i\theta_m(t)]G_m(x,\Delta L)$$

where

$$G_m(x,\Delta L) = \begin{cases} A_m\cos[k_m(x+L_1)], & -L_1 < x < 0 \\ B_m\cos[k_m(x-L_2)], & 0 < x < L_2 \end{cases} \quad (4.9)$$

and c is the speed of light. Therefore, the radiation pressure due to a monochromatic wave of frequency ω_m (ignoring the $\epsilon\frac{\partial}{\partial t}[a_m(t)U_m(x,t)]$ term) is

$$\begin{aligned} \mathcal{P}_m &= \frac{\mu_0}{2}\left\{H_z^2\right\}_{\text{Right interface}}^{\text{Left interface}} \\ &= \frac{\epsilon_0}{2}a_m^2(t)\left\{A_m^2\cos^2(k_m L_1) - B_m^2\cos^2(k_m L_2)\right\}. \end{aligned} \quad (4.10)$$

Now that we have a formula for the radiation pressure force on the central mirror, we can check its accuracy. We have simulations of the odd/even adiabatic amplitudes, $a_{1/2}(t)$, defined in Eqn. (3.2) for a linear sweep of the mirror near an avoided crossing. From these simulations, we can determine the energy

difference per unit area using Eqn. (3.10) to be

$$\frac{\Delta\mathcal{E}(\tau)}{\mathcal{A}} \approx \epsilon_0 \left\{ |a_1(\tau)|^2 + |a_2(\tau)|^2 - 1 \right\} \tag{4.11}$$

assuming that we pick the initial amplitude sum to be 1.

From the radiation pressure calculation, we find that the work done by the mirror on the light field is

$$\frac{\Delta\mathcal{E}(\tau)}{\mathcal{A}} = -v \int_{-1}^{\tau} \mathrm{d}\tau' \left[\mathcal{P}_1(\tau') + \mathcal{P}_2(\tau') \right] \tag{4.12}$$

where τ is a linear reparametrization of time such that $\tau = -1..1$, when $t = -T_0..T_0$. Hence, we find the net radiation pressure due to light by summing the radiation pressure due to each monochromatic light field separately. The radiation pressure force seems to work for the lower reflectivity cases in Fig. 4.1, but the work and energy curves corresponding to 98% reflectivity does not fit perfectly.

Instead of summing up the forces due to individual frequencies of light, we find the force due to the net electromagnetic field. The electric field is

$$\vec{E}(x,t) = \hat{y} \left\{ a_1(t) \exp[-i\theta_1(t)] U_1(x,t) + a_2(t) \exp[-i\theta_2(t)] U_2(x,t) \right\}. \tag{4.13}$$

The magnetizing field satisfies

$$\partial_x H_z \hat{y} = \hat{y} \sum_{m=1,2} \{ i\epsilon a_m(t) \omega_m(t) \exp[-i\theta_m(t)] U_m(x,t) - \epsilon \exp[-i\theta_m(t)] \frac{\partial}{\partial t} [a_m(t) U_m(x,t)] \Big\}. \tag{4.14}$$

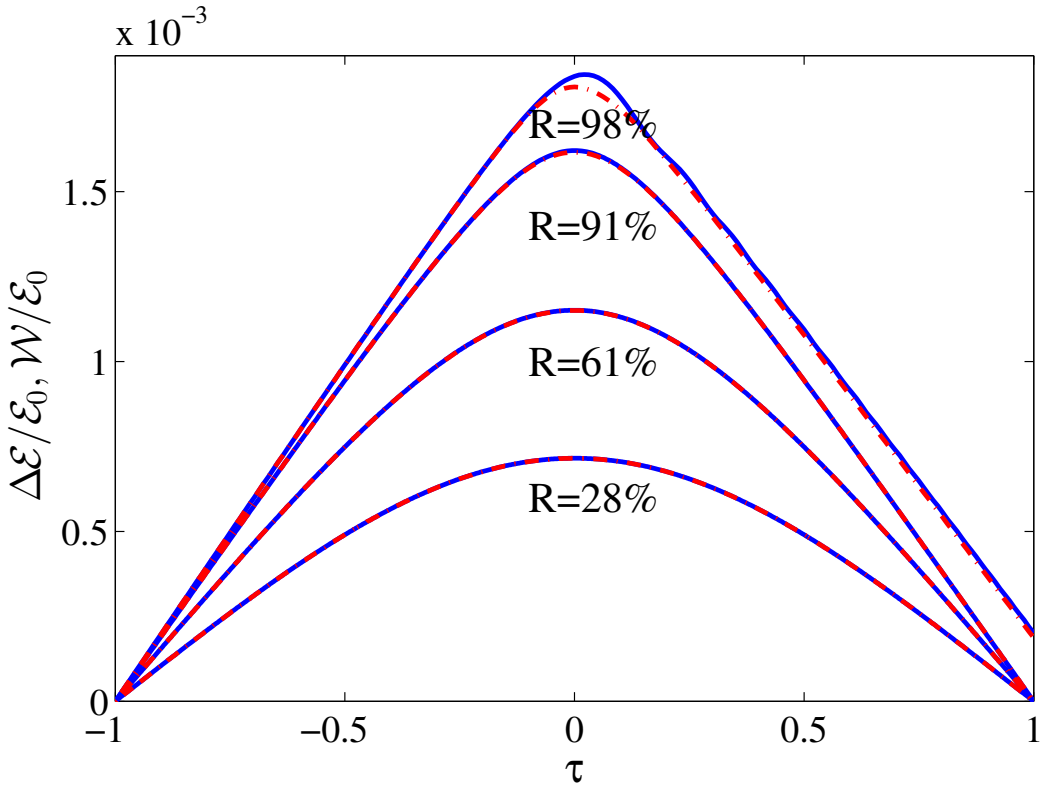

Figure 4.1: Comparison of the work done by the external source driving the mirror and the change in energy of the light field. This figure shows that the ratio of the work done ($\mathcal{W}$) to the initial light energy ($\mathcal{E}_0$) to overcome the radiation pressure on the mirror closely resembles the fractional energy change ($\Delta\mathcal{E}/\mathcal{E}_0$) of the light field inside the cavity. The work and energy are plotted as a function of some re-scaled time co-ordinate (τ). However, the radiation pressure formula used here is not quite correct. As can be seen in the next figure, the formula corresponding to that one is much better. The red, solid curve is generated using equation (3.4). The blue, dotted curve is generated using equation (4.12). The central mirror speed is 5000 ms^{-1}, mirror displacement $1 \times 10^{-3} L$ and light initially localized on the right side of the cavity.

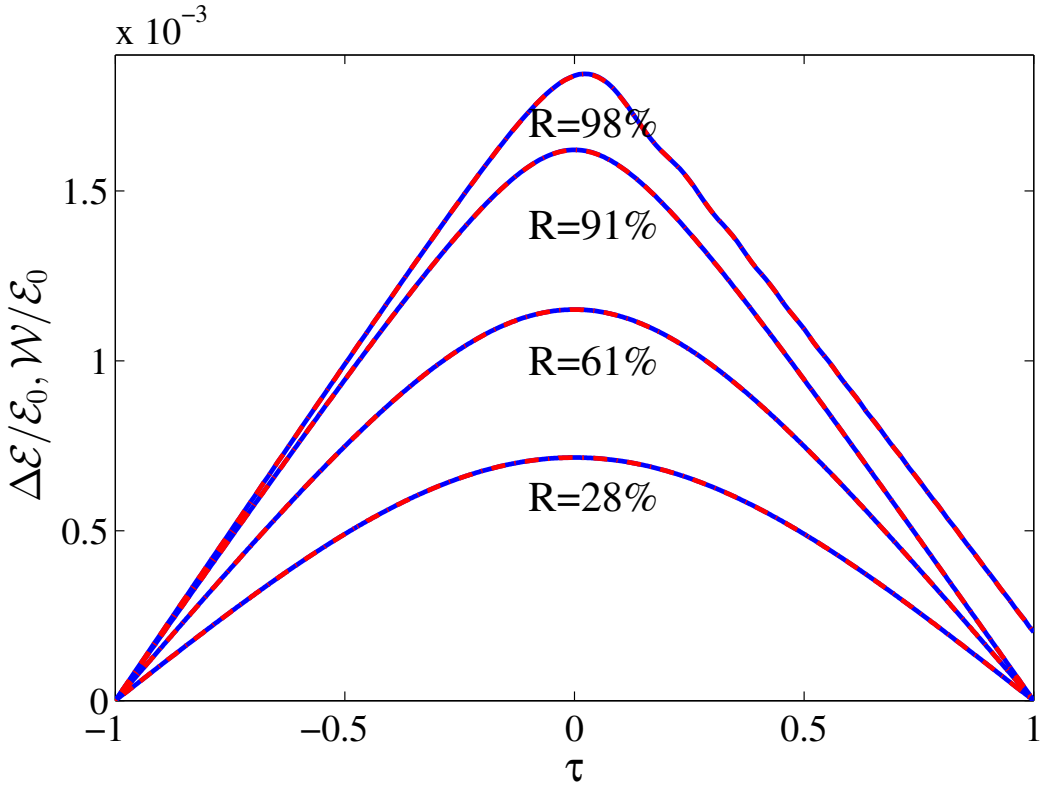

Figure 4.2: Comparison of the work done by the external source driving the mirror and the change in energy of the light field. This agreement between the fractional change in energy ($\Delta\mathcal{E}/\mathcal{E}_0$) and the ratio of work done to the initial energy of the light field ($\mathcal{W}/\mathcal{E}_0$) is a strong indicator that the numerical simulation codes and the formalism used is self consistent. The red, solid line is simulated by equation (3.4), while the dotted, blue curve is simulated using equation (4.16).

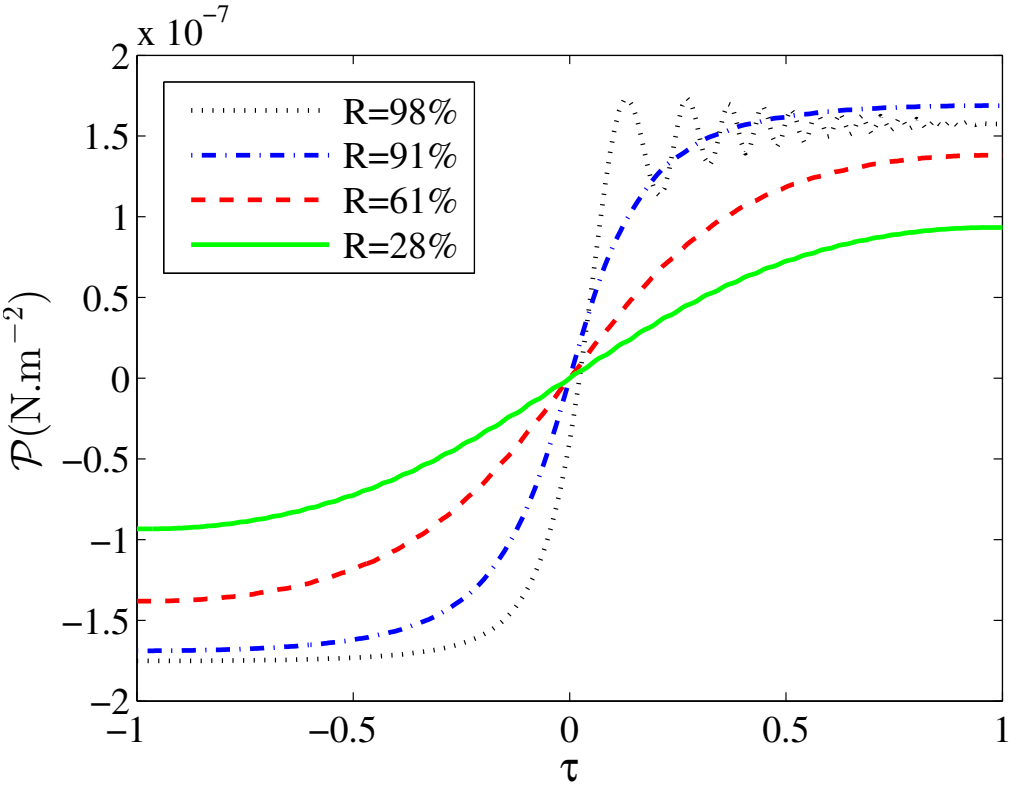

Figure 4.3: Radiation pressure as a function of time for different mirror reflectivities. Here, we plot the radiation pressure of light on the central mirror inside the cavity as a function of time using equation (4.16). We keep the mirror velocity fixed and vary the mirror reflectivity. We find that the initial radiation pressure magnitude increases as the mirror reflectivity is increased. The greater the reflection of light at the central mirror, the greater the change in momentum imparted on the mirror and hence this leads to a higher radiation pressure. One can see that for a reflectivity of 98% the radiation pressure exhibits some oscillatory behaviour. This is due to the non-adiabatic nature of the sweep through the avoided crossing. As the reflectivity approaches unity, the gap at the avoided crossing becomes smaller. A non-adiabatic sweep then causes the mode populations to be swapped back and forth leading to a oscillatory radiation pressure.

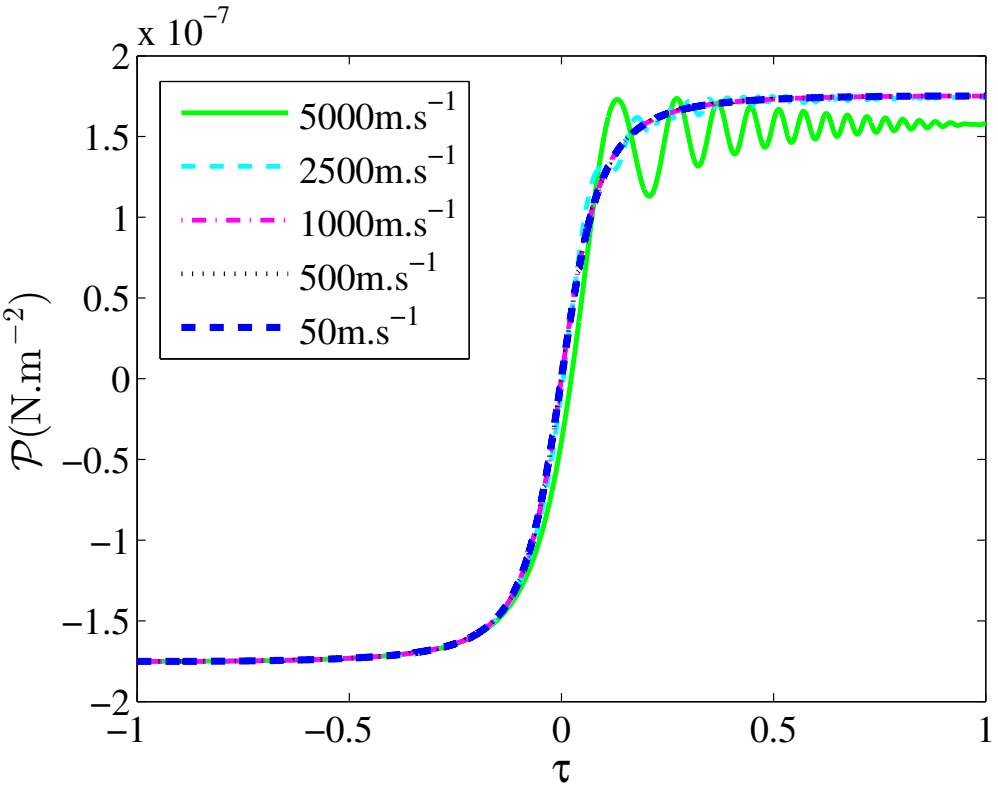

Figure 4.4: Radiation pressure as a function of time for different mirror velocities. In this plot, the radiation pressure is simulated using equation (4.16), while holding the reflectivity constant at 98% and changing the mirror speed from non-adiabatic to adiabatic velocities. In Fig. 4.3, we saw that for a reflectivity of 98% and mirror speed 5000 ms^{-1}, the radiation force showed some oscillatory behaviour. We postulated that it was due to the non-adiabatic nature of the mirror motion causing transitions amongst the two states. Indeed, in this plot we find that as the mirror speed goes down, so does the swapping of population amongst the two modes and consequently the oscillatory behaviour of the radiation pressure. This figure corresponds to the light dynamics shown in Figs. 4.6 and 4.5.

Again we ignore the last term to find

$$\vec{H}_m(x,t) = -\hat{z}\epsilon_0 c \cdot i \left\{ a_1(t)\exp[-i\theta_1(t)]G_1(x,\Delta L) + a_2(t)\exp[-i\theta_2(t)]G_2(x,\Delta L) \right\}. \quad (4.15)$$

Therefore, the radiation pressure due to a dichromatic wave of frequencies $\omega_{1/2}$ terms is given by

$$\mathcal{P} = \frac{\epsilon_0}{2}\left\{ \left| a_2(t)\exp[-i\theta_2(t)]A_2(t)\cos(k_2 L_1) + a_1(t)\exp[-i\theta_1(t)]A_1\cos(k_1 L_1)\right|^2 - \left| a_2(t)\exp[-i\theta_2(t)]B_2\cos(k_2 L_2) + a_1(t)\exp[-i\theta_1(t)]B_1\cos(k_1 L_2)\right|^2 \right\}. \quad (4.16)$$

Previously, when we added the radiation pressures due to the individual frequencies, we were missing the cross terms that are included in Eqn. (4.16). Taking into account the cross terms due to the dichromatic nature of the electromagnetic waves inside the cavity, as can be seen in Fig. 4.2, we have perfect agreement in the work and energy curves. This is a self-consistency check that strongly validates the numerical codes.

4.4 Adiabatic Condition of Double Cavity Dynamics with a Driven Mirror: Maxwell versus Schrödinger

In this section we investigate adiabaticity of the Maxwell wave equation describing light in the double cavity. The most basic aspect of adiabaticity for the Schrödinger wave equation of a time dependent system is that if the ini-

tial state is an instantaneous eigenstate the system continues to remain in the same instantaneous eigenstate of the Hamiltonian with probability equal to one. Thus, as we change the system more and more slowly, the population transfer from the initially occupied instantaneous eigenstate to others will approach zero as the sum of the squares of the amplitudes is constrained to equal one. Analogous to changing the potential function in the Schrödinger equation, here we consider changing the mirror position or dielectric function of the double cavity from some initial to final position. In this section, we find that decreasing mirror speed is a sufficient criterion for achieving adiabaticity in the Maxwell wave equation, but that even in this slow mirror speed limit we do not achieve energy conservation. This requires a bit of elaboration to fully appreciate. Though the Maxwell and Schrödinger wave equations describe the time evolution of wave functions, physically, the former represent classical field amplitudes while the latter represent probability amplitudes. While the sum of the squares of the field amplitudes is conserved under the Schrödinger wave equation, it is not under the Maxwell wave equation. Since for classical electromagnetic fields the sum of the squares of the field amplitudes is the energy, this implies that under the Maxwell wave equation energy is in general not conserved, whereas under the Schrödinger-like first order approximation energy is artificially conserved. Of course, this is expected since the light field interacts with the mirror via radiation pressure and as a result energy can be transferred back and forth between the field and the mirror.

If the electric field is an instantaneous eigenstate of the double cavity corresponding to the starting position of the central mirror, moving the mirror more and more slowly will ensure that the electric field continues to remain in the same instantaneous eigenstate of the cavity. Under the Schrödinger-like

equation, if the initially occupied mode has amplitude 1, the final amplitude of the eigenstate level will approach 1 in the adiabatic limit. However, under the Maxwell wave equation, starting from the initial mode amplitude 1, no matter how slowly we move the mirror, the final amplitude in general will not be 1. Due to radiation pressure, some energy is always pumped into/ out of the system regardless of how slowly the central mirror is being moved. This feature, that the field can remain in the same eigenstate and yet evolve to a different amplitude is a basic and interesting difference between adiabaticity in the Schrödinger and Maxwell wave equations.

Let us consider the question of adiabaticity for a double cavity more quantitatively. A central mirror moves at a constant velocity from position $x = -L_0$ to L_0 over time $t = -T_0$ to T_0. The displacement of the mirror from the center is given by $\Delta L/2$. Then, the mirror displacement function can be written

$$\frac{\Delta L(t)}{2} = \frac{L_0}{T_0} t. \tag{4.17}$$

The mirror speed is given by $v = L_0/T_0$. We fix L_0 and change the parameter T_0. To have a clearer understanding of the role of decreasing mirror speed in adiabaticity of the Maxwell wave equation, consider the following change of variable

$$\tau = \frac{t}{T_0} = \lambda t, \ -1 \leq \tau \leq 1 \tag{4.18}$$

i.e. $\lambda = \frac{1}{T_0}$. Eqn. (3.4), i.e. the adiabatic basis equations, can now be rewritten as

$$\frac{dc_m}{d\tau} = -\frac{d\omega_m}{d\tau}\frac{c_m}{2\omega_m} - \frac{i\lambda}{2\omega_m}\frac{d^2c_m}{d\tau^2} - \sum_n \left\{ \left[\frac{i\lambda}{\omega_m}\frac{dc_n}{d\tau} + \frac{\omega_n}{\omega_m}c_n \right] \bar{P}_{mn} + \frac{i\lambda}{2\omega_m} c_n \bar{Q}_{mn} \right\} \tag{4.19}$$

where

$$\bar{\theta}_{mn} = \frac{1}{\lambda}\int_{\tau_0}^{\tau} [\omega_m(\tau') - \omega_n(\tau')]\, d\tau'$$

$$\bar{P}_{mn} = \int_{-L/2}^{L/2} \frac{\epsilon(\tau,x)}{\epsilon_0} U_m(\tau,x)\partial_\tau U_n(\tau,x) dx e^{i\bar{\theta}_{mn}}$$

$$\bar{Q}_{mn} = \int_{-L/2}^{L/2} \frac{\epsilon(\tau,x)}{\epsilon_0} U_m(\tau,x)\partial_\tau^2 U_n(\tau,x) dx e^{i\bar{\theta}_{mn}}.$$

Note that in Eqn. (4.19), which the adiabatic criterion analysis is based on, we do not assume that the dynamics takes place close to an avoided crossing or make a two level approximation. As a specific example of the adiabaticity, however, we numerically simulate the case of a mirror being swept close to the avoided crossing and apply a two level approximation. The deductions made in this section about adiabaticity in the double cavity hold even for a mirror moving through multiple avoided crossings.

Let us assume that the mode c_i (in the adiabatic basis) is initially populated and all other modes are empty. When $T_0 \to \infty$, we have that $\lambda \to 0$ and the terms P_{nm} for $n \neq m$ approach zero due to the presence of the phase term which oscillates more and more wildly in that limit. The term P_{ii} lacks a similar phase term and so remains finite. The term, $\frac{d\omega_i}{d\tau}\frac{c_i}{2\omega_i}$ in Eqn. (4.19) is related to the slope of the frequency function and is non-zero everywhere except exactly at the avoided crossing. Since the first and third terms on the right hand side of Eqn. (4.19) do not approach zero in the adiabatic or equivalently, the slow mirror limit, $\frac{dc_i}{d\tau}$ does not approach zero. Meanwhile, the rate of change of all initially unpopulated states do approach zero in the adiabatic limit because the first term of Eqn. (4.19) depends on the mode population. This shows that all the initially vacant modes continue to remain vacant in the slow mirror limit,

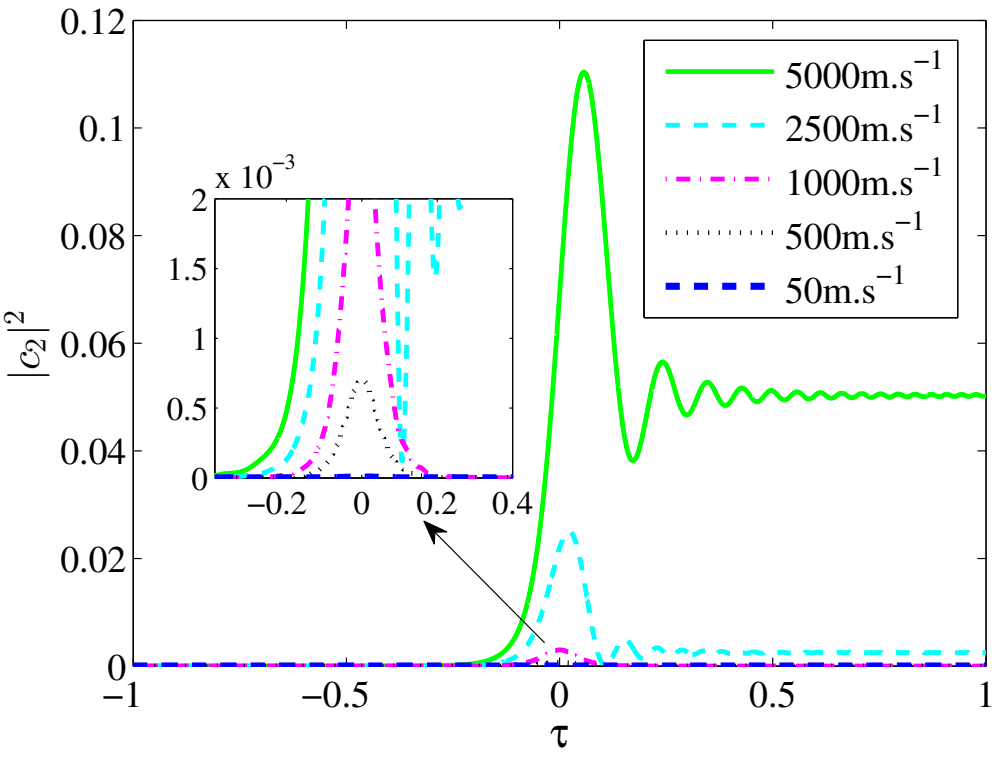

Figure 4.5: Approach to adiabaticity under the Maxwell wave equation. The vertical axis of this figure shows $|c_2|^2$, i.e. mode 2 amplitude in the adiabatic basis, as a function of a time co-ordinate normalized for the sake of comparison. The initial condition for the dynamics is $c_1 = 1$ and $c_2 = 0$. We can see that as the mirror speed goes down, the unpopulated mode amplitude approaches the zero. Parameters: Mirror reflectivity, 98% and mirror displacement, $1 \times 10^{-3} L$, where L is the total length of the double cavity. We have simulated the light field dynamics according to Eqn. (4.19) in the two level approximation near an avoided crossing.

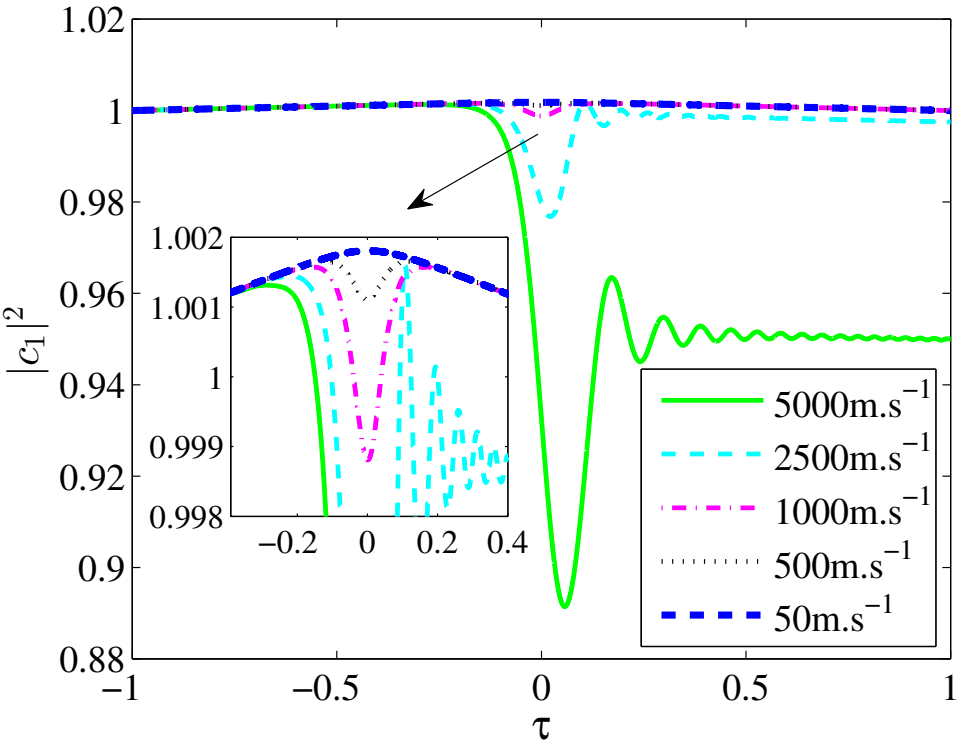

Figure 4.6: Demonstration that field amplitudes are not conserved under adiabatic evolution of Maxwell fields. In this figure, we plot the quantity $|c_1|^2$, corresponding to the setup in Fig. 4.5. We can see that as the mirror speed is decreased the amplitude function of the initially populated mode does not approach unity. This is because, whilst the slowly moving mirror limit is sufficient to achieve adiabaticity, the amplitude sum still tends to a finite limit.

as can be seen in Fig. 4.5. However, the mode that was initially populated will change in magnitude. Hence, no matter how slowly the mirror is moved, there will always be some minimum energy transferred into or out of the populated mode from or to the mirror. This can be seen in Fig. 4.6. Furthermore, in Fig. 4.7, we look at the energy of the system. It was shown in Sec. 3.3 that the difference of the amplitude sum from unity gives the change in energy as a function of time divided by the energy, i.e. $|c_1|^2 + |c_2|^2 - 1 = \Delta\mathcal{E}_{\mathrm{ASOE}}/\mathcal{E}_0$. One can see that no matter how slowly the mirror is being moved, the difference in amplitude sum from the initial value reaches some non-zero limit.

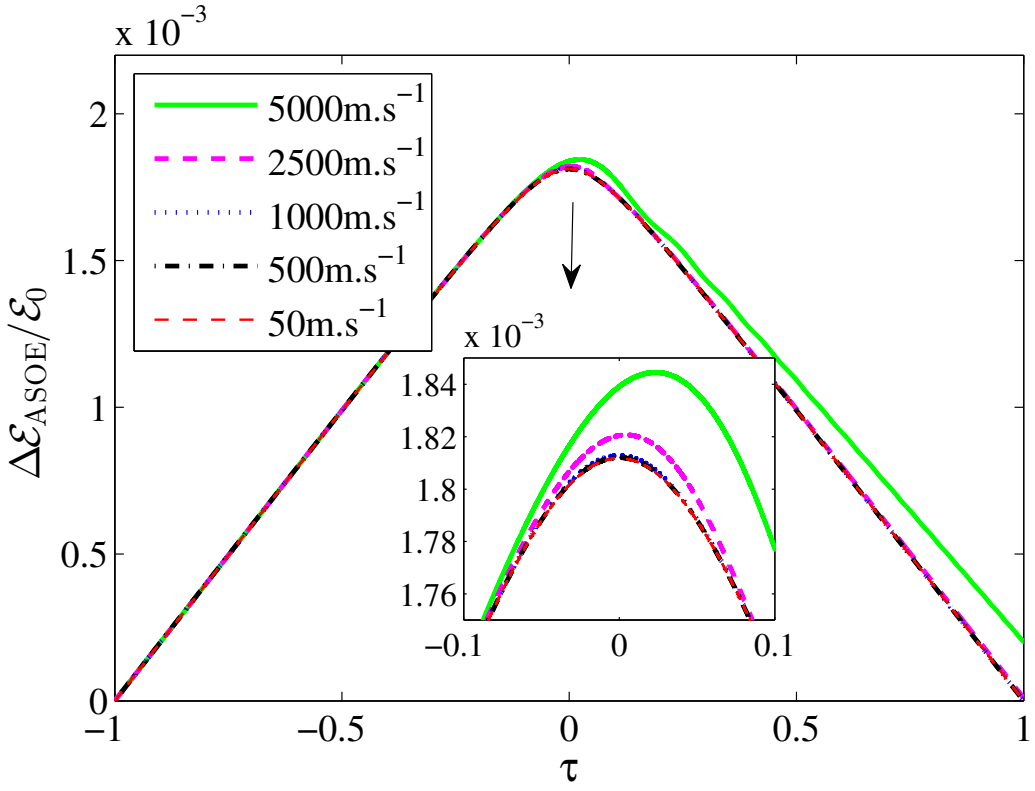

Figure 4.7: Sum of Maxwell field amplitude squared terms tend to a finite non-zero limit in the adiabatic regime. Here, we plot the time evolution of the fractional change ($\Delta\mathcal{E}/\mathcal{E}_0$) in the energy of the light field. This plot shows that as we displace the mirror slower and slower, the energy pumped into the system does not vanish. Furthermore, we see that adiabaticity does not imply conservation of the light field energy.

Chapter 5

Quantum Dynamical Formalism for Light in Double Cavity with a Parametric Mirror

5.1 Introduction

This chapter marks the boundary where we transition from the study of classical dynamics of light in a double cavity to the quantum dynamics. Both the classical and quantum dynamics are non-trivial due to the time-dependence of the boundary condition manifested as the moving central mirror. In particular, we are interested in the dynamical Casimir effect (DCE) in the double cavity. The static Casimir force was discovered by Hendrik B. G. Casimir as being due to the presence of vacuum modes of the electromagnetic field in reference [18]. In the last chapter we saw energy change in the light field due to the interaction of the moving mirror with the light field via the radiation pressure. The DCE is the creation of photons due to the movement of the

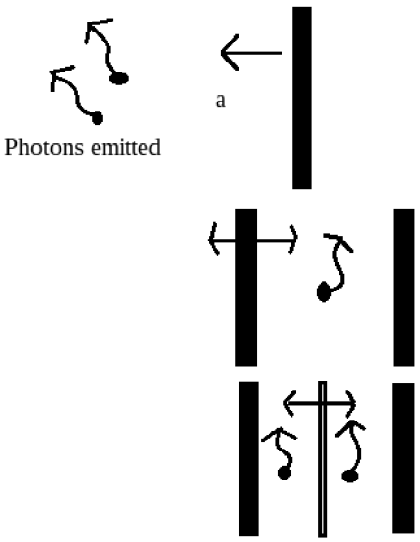

Figure 5.1: Accelerating the cavity mirror converts vacuum photons into real photons inside the cavity.

mirror and the presence of the vacuum light field. One of the earliest works on the excitation of the vacuum modes due to dynamical effects was done by G. T. Moore in reference [5]. G. T. Moore showed that the number of photons created due to the time dependence of boundary conditions is a convergent term and rather small in the non-relativistic regime. We begin by studying the quantum mechanical effective Hamiltonian for the double cavity system in Sec. 5.2. Inspecting the effective Hamiltonian, we see that photon creation in a non-stationary double cavity is due to a combination of squeezing and an acceleration effect, with implicit and explicit dependence on the mirror velocity $\dot{q}$. Furthermore, the acceleration term contains both light scattering terms and parametric oscillator terms. In Sec. 5.3, we write down the equations of motion of the creation/annihilation operators to understand the resonance condition when the frequency of the sinusoidally driven central mirror is tuned to generate the most photons. For the initial vacuum state, the dynamics is

dominated by the parametric oscillator term for short times [49] and driving the mirror at approximately twice that of a cavity mode frequency leads to parametric amplification of the corresponding light mode energy [59]. An analogous example would be the optical parametric oscillator which involves an intense laser beam shining on some non-linear crystal (β-barium borate for example) which causes the electric dipoles in the atoms of the crystal to vibrate with the pump frequency (ω_p) and emit electromagnetic radiation. Due to energy conservation, when the pump frequency satisfies $\omega_p = 2\omega_0$, where ω_0 is the frequency of the output radiation, a pair of photons of the corresponding frequency can be radiated [60] in a process known as degenerate parametric amplification (the photons are emitted in pairs due to invariance under charge conjugation). In Sec. 5.4, we review the formalism already present in the literature [24, 22, 28, 2] which is extremely convenient for numerically simulating the quantum dynamics propagator. This is the approach we take to simulate the quantum dynamics in this thesis. We numerically generate the propagator of the dynamics for a certain cutoff frequency determined according to our accuracy needs. Then, depending on the initial state of the light field (vacuum, general coherent states etc.), the propagator determines the photon numbers corresponding to the evolved light state at later times.

5.2 Effective Quantum Mechanical Hamiltonian of Light in The Double Cavity

In this section we review the effective Hamiltonian formulation for a cavity with a parametric driven mirror due entirely to C. K. Law [49]. Consider a

double cavity system consisting of an optical cavity with perfect end mirrors and a partially transmissive central mirror that is moved parametrically. The Lagrangian density of the electromagnetic (light) field inside the system is given by [61]

$$\mathcal{L}_F = \frac{1}{2}\left[\epsilon(x,q(t))(\partial_t A)^2 - (\partial_x A)^2/\mu_0\right], \tag{5.1}$$

and the corresponding conjugate momentum is given by

$$\Pi(x,t) = \epsilon(x,q(t))\partial_t A(x,t), \tag{5.2}$$

where $q(t)$ denotes the position function of the central mirror. Furthermore, we can write down the quantized vector potential function and its conjugate momentum in the instantaneous eigenstate basis of the system denoted, $\{\phi_k(x,q)\}$, given by

$$\begin{aligned} \hat{A}(x,t) &= \frac{1}{\sqrt{\epsilon_0}}\sum_k \hat{Q}_k(t)\phi_k(x,q(t)) \\ \hat{\Pi}(x,t) &= \frac{\epsilon(x,q(t))}{\sqrt{\epsilon_0}}\sum_k \hat{P}_k(t)\phi_k(x,q(t)). \end{aligned} \tag{5.3}$$

Since, $\{\phi_k(x,q)\}$ satisfies the Sturm-Liouville equation given by

$$\frac{\partial^2\phi_k(x,q(t))}{\partial x^2} + \mu_0\epsilon(x,q(t))\omega_k^2(q(t))\phi_k(x,q(t)) = 0, \tag{5.4}$$

it forms an orthonormal basis satisfying

$$\int_0^l \frac{\epsilon(x,q(t))}{\epsilon_0}\phi_j(x,q(t))\phi_k(x,q(t))\mathrm{dx} = \delta_{jk}. \tag{5.5}$$

The dynamics of light corresponding to the Lagrangian above is given by

the Euler-Lagrange equation, $\partial_x \left\{ \frac{\partial \mathcal{L}_F}{\partial(\partial_x A)} \right\} + \partial_t \left\{ \frac{\partial \mathcal{L}_F}{\partial(\partial_t A)} \right\} - \frac{\partial \mathcal{L}_F}{\partial A} = 0$, which implies that

$$\partial_x^2 A(x,t)/\mu_0 - \partial_t\{\epsilon(x,q(t))\partial_t A(x,t)\} = 0. \tag{5.6}$$

For a stationary double cavity, the co-ordinates $\{\hat{Q}_k, \hat{P}_k\}$ are canonical variables of the quantized simple harmonic oscillator corresponding to the eigenmode, $\omega_k(q)$. Since we do not treat the mirror position and momentum as dynamical variables, we cannot proceed from the Lagrangian to the Hamiltonian via Legendre transformations. The Hamiltonian of a single and double cavity is quantized in references [16, 17], respectively, by treating both the light field and the central mirror in terms of dynamical variables i.e. the motion of the mirror is not a prescribed function of time but evolves under the combination of radiation pressure and a conservative potential. In [49], the formalism for the effective Hamiltonian is derived by examining the dynamics of light in terms of the canonical variables $\{\hat{Q}_k, \hat{P}_k\}$ or $\{\hat{a}_k, \hat{a}_k^\dagger\}$. One feature that we will see later is that if we wish to change from one set of canonical variables to another, expecting Hamilton's equations to hold, we cannot just simply substitute the old variables in terms of the new. [One cannot derive a Hamiltonian via a Legendre transformation applied to the Lagrangian and Hamilton's equations are not preserved under canonical transformations.] To write down an effective Hamiltonian in terms of any canonical variables, we would have to examine the dynamics in terms of the new variables and then back-engineer the corresponding Hamiltonian. Hence, this is not a true Hamiltonian but rather an effective one that satisfies Hamilton's equations for some variables of interest [49]. In our study of light in the double cavity, due to the parametric nature of the mirror motion, it is implicit that a true Hamiltonian

cannot be written down. If one wished to study the dynamics of this system via the Schrödinger equation, one would have to rely on an effective Hamiltonian. From Eqns. (5.4) and (5.5) the amplitudes $\{\hat{Q}_k, \hat{P}_k\}$ can be projected out and found to be

$$\begin{aligned} \hat{Q}_k(t) &= \frac{1}{\sqrt{\epsilon_0}} \int_0^l \epsilon(x, q(t)) \hat{A}(x,t) \phi_k(x, q(t)) \mathrm{dx}, \\ \hat{P}_k(t) &= \frac{1}{\sqrt{\epsilon_0}} \int_0^l \hat{\Pi}(x,t) \phi_k(x, q(t)) \mathrm{dx}. \end{aligned} \tag{5.7}$$

We are interested in the scenario where the boundary conditions in the double cavity are changing via a moving central mirror. To find the dynamics of the electromagnetic field, we take the time derivatives of $\{\hat{Q}_k, \hat{P}_k\}$. We find that,

$$\begin{aligned} \frac{d\hat{Q}_k}{dt} &= \frac{1}{\sqrt{\epsilon_0}} \int_0^l \Bigg[\frac{\partial \epsilon(x, q(t))}{\partial t} \hat{A}(x,t) \phi_k(x, q(t)) + \\ &\quad \epsilon(x, q(t)) \frac{\partial \hat{A}(x,t)}{\partial t} \phi_k(x, q(t)) + \epsilon(x, q(t)) \hat{A}(x,t) \frac{\partial \phi_k(x, q(t))}{\partial t} \Bigg] \mathrm{dx} \\ &= \frac{1}{\sqrt{\epsilon_0}} \int_0^l \hat{\Pi}(x,t) \phi_k(x, q(t)) \mathrm{dx} + \frac{1}{\sqrt{\epsilon_0}} \int_0^l \Bigg[\frac{\partial \epsilon(x, q(t))}{\partial t} \hat{A}(x,t) \phi_k(x, q(t)) + \\ &\quad \epsilon(x, q(t)) \hat{A}(x, q(t)) \frac{\partial \phi_k(x, q(t))}{\partial t} \Bigg] \mathrm{dx} \\ &= \hat{P}_k(t) - \sum_j G_{kj}(q(t)) \hat{Q}_j(t), \end{aligned} \tag{5.8}$$

where,

$$G_{kj}(q(t)) = \dot{q} \bar{G}_{kj}, \tag{5.9}$$

where, $\bar{G}_{kj}(q) = \int_0^l \mathrm{dx} \frac{\epsilon(x,q)}{\epsilon_0} \phi_k(x,q) \frac{\partial \phi_j(x,q)}{\partial q}$. This separates the purely dynamical effect of the mirror velocity in G_{kj} from the stationary properties of the cavity denoted by $\bar{G}_{kj}$. To go from line 2 to line 3 of Eqn. (5.8) we use the orthogonality of the ϕ_k basis given in Eqn. (5.5) to reduce the first term to

$\hat{P}_k(t)$. The second and third terms are reduced by observing that

$$\begin{aligned}
&\int_0^l \frac{1}{\sqrt{\epsilon_0}}\left[\frac{\partial\epsilon(x,q(t))}{\partial t}\hat{A}(x,t)\phi_k(x,q(t))+\right. \\
&\left.\epsilon(x,q(t))\hat{A}(x,t)\frac{\partial\phi_k(x,q(t))}{\partial t}\right]\mathrm{dx} \\
= &\sum_j \hat{Q}_j(t)\int_0^l\left[\frac{\partial}{\partial t}\frac{\epsilon(x,q(t))}{\epsilon_0}\phi_j(x,q(t))\phi_k(x,q(t))+\right. \\
&\left.\frac{\epsilon(x,q(t))}{\epsilon_0}\phi_j(x,q(t))\frac{\partial\phi_k(x,q(t))}{\partial t}\right]\mathrm{dx} \\
= &-\sum_j \hat{Q}_j(t)\int_0^l \frac{\epsilon(x,q(t))}{\epsilon_0}\phi_k(x,q(t))\frac{\partial\phi_j(x,q(t))}{\partial t}\mathrm{dx} \\
= &-\sum_j G_{kj}(q(t))\hat{Q}_j(t),
\end{aligned} \tag{5.10}$$

where the first equality follows from substituting to expansion in 5.4 for $\hat{A}(x,t)$ and the second equation from differentiating the normalization condition

$$\begin{aligned}
0 = &\frac{\partial}{\partial t}\int_0^l \frac{\epsilon(x,q(t))}{\epsilon_0}\phi_k(x,q(t))\phi_j(x,q(t))\mathrm{dx} \\
= &\int_0^l\left[\frac{\partial}{\partial t}\frac{\epsilon(x,q(t))}{\epsilon_0}\phi_k(x,q(t))\phi_j(x,q(t))+\frac{\epsilon(x,q(t))}{\epsilon_0}\frac{\partial\phi_k(x,q(t))}{\partial t}\phi_j(x,q(t))+\right. \\
&\left.\frac{\epsilon(x,q(t))}{\epsilon_0}\phi_k(x,q(t))\frac{\partial\phi_j(x,q(t))}{\partial t}\right]\mathrm{dx}.
\end{aligned} \tag{5.11}$$

The equation of motion for $\hat{P}_k$ is obtained similarly. Differentiating Eqn. (5.8) we find that

$$\frac{d\hat{P}_k}{dt} = \frac{1}{\sqrt{\epsilon_0}}\int_0^l\left[\frac{\partial\hat{\Pi}(x,t)}{\partial t}\phi_k(x,q(t))+\hat{\Pi}(x,t)\frac{\partial\phi_k(x,q(t)}{\partial t}\right]. \tag{5.12}$$

The first term is treated by differentiating Eqn. (5.2) and making use of the

Euler-Lagrange equation 5.6 to give

$$\begin{aligned}\frac{1}{\sqrt{\epsilon_0}}\int_0^l \partial_t\hat{\Pi}(x,t)\phi_k(x,q(t))\mathrm{dx} &= \frac{1}{\sqrt{\epsilon_0}\mu_0}\int_0^l \partial_x^2\hat{A}(x,t)\phi_k(x,q(t))\mathrm{dx} \\ &= \frac{1}{\epsilon_0\mu_0}\sum_j \hat{Q}_j(t)\int_0^l \partial_x^2\phi_j(x,q(t))\phi_k(x,q(t))\mathrm{dx} \\ &= -\omega_k^2(q(t))\hat{Q}_k(t),\end{aligned} \tag{5.13}$$

where to obtain the final equality, the Helmholtz equation 5.4 has been used. The second term in Eqn. (5.12) is treated as follows

$$\begin{aligned}&\frac{1}{\sqrt{\epsilon_0}}\int_0^l \hat{\Pi}(x,t)\partial_t\phi_k(x,q(t))\mathrm{dx} \\ =\ &\sum_j \hat{P}_j(t)\int_0^l \frac{\epsilon(x,q(t))}{\epsilon_0}\phi_j(x,q(t))\partial_t\phi_k(x,q(t))\mathrm{dx} \\ =\ &\sum_j \hat{P}_j(t)G_{jk}(q(t)),\end{aligned} \tag{5.14}$$

so that Eqn. (5.12) becomes

$$\frac{d\hat{P}_k}{dt} = -\omega_k^2(q(t))\hat{Q}_k(t) + \sum_j \hat{P}_j(t)G_{jk}(q(t)). \tag{5.15}$$

The effective Hamiltonian corresponding to the variables $\{\hat{Q}_k, \hat{P}_k\}$ can be written as

$$\hat{\mathcal{H}}_{\text{eff}} = \frac{1}{2}\sum_k \left[\hat{P}_k^2 + \omega_k^2(q(t))\hat{Q}_k^2 - G_{kk}(q(t))\left\{\hat{P}_k\hat{Q}_k + \hat{Q}_k\hat{P}_k\right\}\right] - \sum_{j\neq k}\hat{P}_k G_{kj}\hat{Q}_j \tag{5.16}$$

because it satisfies Hamilton's equations Eqns. (5.8) and (5.15) for the variables $\{Q_k, P_k\}$. If we want an effective Hamiltonian in terms of the variables $\{\hat{a}_k^\dagger, \hat{a}_k\}$, we would have to look at the equations of motion for those variables

and back-engineer the corresponding Hamiltonian. Note, we cannot simply transform from $\{Q_k, P_k\}$ to $\{\hat{a}_k^\dagger, \hat{a}_k\}$ as the resulting Hamiltonian would lead to erroneous equations of motion. The terms in Eqn. (5.16) resembling the harmonic oscillator with time dependent frequencies (i.e. the terms without the coupling terms G_{mn}) are responsible for the squeezing effect in the DCE [29]. Meanwhile, the remaining terms involving the coupling coefficient terms are responsible for the so-called acceleration effect in the DCE [29] since G_{mn} explicitly contains the motional $\dot{q}$ term according to the definition in Eqn. (5.9). Note that despite the naming of this part of the Hamiltonian as the acceleration effect, it still contributes to the DCE even for a mirror moving at a constant velocity. Even though the acceleration effect in the effective Hamiltonian appears as a higher order relativistic correction, the squeezing and the acceleration parts contribute to the DCE on an equal footing according to the authors in reference [29]. The acceleration part of the effective Hamiltonian leads to both photon hopping between modes and parametric amplification when there is a mode pair whose frequencies add up to the driving frequency. In references [62, 63], the time evolution of states in the time-dependent harmonic oscillator potential given by the Hamiltonian

$$\hat{\mathcal{H}}(Q_k, P_k, t) = \frac{\hat{P}_k^2}{2} + \frac{\omega_k^2(t)}{2}\hat{Q}_k^2. \tag{5.17}$$

The squeezing part of the Hamiltonian is comprised of these time dependent harmonic oscillator Hamiltonians corresponding to each cavity frequency function. More specifically, the ground state corresponding to the initial frequency

of the potential ($\omega_k(t_0) = \omega_k^0$), given by

$$\psi_0(q', t = 0) = \left(\frac{\omega_k^0}{\pi}\right)^{1/4} \exp\left\{-\frac{\omega_k^0}{2} q'^2\right\} \tag{5.18}$$

will evolve as

$$\psi_0(q', t) = \left(\frac{\omega_k^0}{\pi}\right)^{1/4} \frac{1}{\sqrt{u(t)}} \exp\left\{\frac{i}{2}\frac{\dot{u}(t)}{u(t)} q'^2\right\}, \tag{5.19}$$

where,

$$\ddot{u} + \omega_k^2(t) u = 0 \tag{5.20}$$

with initial conditions $u(0) = 1$, $\dot{u}(0) = i\omega_k^0$. However, the evolved state does not correspond to the instantaneous ground state of the potential since the width is determined by the time dependence of the instantaneous frequency and in general $\frac{\dot{u}}{u} \neq \omega(t)$. Furthermore, this squeezed state has some non-zero population in the excited states of the Fock basis corresponding to the instantaneous frequency. Hence, due to the presence of the time dependent boundary condition, vacuum photons are excited to real photons. Though the time evolved states are not minimum uncertainty states (MUS) with respect to the Heisenberg uncertainty relation ($\sigma_x \sigma_p \geq \hbar/4$), they are MUS corresponding to the weaker Schrödinger-Robertson uncertainty relation ($\sigma_x \sigma_p - \sigma_{px}^2 \geq \hbar/4$) as shown in references [23, 63]. These states are known as correlated squeezed states [64]. Parametric amplification processes leading to pair production in such squeezed states were discussed in reference [65]. Since the photons are created in pairs, the must be correlated and were crucial in the observation of the DCE [35] for the quantum signature they provide.

5.3 Resonance condition between driving frequency and Photon Creation

The following treatment loosely follows C. K. Law's observation on the resonance condition in reference [49]. In this section, we are interested in the resonance between photon creation and the driving frequency of the central mirror. To gain an understanding of the connection between the two, we analyze the time dependence of the creation operators in the Heisenberg picture and the role of the driving frequency of the sinusoidal mirror motion. The effective Hamiltonian for light in a double cavity with a parametric central mirror in terms of the creation/annihilation operators is given by [49]

$$\hat{\tilde{\mathcal{H}}} = \sum_k \omega_k(t)\hat{a}_k^\dagger\hat{a}_k - \frac{i}{2}\sum_k \left\{G_{kk}(t) - \frac{\dot{\omega}_k}{2\omega_k}\right\}\left[\left(\hat{a}_k^\dagger\right)^2 - \hat{a}_k^2\right] - \frac{i}{2}\sum_{\substack{j,k \\ j\neq k}}\sqrt{\frac{\omega_k(t)}{\omega_j(t)}}G_{kj}(t)\left(\hat{a}_k^\dagger\hat{a}_j^\dagger + \hat{a}_k^\dagger\hat{a}_j - \hat{a}_j\hat{a}_k - \hat{a}_j^\dagger\hat{a}_k\right), \quad (5.21)$$

where

$$G_{kj}(t) = \int_0^l \mathrm{dx}\frac{\epsilon(x,q(t))}{\epsilon_0}\phi_k(x,q(t))\frac{\partial\phi_j(x,q(t))}{\partial t} \quad (5.22)$$

and is equivalent to Eqn. (5.9). Note that the time dependence of the boundary condition leads to both zero photon processes (scattering) via terms $\hat{a}_k^\dagger\hat{a}_j - \hat{a}_j^\dagger\hat{a}_k$, as well as two photon processes due to terms $\hat{a}_k^\dagger\hat{a}_j^\dagger - \hat{a}_j\hat{a}_k$. For a sinusoidally driven mirror, the latter term is responsible for second harmonic generation (for $k = j$) and parametric down conversion (for $k \neq j$). The harmonic oscillator Hamiltonian with time dependent frequencies in Eqn. (5.21) is defined as the squeezing part while the other terms involving G_{kj} and $\dot{\omega}_k/\omega_k$ is defined

as the acceleration part in the DCE. The acceleration part of the effective Hamiltonian does contain terms that correspond to the squeeze operator (Appendix B.1) and ironically enough, without the demonstration in Sec. 5.2 it is not as obvious that the "squeezing part" leads to a squeezing of the vacuum state. The Heisenberg equations of motion for the creation operators, continued from Hamilton's equations, are given by

$$\dot{\hat{a}}_n = -i\frac{\partial\hat{\tilde{\mathcal{H}}}}{\partial\hat{a}_n^\dagger} \text{ and } \dot{\hat{a}}_n^\dagger = i\frac{\partial\hat{\tilde{\mathcal{H}}}}{\partial\hat{a}_n}. \tag{5.23}$$

Defining

$$\begin{aligned} e_{kn}(t) &\equiv \sqrt{\frac{\omega_k(t)}{\omega_n(t)}}G_{kn}(t) + \sqrt{\frac{\omega_n(t)}{\omega_k(t)}}G_{nk}(t) \\ f_{kn}(t) &\equiv \sqrt{\frac{\omega_k(t)}{\omega_n(t)}}G_{kn}(t) - \sqrt{\frac{\omega_n(t)}{\omega_k(t)}}G_{nk}(t). \end{aligned} \tag{5.24}$$

we have that

$$\dot{\hat{a}}_n = -i\omega_n(t)\hat{a}_n - \left[G_{nn} - \frac{\dot{\omega}_n}{2\omega_n}\right]\hat{a}_n^\dagger + \sum_{k\neq n}\left[f_{kn}\hat{a}_k - e_{kn}\hat{a}_k^\dagger\right]. \tag{5.25}$$

Even for a static cavity, in analogy with the creation/annihilation operators in the simple harmonic oscillator, $\hat{a}_n$ contains a fast oscillating phase term of $\exp\left[-i\int_{t_0}^t \omega_n(t')\mathrm{d}t'\right]$. For the time dependent cavity case, we can transform the analogous phase away via the following change of variable

$$\hat{a}_k = \exp\left[-i\int_{t_0}^t \omega_n(t')\mathrm{d}t'\right]\hat{b}_k = e^{-i\theta_k(t)}\hat{b}_k. \tag{5.26}$$

Hence, the equations of motion become

$$\dot{\hat{b}}_n = -\dot{q}\left[\bar{G}_{nn} - \frac{\partial_q \omega_n}{2\omega_n}\right] e^{2i\theta_n}\hat{b}_n^\dagger + \dot{q}\sum_{k\neq n}\left[\bar{f}_{kn}\hat{b}_k e^{i(\theta_n-\theta_k)} - \bar{e}_{kn}\hat{b}_k^\dagger e^{i(\theta_n+\theta_k)}\right]. \quad (5.27)$$

Assuming a sinusoidal vibration of the central mirror, i.e.

$$q(t) = l_0 + \epsilon \sin(\Omega_D t), \quad (5.28)$$

the mirror velocity $\dot{q} = \epsilon\Omega_D \cos(\Omega_D t) = \frac{\epsilon\Omega_D}{2}\left[e^{i\Omega_D t} + e^{-i\Omega_D t}\right]$. Resonance occurs due to the cancellation of the mirror driving phase term and the phase terms in the equations of motion. There are three sets of phase terms in the equation of motion: $2\theta_n$, $\theta_n - \theta_k$, $\theta_n + \theta_k$. To get a handle on the resonance condition, let us look at the time dependence of the term $\hat{N}_n = \hat{b}_n^\dagger \hat{b}_n$. We have that

$$\begin{aligned}
\dot{\hat{N}}_n &= \dot{\hat{b}}_n^\dagger \hat{b}_n + \hat{b}_n^\dagger \dot{\hat{b}}_n \quad (5.29)\\
&= -\left[G_{nn} - \frac{\dot{\omega}_n}{2\omega_n}\right]\left\{\hat{b}_n^2 e^{-2i\theta_n} + \left(\hat{b}_n^\dagger\right)^2 e^{2i\theta_n}\right\}\\
&\quad + \sum_{k\neq n}\left[f_{kn}\left\{\hat{b}_k^\dagger \hat{b}_n e^{-i\alpha_{nk}} + \hat{b}_n^\dagger \hat{b}_k e^{i\alpha_{nk}}\right\}\right.\\
&\quad \left. - e_{nk}\left\{\hat{b}_n \hat{b}_k e^{-i\beta_{nk}} + \hat{b}_n^\dagger \hat{b}_k^\dagger e^{i\beta_{nk}}\right\}\right]
\end{aligned}$$

where $\alpha_{nk} = \theta_n - \theta_k = -\alpha_{kn}$ and $\beta_{nk} = \theta_n + \theta_k = \beta_{kn}$. The terms containing phase α_{nk} are responsible for photon transfer amongst the modes. Then, there are the phases β_{nk} and $2\theta_n$ which are much larger. However, the mirror velocity prefactor from Eqn. (5.27) can lead to a partial cancellation of the phase. A large net phase would lead to a small contribution to the growth in photon numbers. Hence, for net photon growth, we require a driving frequency that

will reduce the order of magnitude of the β_{nk} and $2\theta_n$ phases. For photon transfer amongst modes, we require a driving frequency twice size of the gap between the modes.

The total number of photons $\hat{N} = \sum_n \hat{N}_n$ and we have that

$$\begin{aligned}
\dot{\hat{N}} &= \sum_n \dot{\hat{N}}_n \qquad (5.30)\\
&= \dot{\hat{b}}_n^\dagger \hat{b}_n + \hat{b}_n^\dagger \dot{\hat{b}}_n \\
&= -\sum_n \left[G_{nn} - \frac{\dot{\omega}_n}{2\omega_n} \right] \left\{ \hat{b}_n^2 e^{-2i\theta_n} + \left(\hat{b}_n^\dagger \right)^2 e^{2i\theta_n} \right\} \\
&\quad + \sum_{\substack{k,n \\ k\neq n}} \Big[f_{kn} \left\{ \hat{b}_k^\dagger \hat{b}_n e^{-i\alpha_{nk}} + \hat{b}_n^\dagger \hat{b}_k e^{i\alpha_{nk}} \right\} \\
&\quad - e_{nk} \left\{ \hat{b}_n \hat{b}_k e^{-i\beta_{nk}} + \hat{b}_n^\dagger \hat{b}_k^\dagger e^{i\beta_{nk}} \right\} \Big] \\
&= -\dot{q} \sum_n \left[\bar{G}_{nn} - \frac{\partial_q \omega_n}{2\omega_n} \right] \left\{ \hat{b}_n^2 e^{-2i\theta_n} + \left(\hat{b}_n^\dagger \right)^2 e^{2i\theta_n} \right\} \\
&\quad - 2\dot{q} \sum_{\substack{k,n \\ k<n}} \bar{e}_{nk} \left\{ \hat{b}_n \hat{b}_k e^{-i\beta_{nk}} + \hat{b}_n^\dagger \hat{b}_k^\dagger e^{i\beta_{nk}} \right\}.
\end{aligned}$$

Not surprisingly, the effect of photon scattering terms cancel out in the total photon number of the cavity. Now we can see that taking the driving frequency to be twice the initial frequency corresponding to any mode will cancel out some of the fast oscillating terms and cause the photon number to grow. Otherwise, the fast oscillating terms keep the photon growth close to zero. This resonance condition holds true for both the single and the double cavity. In the double cavity, as we will see later, due to the close proximity of the eigenstates in the avoided crossing, we get further interference between phases which leads to some extra features not present in the single cavity DCE.

5.4 Formalism to Numerically Simulate the Propagator

We assume from this section onwards that $\hbar = c = \epsilon_0 = 1$. We follow the formalism first used by [24] in a quantum mechanical context. The notation in this section closely follows that of Ruser in references [2, 3] The method depends on a reformulation of the equations of motion starting from the Heisenberg equations of motion for $\{\hat{Q}_n, \hat{P}_n\}$ given by

$$\begin{aligned} \frac{d\hat{Q}_n}{dt} &= \hat{P}_n(t) - \sum_j G_{nj}(q(t))\hat{Q}_j(t) \\ \frac{d\hat{P}_n}{dt} &= -\omega_n^2(t)\hat{Q}_n(t) + \sum_j \hat{P}_j(t)G_{jn}(q(t)). \end{aligned} \tag{5.31}$$

Combining the two equations, we find that

$$\begin{aligned} \ddot{\hat{Q}}_n &= \dot{\hat{P}}_n - \sum_j \dot{G}_{nj}\hat{Q}_j - \sum_j G_{nj}\dot{\hat{Q}}_j \\ &= -\omega_n^2(t)\hat{Q}_n + \sum_m G_{mn}\hat{P}_m - \sum_j \dot{G}_{nj}\hat{Q}_j - \sum_j G_{nj}\dot{\hat{Q}}_j \\ &= -\omega_n^2(t)\hat{Q}_n + \sum_m \left[G_{mn}\dot{\hat{Q}}_m - G_{nm}\dot{\hat{Q}}_m - \dot{G}_{nm}\hat{Q}_m\right] - \sum_{m,j} G_{mn}G_{mj}\hat{Q}_j. \end{aligned} \tag{5.32}$$

Assume that the mirror motion begins at some time t_0. We are interested in the photon number (or energy) of the light field at some later time t_1 when the mirror comes back to rest. We take the mirror to be at rest at time t_1, since the photon number for changing boundary conditions is ambiguous. Let, $\omega_n(t_0) = \omega_n^0$ and $\omega_n(t_1) = \omega_n^1$. Let $\{\hat{a}_n, \hat{a}_n^\dagger\}$ and $\{\hat{A}_n, \hat{A}_n^\dagger\}$ be the creation/annihilation operators at times t_0 and t_1 respectively. Then, the vacuum states at the

different times satisfy

$$\begin{aligned} \hat{a}_n|0,t_0\rangle &= 0 \\ \hat{A}_n|0,t_1\rangle &= 0. \end{aligned} \tag{5.33}$$

For the sake of clarity, we must point out that $|0,t_1\rangle$ is not the time evolved state corresponding to $|0,t_0\rangle$, but rather $|0,t_{0/1}\rangle$ are the ground states corresponding to the instantaneous creation/annihilation operators. We connect the creation/annihilation operators at different times via Bogoliubov transformations,

$$\hat{A}_n = \sum_m \left[A_{mn}(t_1)\hat{a}_m + B^*_{mn}(t_1)\hat{a}^\dagger_m\right]. \tag{5.34}$$

From the commutation relations $[\hat{A}_n, \hat{A}_k] = 0$ and $[\hat{A}_n, \hat{A}^\dagger_k] = \delta_{nk}$, writing

$$\hat{A}^\dagger_k = \sum_j \left[A^*_{jk}(t_1)\hat{a}^\dagger_j + B_{jk}(t_1)\hat{a}_j\right], \tag{5.35}$$

we have that

$$\begin{aligned} 0 &= [\hat{A}_n, \hat{A}_k] \\ &= \sum_{m,j} \left\{A_{mn}(t_1)B^*_{jk}(t_1)[\hat{a}_m, \hat{a}^\dagger_j] - A_{jk}(t_1)B^*_{mn}(t_1)[\hat{a}_j, \hat{a}^\dagger_m]\right\} \\ &= \sum_m \left\{A_{mn}(t_1)B^*_{mk}(t_1) - A_{mk}(t_1)B^*_{mn}(t_1)\right\}, \end{aligned} \tag{5.36}$$

and

$$\begin{aligned}\delta_{nk} &= [\hat{A}_n, \hat{A}_k^\dagger] \\ &= \sum_{m,j} \left\{ A_{mn}(t_1) A^*_{jk}(t_1) [\hat{a}_m, \hat{a}_j^\dagger] - B^*_{mn}(t_1) B_{jk}(t_1) [\hat{a}_j, \hat{a}_m^\dagger] \right\} \\ &= \sum_m \left\{ A_{mn}(t_1) A^*_{mk}(t_1) - B^*_{mn}(t_1) B_{mk}(t_1) \right\}.\end{aligned} \tag{5.37}$$

Let us denote the time evolution operator by $\hat{U} \equiv \hat{U}(t, t_0)$. Then, write the time evolution of the initial co-ordinate values $\{\hat{Q}_n(t_0), \hat{P}_n(t_0)\}$ in terms of some ansatz comprised of complex coefficients $\epsilon_n^{(m)}(t)$ and the initial creation/annihilation operators

$$\begin{aligned}\hat{Q}_n(t) = \hat{U}^\dagger \hat{Q}_n(t_0) \hat{U} &= \sum_m \frac{\hat{a}_m}{\sqrt{2\omega_m^0}} \epsilon_n^{(m)}(t) + h.c. \\ \hat{P}_n(t) = \hat{U}^\dagger \hat{P}_n(t_0) \hat{U} &= \sum_m \frac{\hat{a}_m}{\sqrt{2\omega_m^0}} \left[\dot{\epsilon}_n^{(m)}(t) + \sum_k G_{nk}(q(t)) \epsilon_k^{(m)}(t) \right] + h.c.\end{aligned} \tag{5.38}$$

Furthermore, by substituting the new form of $\hat{Q}_n(t)$ in the equations of motion, we find that for every fixed m, $\epsilon_n^{(m)}(t)$ satisfies the exact same equation of motion as $\hat{Q}_n$ with the initial conditions

$$\begin{aligned}\epsilon_n^{(m)}(t_0) &= \delta_{nm} \\ \dot{\epsilon}_n^{(m)}(t_0) &= -i\omega_n^0 \delta_{nm} + G_{nm}(q(t_0)),\end{aligned} \tag{5.39}$$

since Eqn. (5.39) is motivated by the $\{\hat{Q}_n, \hat{P}_n\}$ operators for the static quantum harmonic oscialltor and its relation to the creation/annihilation operators. The

initial condition comes from the observation that

$$\begin{aligned} \hat{Q}_n(t_0) &= \frac{\hat{a}_n}{\sqrt{2\omega_n^0}} + h.c. \\ \hat{P}_n(t_0) &= i\sqrt{\frac{\omega_n^0}{2}}\hat{a}_n^\dagger + h.c., \end{aligned} \tag{5.40}$$

and comparing it to the previous form in terms of $\epsilon_n^{(m)}(t)$. There is an important point to be made in view of these initial conditions. We need to impose a cutoff frequency to compute the photon number and similar quantities. Physically, we note that the high frequencies in the double cavity would not 'see' the end mirrors. Moreover, if we look at the $\dot{\epsilon}_n^{(m)}(t_0)$ term, we see that for a moving system, arbitrarily high frequencies can be excited due to the presence of the $G_{nm}(q(t_0))$ term. A cutoff frequency ensures that total light energy and photon number do not diverge in finite time due to the presence of these excitations. Furthermore, at time t_1, we have that

$$\begin{aligned} \hat{Q}_n(t_1) &= \frac{\hat{A}_n + \hat{A}_n^\dagger}{\sqrt{2\omega_n^1}} \\ \hat{P}_n(t_1) &= i\sqrt{\frac{\omega_n^1}{2}}\left[\hat{A}_n^\dagger - \hat{A}_n\right]. \end{aligned} \tag{5.41}$$

Since

$$\begin{aligned} \hat{A}_n &= \sum_m \left[A_{mn}(t_1)\hat{a}_m + B_{mn}^*(t_1)\hat{a}_m^\dagger\right] \\ \hat{A}_n^\dagger &= \sum_m \left[A_{mn}^*(t_1)\hat{a}_m^\dagger + B_{mn}(t_1)\hat{a}_m\right], \end{aligned} \tag{5.42}$$

we have that

$$\begin{aligned}\hat{A}_n + \hat{A}_n^\dagger &= \sum_m \{[A_{mn}(t_1) + B_{mn}(t_1)]\,\hat{a}_m + \\ &\quad [A^*_{mn}(t_1) + B^*_{mn}(t_1)]\,\hat{a}_m^\dagger\} \\ \hat{A}_n^\dagger - \hat{A}_n &= \sum_m \left\{[B_{mn}(t_1) - A_{mn}(t_1)]\,\hat{a}_m + [A^*_{mn}(t_1) - B^*_{mn}(t_1)]\,\hat{a}_m^\dagger\right\}.\end{aligned} \tag{5.43}$$

Then, we can say that

$$\begin{aligned}A_{mn}(t_1) + B_{mn}(t_1) &= \sqrt{\frac{\omega_n^1}{\omega_m^0}}\epsilon_n^{(m)}(t_1) \\ A_{mn}(t_1) - B_{mn}(t_1) &= \frac{i}{\sqrt{2\omega_m^0\omega_n^0}}\left[\dot{\epsilon}_n^{(m)}(t_1) + \sum_k G_{nk}(q(t_1))\epsilon_k^{(m)}(t_1)\right].\end{aligned} \tag{5.44}$$

Solving the previous set of equations, we find that

$$\begin{aligned}A_{mn}(t_1) &= \frac{1}{2}\sqrt{\frac{\omega_n^1}{\omega_m^0}}\left\{\epsilon_n^{(m)}(t_1) + \right. \\ &\quad \left.\frac{i}{\omega_n^1}\left[\dot{\epsilon}_n^{(m)}(t_1) + \sum_k G_{nk}(q(t_1))\epsilon_k^{(m)}(t_1)\right]\right\} \\ B_{mn}(t_1) &= \frac{1}{2}\sqrt{\frac{\omega_n^1}{\omega_m^0}}\left\{\epsilon_n^{(m)}(t_1) - \right. \\ &\quad \left.\frac{i}{\omega_n^1}\left[\dot{\epsilon}_n^{(m)}(t_1) + \sum_k G_{nk}(q(t_1))\epsilon_k^{(m)}(t_1)\right]\right\}\end{aligned} \tag{5.45}$$

expressing the Bogoliubov coefficients in terms of the complex coefficients, $\epsilon_n^{(m)}(t)$ and its time derivative. Since $\hat{A}_k = \hat{a}_k$ for $t_1 = t_0$, $A_{mn}(t_0) = \delta_{mn}$ and $B_{mn}(t_0) = 0$.

Our end goal is to reformulate the Heisenberg equations in terms of first order in time differential equations that yield the propagator for the dynamics. Now, let us motivate the introduction of the auxillary variables $\xi_n^{(m)}$ and $\eta_n^{(m)}$.

Defining, $\hat{b}_n(t) \equiv \hat{U}^\dagger \hat{a}_n \hat{U}$, where $\hat{a}_n = \frac{1}{\sqrt{2}}\left[\sqrt{\omega_n^0}\hat{Q}_n(t_0) + \frac{i}{\sqrt{\omega_n^0}}\hat{P}_n(t_0)\right]$, we have that

$$\begin{aligned}\hat{b}_n(t) &= \frac{1}{\sqrt{2}}\left[\sqrt{\omega_n^0}\hat{U}^\dagger\hat{Q}_n(t_0)\hat{U} + \frac{i}{\sqrt{\omega_n^0}}\hat{U}^\dagger\hat{P}_n(t_0)\hat{U}\right] \\ &= \frac{1}{\sqrt{2}}\left[\sqrt{\omega_n^0}\hat{Q}_n(t) + \frac{i}{\sqrt{\omega_n^0}}\hat{P}_n(t)\right].\end{aligned} \tag{5.46}$$

Defining

$$\Delta^{\pm}(t) \equiv \frac{1}{2}\left[1 \pm \frac{\omega_n^0}{\omega_n(t)}\right], \tag{5.47}$$

and

$$\begin{aligned}\xi_n^{(m)}(t) &= \epsilon_n^{(m)}(t) + \frac{i}{\sqrt{\omega_n^0}}\left[\dot{\epsilon}_n^{(m)}(t) + \sum_k G_{nk}(q(t))\epsilon_k^{(m)}(t)\right] \\ \eta_n^{(m)}(t) &= \epsilon_n^{(m)}(t) - \frac{i}{\sqrt{\omega_n^0}}\left[\dot{\epsilon}_n^{(m)}(t) + \sum_k G_{nk}(q(t))\epsilon_k^{(m)}(t)\right]\end{aligned} \tag{5.48}$$

we find that the auxillary variables contain information regarding the time evolution of the Bogoliubov coefficients since

$$\hat{b}_n(t) = \sum_m \frac{1}{2}\left[\xi_n^{(m)}(t)\hat{a}_m + \eta_n^{(m)^*}(t)\hat{a}_m^\dagger\right]. \tag{5.49}$$

Following these changes of variables

$$\begin{aligned}A_{mn}(t_1) &= \frac{1}{2}\sqrt{\frac{\omega_n^1}{\omega_m^0}}\left[\Delta_n^+(t_1)\xi_n^{(m)}(t_1) + \Delta_n^-(t_1)\eta_n^{(m)}(t_1)\right] \\ B_{mn}(t_1) &= \frac{1}{2}\sqrt{\frac{\omega_n^1}{\omega_m^0}}\left[\Delta_n^-(t_1)\xi_n^{(m)}(t_1) + \Delta_n^+(t_1)\eta_n^{(m)}(t_1)\right].\end{aligned} \tag{5.50}$$

Furthermore, using Eqn. (5.49) and the Heisenberg equations of motion satis-

fied by $\epsilon_n^{(m)}(t)$ one can check that

$$\begin{aligned}\dot{\xi}_n^{(m)} &= -i\left[a_{nn}^{+}\xi_n^{(m)} - a_{nn}^{-}\eta_n^{(m)}\right] - \sum_k \left[c_{nk}^{-}\xi_k^{(m)} + c_{nk}^{+}\eta_k^{(m)}\right] \\ \dot{\eta}_n^{(m)} &= -i\left[a_{nn}^{-}\xi_n^{(m)} - a_{nn}^{+}\eta_n^{(m)}\right] - \sum_k \left[c_{nk}^{+}\xi_k^{(m)} + c_{nk}^{-}\eta_k^{(m)}\right],\end{aligned} \tag{5.51}$$

with the initial conditions $\xi_n^{(m)}(t_0) = 2\delta_{mn}$ and $\eta_n^{(m)}(t_0) = 0$, where

$$a_{nn}^{\pm}(t) = \frac{\omega_n^0}{2}\left\{1 \pm \left[\frac{\omega_n(t)}{\omega_n^0}\right]^2\right\} \tag{5.52}$$

and

$$c_{nk}^{\pm}(t) = \frac{1}{2}\left[G_{nk}(q(t)) \pm \frac{\omega_k^0}{\omega_n^0}G_{kn}(q(t))\right]. \tag{5.53}$$

These relations completely describe the dynamics of the system by giving us the propagator in terms of first order in time equations of motion without having to compute the $\sum_{m,j} G_{mn}G_{mj}\hat{Q}_j$ terms in Eqn. (5.33) which is computationally intensive. To find the photon number, we merely need to simulate $\xi_n^{(m)}$ and $\eta_n^{(m)}$ and then find B_{mn} which gives us the photon number starting with a vacuum state as shown later. From the same information, one can find the energy of the field as well. Simulating these quantities give us the propagator for the quantum dynamics. Then, depending on the inititial state of the light field, we can easliy find the time of evolution of the particular initial state. In other words, once we have the propagator, the hard part of the numerical study is done. We merely need to project the initial state into the Fock basis and recombine using the propagator coefficients to generate the photon numbers and energy corresponding to the time evolved state.

5.4.1 Photon Number for Light in an initial Vacuum and also a General Coherent State

At this point, let us consider the quantity $\hat{N}_n(t_1) = \hat{A}_n^\dagger \hat{A}_n$, which gives us the number of photons corresponding to the frequency ω_n^1. If the initial state of light was the vacuum state, i.e.

$$|0, t_0\rangle = |0, t_0\rangle_{\omega_1^0} |0, t_0\rangle_{\omega_2^0} ... |0, t_0\rangle_{\omega_k^0} ..., \tag{5.54}$$

the photon number corresponding to ω_n^1 is given (in the Heisenberg picture) by $\langle 0, t_0 | \hat{N}_n(t_1) | 0, t_0 \rangle$. Since the action of the instantaneous annihilation operator on the initial state is given by

$$\begin{aligned} \hat{A}_n |0, t_0\rangle &= \sum_m \left[A_{mn}(t_1) \hat{a}_m + B_{mn}^*(t_1) \hat{a}_m^\dagger \right] |0, t_0\rangle \\ &= \sum_m B_{mn}^*(t_1) |0, t_0\rangle_{\omega < \omega_n^0} |1, t_0\rangle_{\omega_n^0} |0, t_0\rangle_{\omega > \omega_n^0} \end{aligned} \tag{5.55}$$

we have that the photon number in mode n at time t_1 is given by

$$\langle 0, t_0 | \hat{N}_n(t_1) | 0, t_0 \rangle = \sum_m |B_{mn}(t_1)|^2, \tag{5.56}$$

and the total energy is given by $E(t_1) = \sum_n \omega_n^1 \hat{N}_n(t_1)$. In the case of the initial state being some general coherent state rather than the vacuum state, i.e.

$$|\psi(t_0)\rangle = |\alpha_1, t_0\rangle_{\omega_1(t_0)} |\alpha_2, t_0\rangle_{\omega_2(t_0)} ... = |\vec{\alpha}, t_0\rangle, \tag{5.57}$$

the process for determining the photon number is similar.

$$\begin{aligned}\hat{N}_n(t_1) &= \sum_{i,j}\left[A^*_{in}(t_1)\hat{a}^\dagger_i + B_{in}(t_1)\hat{a}_i\right]\left[A_{jn}(t_1)\hat{a}_j + B^*_{jn}(t_1)\hat{a}^\dagger_j\right] \quad (5.58)\\ &= \sum_{i,j}\Big[A^*_{in}(t_1)A_{jn}(t_1)\hat{a}^\dagger_i\hat{a}_j + A^*_{in}(t_1)B^*_{jn}(t_1)\hat{a}^\dagger_i\hat{a}^\dagger_j + \\ &\quad B_{in}(t_1)A_{jn}(t_1)\hat{a}_i\hat{a}_j + B_{in}(t_1)B^*_{jn}(t_1)\hat{a}_i\hat{a}^\dagger_j\Big].\end{aligned}$$

Then, using that $[\hat{a}_i, \hat{a}^\dagger_j] = \delta_{ij}$, we find that

$$\begin{aligned}&\langle\vec{\alpha}, t_0|\hat{N}_n(t_1)|\vec{\alpha}, t_0\rangle \quad (5.59)\\ &\qquad = \sum_{i,j}\left(A^*_{in}\alpha^*_i + B_{in}\alpha_i\right)\left(A_{jn}\alpha_j + B^*_{jn}\alpha^*_j\right) + \sum_i |B_{in}|^2.\end{aligned}$$

This result is true in general, regardless of perfect or open single cavity or double cavity DCE.

Chapter 6

Numerical Simulation of the Dynamical Casimir Effect in a Double Cavity

6.1 Introduction

In this chapter we study the dynamical Casimir effect for a semi-open single cavity with the aid of numerical simulations. The semi-open single cavity has a stationary, perfectly reflecting mirror at one end and a sinusoidally driven, partially transmissive mirror at the other end. We build up to simulating the semi-open cavity by first simulating the perfect single cavity and then moving onto a symmetric double cavity before finally using an asymmetric double cavity to simulate the semi-open single cavity. The DCE in the double cavity has been analytically studied by Soff et al in reference [66] where they vibrate one of the perfect end mirrors. We, on the other hand, study the case where the partially transmissive central mirror is driven. Because photon production from the vacuum is tiny except at relativistic mirror speeds, we take this opportunity to remind the reader that an equivalent of the DCE can be

studied where the properties of a background dielectric or mirror in the cavity are manipulated [67, 68, 25]. This results in a variation of the optical length (Appendix A.1) allowing for higher *effective* mirror velocities in experiments. In fact, the confirmation of the DCE in the experiment by Wilson et al in reference [35] uses an analogue system (superconducting circuit) to simulate a moving mirror.

Extensive analytical work has been done on the dynamical Casimir effect (DCE) for the perfect single cavity [22, 28, 27, 30, 31]. A numerical study and confirmation of analytical results have been done in references [2]. In such a system, an end mirror driven with a frequency twice some cavity mode frequency leads to a resonance effect and the photon number corresponding to that mode grow non-linearly (quadratic for short times). This begs the question as to what happens to the number of photons if the driven mirror were to be partially transmissive and the cavity was coupled to an external environment? Analytically this topic has been studied using several different approaches: master equation formulation [37, 66, 38], scattering approach [39, 40, 25] and using cavity quasi-modes [26]. In references [26, 25] where a partially transmissive mirror of an open cavity is driven, it is predicted that after an initial quadratic growth of photons in the resonant mode, the photon number would become saturated. This result is in contrast to the perfect single cavity case and is not surprising because the photons leak out of the cavity at a constant rate Γ, say $\dot{N} = -\Gamma N$, and also since the coupling between the driven mirror and the vacuum field is lower for transmissive mirrors, which therefore perturb the vacuum field less, we expect the rate of photon production to be smaller than in the case of a driven perfect mirror. On the other hand, in reference [66], where it is the perfect mirror of a semi-open cavity that

is driven, the photon growth rate is not drastically modified for high enough reflectivites of the (static) partially transmissive mirror.

In this chapter, we answer the question of photon growth rate in the semi-open single cavity by numerically simulating the dynamics. Theoretically, such a cavity admits a continuum of modes which poses a difficulty in the simulation of the dynamics. We get around this obstacle by recognizing that a semi-open single cavity is just a single cavity coupled to an external environment by making one of the end mirrors partially transmissive. If we approximate the environment by a very long cavity, then we end up with an asymmetric (one cavity half much longer than the other) double cavity. Since the wavenumber structure in this asymmetric double cavity is discrete, numerical simulations of the dynamics becomes possible. In the limit the environment cavity length approaches infinity, the wavenumber structure approaches a continuum and the asymmetric double cavity model approaches an ideal semi-open single cavity. This approach to modelling an open cavity via a double cavity has been used in a classical context in references [10, 42] with success. The drawback of the method is that due to the finite size of the environment cavity, the photons that have decayed into the environment will eventually slosh back into the open cavity. For high enough reflectivities or large enough cavities, however, the time taken for the light to slosh back becomes large.

Neverthless, we find that the photons created in the open cavity converge as the environment cavity length is increased which shows that the approach is justified. Indeed, the numerical simulations show that after an initial exponential growth of the photon number a saturation takes place. In contrast with previous predictions for the open cavity [26], our essentially exact results for the semi-open cavity show that the saturation takes place much earlier,

and the maximum number of photons in the cavity is much lower than the predicted value [26, 25] for open cavities with time-varying dielectrics. This is not surprising considering that even the static Casimir force is strongly reduced for cavities with transmissive mirrors studied as two parallel dielectric plates [69] since the coupling of such a mirror with the vacuum field is weaker. Although our approach to the open cavity seems very similar to the setup studied by [66], the situation is fundamentally different because they drive a perfectly reflective end mirror, whereas we drive the partially transmissive end mirror of the semi-open cavity.

The arrangement of this chapter is as follows: First in parallel to the work in references [3, 2] we numerically simulate the DCE for the perfect single cavity and compare to the analytical works in references [22, 28]. Then we numerically study the DCE in the symmetric double cavity, i.e. a double cavity with two equal halves and a sinusoidally driven, partially transmissive central mirror. This result is already interesting since the double cavity can be thought of as two semi-open cavities coupled to each other. We change the reflectivity of the central mirror and compare the total photon number to the two perfect single cavities case. Then, we simulate the DCE for a semi-open single cavity by letting one of the cavity halves of a double cavity be much longer than the other. Next, we delve into the behaviour of photon growth in the open cavity and compare it to the growth of photon number in the perfect cavity with the decay rate factored in artificially. Lastly, we finish off this chapter by discussing regularization of the energy and photon number in the results presented.

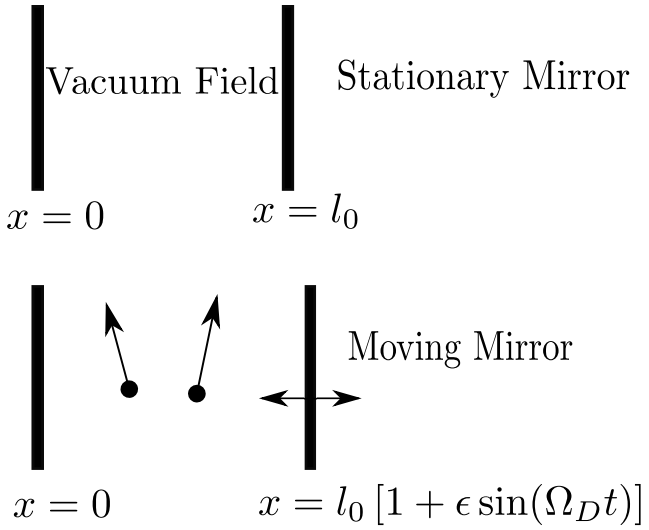

Figure 6.1: As the end mirror of a perfect single cavity begins to move, it excites photons from the vacuum field.

6.2 Numerical Study of DCE in a Single Cavity with Perfect End Mirrors

In this chapter we simulate the DCE in a perfect single cavity. In other words, we study the evolution of photon number in a single cavity with perfect end mirrors assuming that the light field is initially in the vacuum mode. This single cavity is comprised of a perfectly reflective end mirror fixed at position $x = 0$ and another perfectly reflecting end mirror at position $x = l_0[1 + \epsilon \sin(\Omega_D t)]$, where l_0 is the cavity length at time $t = 0$, ϵ is the amplitude of the mirror vibration in units of l_0 and Ω_D is the driving frequency of the mirror. Hence, the cavity length is variable and given by $l(t) = l_0[1 + \epsilon \sin(\Omega_D t)]$. This problem was studied by M. Ruser in reference [2] and we shall follow his approach here (and have checked we reproduce his results). We adopt natural units $\hbar = c = \epsilon_0 = 1$ and set the cavity length to be $l_0 = 1$, and set $\epsilon = 0.001$. The drive frequency $\Omega_D = 2\omega_n^0 = 2n_D\pi$ where $n_D = 1.5, 3$. The highest mirror

driving frequency considered in this thesis is 6π and implies a maximum mirror speed of $0.019c$. The frequency is in units of c/l_0, time in units of l_0/c and length is in units of $\hbar/c$kg from here onwards. For $t \leq 0$, the cavity end mirrors are taken to be at rest. The sudden jump in velocity to a finite value is small for $\epsilon \ll 1$ since it implies a small velocity once the mirror starts moving [3]. This leads to a small discontinuity in initial creation of photons and can be eliminated by considering mirror parametrizations that are smooth. We consider the sinusoidal parametrization, $l(t) = l_0[1 + \epsilon \sin(\Omega_D t)]$, since it has been studied extensively analytically [22, 28, 30]. The initial quantum state of the light field is taken to be the vacuum mode. The two end mirrors will experience a static Casimir force. As the mirror begins moving, work needs to be done to counteract the static Casimir Force and move according to the prescribed sinusoidal motion. Due to this, photons are pumped in and out from the external drive into the cavity. Lastly, the changing cavity frequency causes the vacuum photons to evolve into the excited modes as the Fock basis itself evolves since the cavity frequencies are changing due to the moving mirror. Once vacuum photons are converted to real photons, it leads to further modulation of the photon number in the cavity since the mirror motion now needs to counteract the new radiation pressure due to these real photons on the mirror. In fact, we have already seen the analogous classical effect in chapters 3 and 4. The effects leading to the growth of photon number can also be categorize as being due to the squeezing and the acceleration effect [29]. Non-adiabatic change of cavity length squeezes the initial vacuum state leading to growth in photon number and is referred to as the 'squeezing' effect. In addition, there are photons created due to the *explicit* contribution of velocity and its higher order derivatives referred to as the 'acceleration'

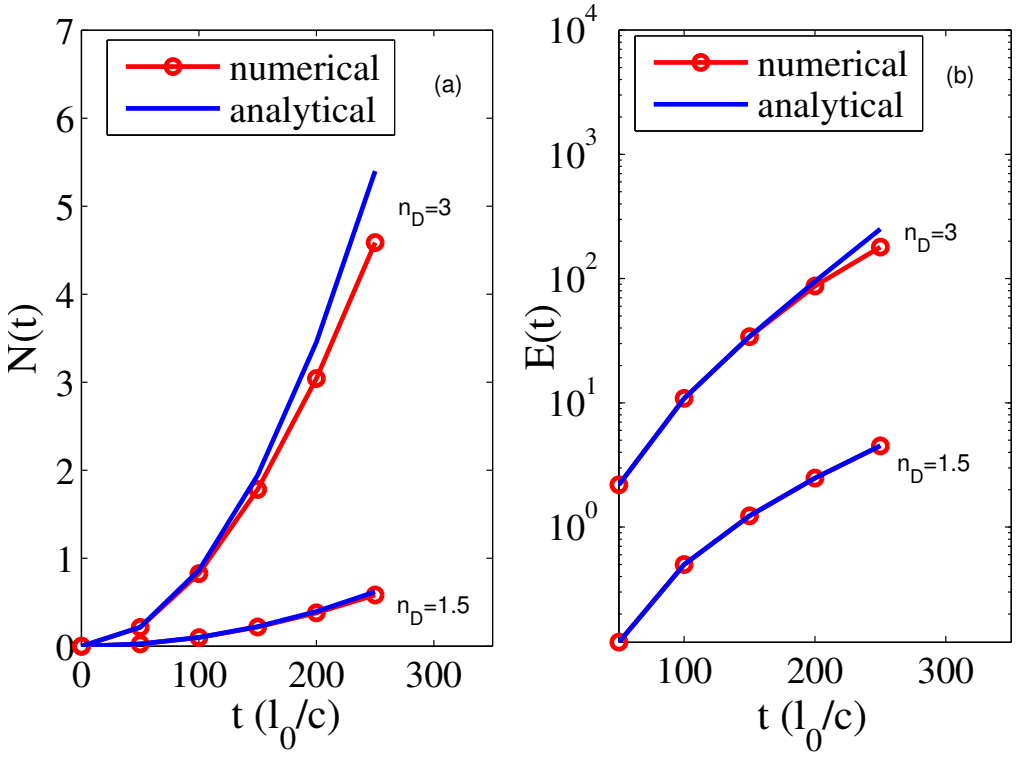

Figure 6.2: This figure shows the total photon number (a) and energy (units of $\hbar c/l_0$) (b) inside a single cavity with perfect end mirrors as a function of time. We compare the numerical results against the analytical results in Eqns. (6.1) and (6.2). These formulae hold for short times, i.e. $t \ll 300$ or $t \approx 30$. We see that after the initial quadratic growth, the photon emission rate slows down. We also see that the total photon energy also grows exponentially. The $n_D = 3$ curve corresponds to a driving frequency of $\Omega_D = 2n_D\pi = 6\pi$ and resonantly enhances the growth of photon number for the frequency $n_D\pi = 3\pi$. Meanwhile, the $n_D = 1.5$ curve corresponds to a driving frequency of $\Omega_D = 3\pi$ and is not resonant with any of the cavity modes.

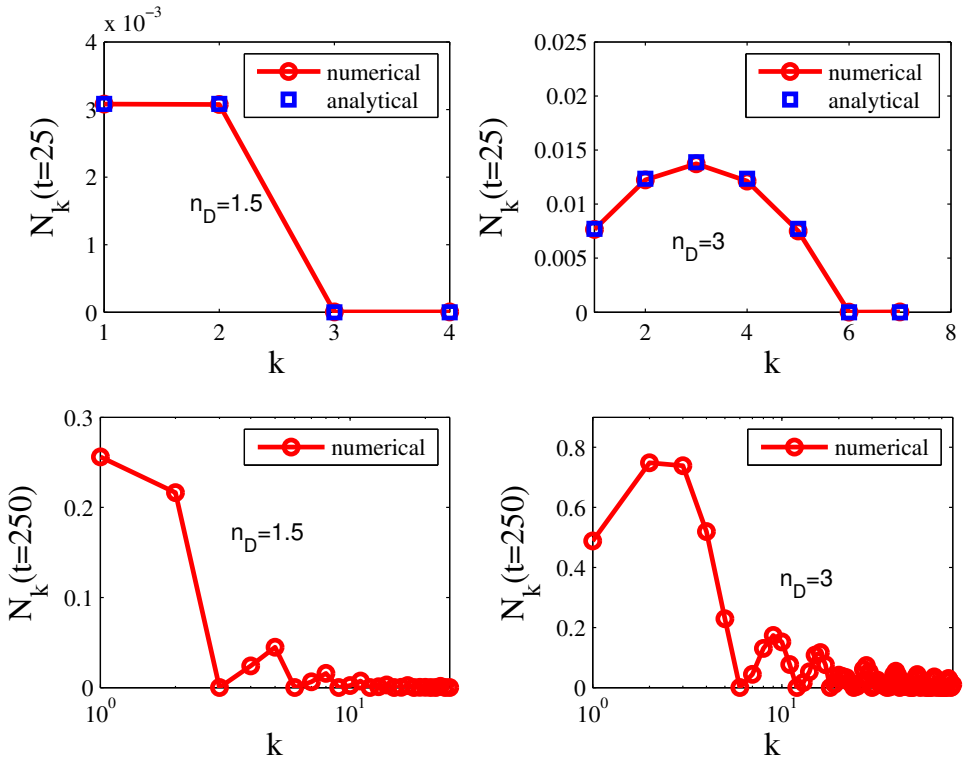

Figure 6.3: This figure shows a snapshot of the population of photons in each cavity mode for both short and long times. For short times, for example $t = 25$, the greatest photon population is centered around the modes the driving frequency is resonant with. For $n_d = 1.5$, this would be the first and second modes, while for $n_D = 3$, this would be the third mode. We compare the numerical results for short time against the analytical result given by Eqn. (6.3).

effect.

For small time, $\epsilon\pi t \ll 1$, analytical formulae for the total photon number and energy due to Dodonov and Klimov [22] and Ji et al [28] are respectively given by

$$N(t) = n_D(4n_D^2 - 1)(10^{-3}\pi t)^2/12 \tag{6.1}$$

and

$$E(t) = (4n_D^2 - 1)\pi \sinh^2(n_D 10^{-3}\pi t)/12. \tag{6.2}$$

We can see in Fig. 6.2 that the numerical and analytical values for total photon number and energy agree very well for short enough times. We see that after the initial quadratic growth in photon number, the rate slows down. Knowing that the analytical results come from a perturbative treatment, it makes sense that higher order corrections come into play for longer times. The light field energy inside the cavity grows non-linearly ($\sinh^2(\cdot)$) as predicted by the analytical result. Meanwhile, the analytical formula for photon number corresponding to a particular cavity mode is given by

$$N_k(t) = (2n_D - k)k(10^{-3}\pi t)^2/4 \tag{6.3}$$

where, $k < 2n_D$ and $N_k(t) = 0$ for all other modes. Note that this is only true for small enough times. As we can see in Fig. 6.3, the analytical formula and the numerical results for the photon numbers in individual modes match very closely. For modes close to the resonant frequency, the photon population is high and it tapers off to zero beyond a width of $2n_D$ around the resonant frequency. This photon population shape is one of the important considerations behind our choice of driving frequencies. Choosing larger driving frequencies

require us to include a larger number of modes for the simulation and hence is computationally too intensive.

Since the growth in photon number inside the cavity is affected by the interaction between the oscillating mirror and the radiation pressure, we expect photons to be pumped out of the cavity as well as into the cavity and hence the photon number growth to be modulated in time. This reasoning is motivated by the classical field results discussed in chapter 4. However, the analytical results and the numerical results in Fig. 6.2 show only monotonic growth in photon number. Assuming that somehow the perturbative nature of the analytic formulae fails to capture the effect of the photons pumped out and that the numerical simulations did not zoom in enough, we simulate the dynamics for a short time of t_f and sample 400 points in the time interval. We plot these results in Fig. 6.4 and sure enough see micromodulations in the total photon number inside the cavity, which has also been observed by M. Ruser in reference [3]. Furthermore, in the same figure we also plot $\left(\dot{l}/l\right)^2$ and find that the period of oscillation coincides with the micromodulation period. For every 2 mirror oscillations, both curves have 4 dips. In reference [30], the authors find periodic behaviour in the Bogoliubov coefficients reminiscent of the micromodulation structure observed in our photon number curves, although they do not compute the photon number explicitly. Also in Fig. 6.4, we plot the growth in photon numbers while ignoring the acceleration term in the effective Hamiltonian given by Eqn. (5.16) and find that the photon creation rate is approximately halved in comparison to the full effective Hamiltonian (squeezing + acceleration). This is in agreement with the analysis in reference [29] that the squeezing and acceleration contributions of the effective Hamiltonian are of the same order of magnitude. Remarkably, we can also discern that there is

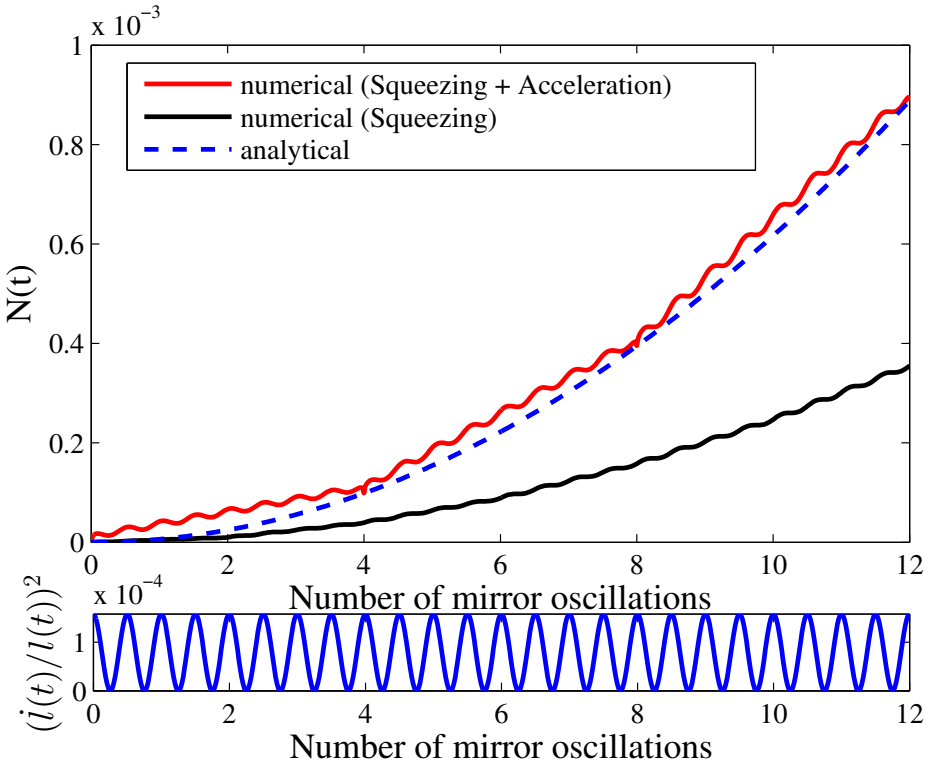

Figure 6.4: This figure shows the total photon number and energy in the cavity for $n_D = 2$ as a function of the number of mirror oscillations. Here, a mirror oscillation denotes the time taken for the driven mirror to come back to its initial position with the initial velocity. The period of the mirror oscillation (T_M) is 0.5 since $\Omega_D = 4\pi = 2\pi/T_M$. Taking many more time samples, we see both micromodulations and an underlying piecewise linear behaviour in the numerical simulation that are not predicted by the simple perturbative formula in Eqn. (6.1). We also see that the squeezing part of the Hamiltonian contributes about half of the DCE and so the acceleration terms in the Hamiltonian (those that depend on velocity) contribute the other half.

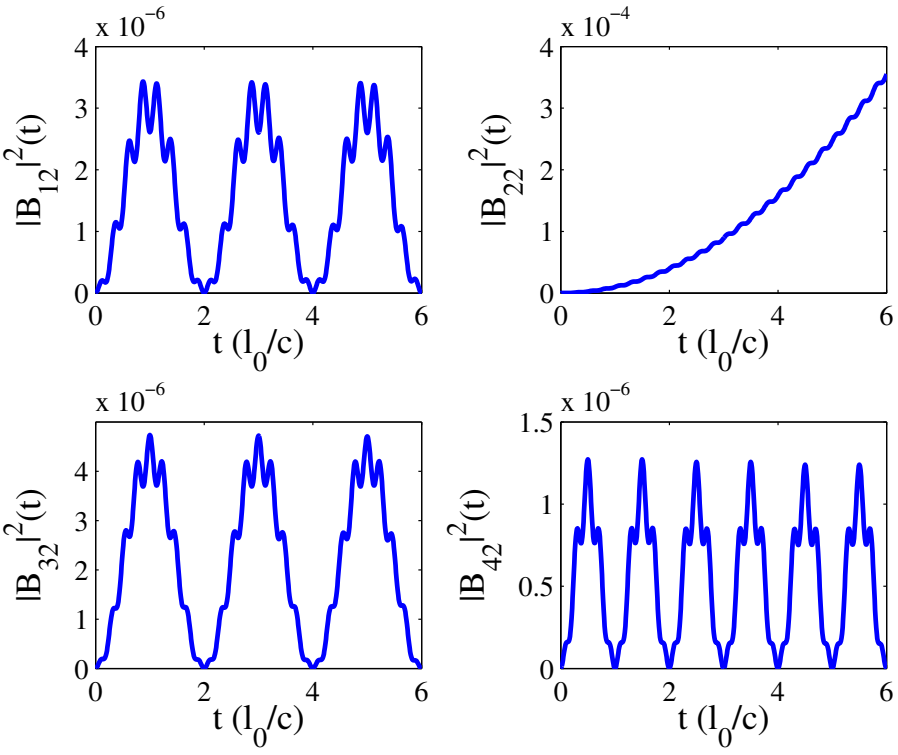

Figure 6.5: Time evolution of Bogoliubov coefficients. We plot the Bogoliubov coefficients, $B_{mn}(t)$ defined in Eqn. (5.35) as a function of time to get a better understanding of the creation of photons of the second mode, i.e. $N_2(t)$. From the definition in Eqn. (5.56), we set $n = 2$. We find that for $m = 2$, the coefficient grows almost monotonically if we ignore the micromodulations. For all other m values, we see a periodic behaviour and the coefficients vanish sharply at times $t = 1$ or 2. The piecewise linear behaviour discernable in Fig. 6.4 is due to the periodic behaviour of these off-diagonal terms.

an underlying piecewise linear growth in the photon number curves, a feature also not predicted by prior analytic work. Furthermore, the mode structures and coupling coefficients used in the code were analytical functions. This gives us confidence that this behaviour is a real feature of the dynamics rather than an error in the simulation code or lack of accuracy. We further investigate the single cavity DCE at high resolution times in Fig. 6.5, where we plot the Bogoliubov coefficients that are summed in Eqn. (5.56) to give the photon population corresponding to the resonant mode. Upon closer inspection, we find that the piecewise linear behaviour is due to B_{mn} for $m \neq n$. The diagonal Bogoliubov coefficient for $m = n = 2$ grows monotonically underneath the micromodulations. The off-diagonal coefficients, which account for the contributions from the off-resonant modes are, interestingly, periodic functions. One might assume that this periodicity is somehow linked to the mirror returning to its initial position and the Bogoliubov transformation reducing to the identity matrix. The period of the coefficients in Fig. 6.5 are 2 for $|B_{12/32}|^2$ and 1 for $|B_{42}|^2$ while the period of the mirror oscillations is 0.5. Hence, we see that the periodicity must be linked to some other factor that the mirror has returned to its initial position with the initial velocity. Nevertheless, it is remarkable that the contribution from the off-diagonal Bogoliubov coefficients gives rise to a linear growth underneath the micromodulations.

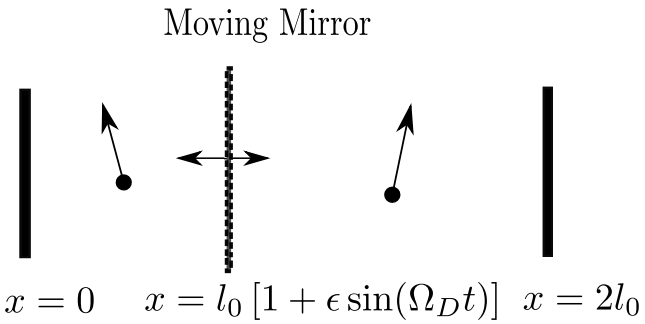

Figure 6.6: The double cavity system is a perfect single cavity with an externally driven partially transmissive central mirror. Photons are created from the vacuum due to the time-dependent boundary condition. The double cavity can also be thought of as two semi-open single cavities coupled to one another.

6.3 Dynamical Casimir Effect in the Double Cavity

In the previous section, we took a brief look at the dynamical Casimir effect for a perfect single cavity. Now we shift our focus to a slightly more elaborate system by symmetrically adding a third mirror to the perfect single cavity system. Moreover, the central mirror is now made partially transmissive as shown in Fig. 6.6, which presents no difficulty in numerical simulations since the wavenumbers in this system are still discrete. Importantly, the moving mirror is not perfectly reflective which means that we do not suffer from pathological problems described by Moore [5] and Barton and Eberlein [6]. On the other hand, if one of the end mirrors was made partially transmissive, we would have to deal with a continuum of modes. The resulting system is just the familiar double cavity that we have dealt with extensively in the first few chapters. The double cavity is comprised of two perfect end mirrors at $x = 0$ and $x = 2l_0$. It has a partially transmissive, driven central mirror with

the position function $x(t) = l_0 [1 + \epsilon \sin(\Omega_D t)]$. As before, ϵ and Ω_D are the amplitude and the driving frequency of the mirror. Since the double cavity can be thought of as two semi-open single cavities coupled to each other, this is a detour along the way to studying an open single cavity coupled to an external environment. It is a good test of our intuition to guess what would happen to the photon creation in the double cavity starting with light in the vacuum state and driving the central mirror sinusoidally. We simulate the dynamics for the exact same parameter values as in the previous section where $l_0 = 1$ in units such that $\hbar = c = \epsilon_0 = 1$, $\epsilon = 0.001$ and $\Omega_D = 2n_D\pi = 3\pi, 4\pi$. The driving frequency corresponding to $n_D = 2$ is resonant with the frequencies near 2π, i.e. photons corresponding to these eigenfrequencies experience the greatest growth. In Fig. 6.7 (a) and (b), we see that the total photon number created in the double cavity, unless for very high reflectivities ($\alpha = 10$), is very modest compared to the perfect central mirror case. The reflectivities corresponding to the resonant eigenfrequencies near 2π are given by $R(\alpha = 1) = 90.8\%$, $R(\alpha = 2) = 97.5\%$, $R(\alpha = 4) = 99.4\%$ and $R(\alpha = 10) = 99.9\%$. Moreover, as the reflectivity of the central mirror approaches 100%, the total photon number asymptotically approaches the sum of $N(t)$ curves of two perfect single cavities. The double cavity where the central mirror is completely reflective ($\alpha = \infty$) is of course just two perfect single cavities.

Mathematically, the photon creation in cavities with time-dependent boundary conditions is due to the squeezing and acceleration parts of the Hamiltonian as discussed at the end of Sec. 5.2. Despite the same mathematical origins for photon creation in a double cavity with a perfectly reflective and partially transmissive driven mirror, the actual photon number curves in Fig. 6.7 have qualitative differences. In the former, the photon number inside the cavity

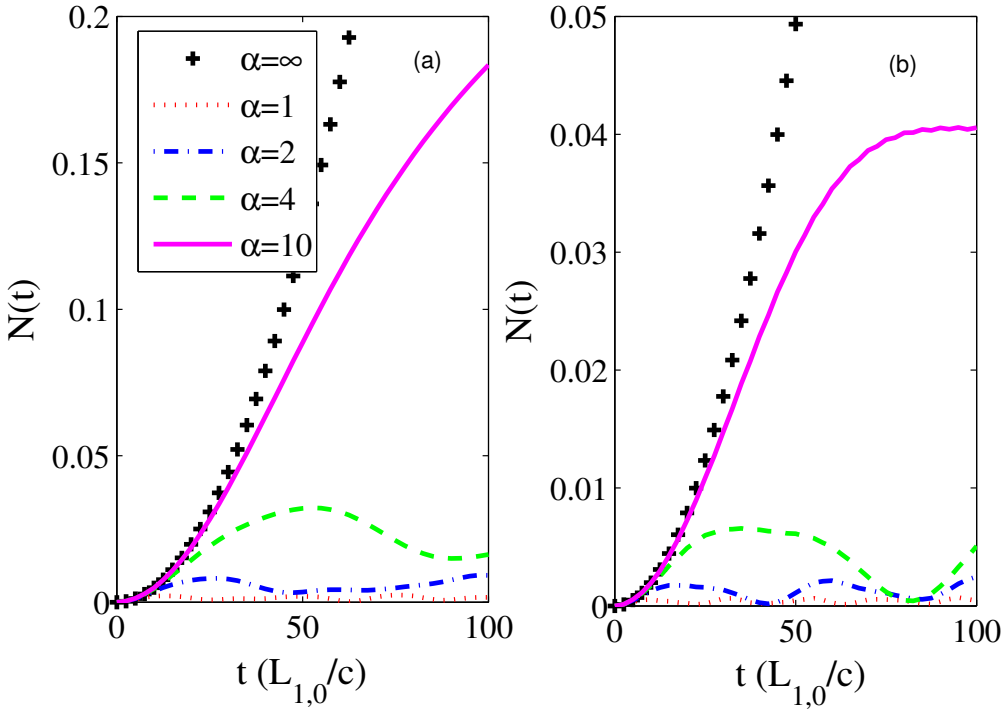

Figure 6.7: In this figure we compare the total number of photons created in the double cavity for the two different central mirror frequencies against the perfectly reflective central mirror case. In (a) $n_D = 2$ and in (b) $n_D = 1.5$. The initial lengths of the cavity halves are $L_1(t_0) = L_{1,0} = 1$ and $L_2(t_0) = L_{2,0} = 1$. We find that after an initial growth in photon number equal to the perfect central mirror case ($\alpha = \infty$), the photon creation rate slows down and reaches a local maximum. Furthermore, we find that as the central mirror reflectivity is increased, the number of photons created inside the double cavity also increases, i.e. the mirror couples to the field more strongly.

more or less grows monotonically (ignoring micromodulations seen in Fig. 6.4), while in the latter case there are dips in the photon number curves. These dips can be explained using a very classical concept that we dealt with in chapters 3 and 4. A major difference between the perfect and the partially transmissive central mirror is that the photons can slosh in back and forth between the two cavity halves when they are coupled together. As we saw in Figs. 4.1 and 4.2, the external source driving the central mirror has to counter the radiation pressure exerted by the real (i.e. non-vacuum state) photons on the driven mirror. As a result of the external source doing work on the cavity light field, photons will be pumped in and out of the cavity.

In the case where the central mirror is perfectly reflective, i.e. the system consists of two perfect single cavities, the photon production is equal in both cavity halves and hence the intensity of the light field on both sides of the central mirror is equal. Since the radiation pressure is proportional to the difference of the light field intensity between the two interfaces of the central mirror, the net radiation pressure ends up being zero. In contrast, from the moment the photons are being created in the transmissive double cavity, the photons begin to slosh back and forth. As the asymmetry in the photon localization increases, due to imbalance in light intensity between the two cavity halves, the central mirror will begin to experience a net radiation pressure. Furthermore, as the light sloshes back and forth, this radiation pressure changes direction as well. Lastly, let us note that higher reflectivity will lead to lower sloshing rate but stronger photon localization imbalance. This might explain why the dips in photon number curves in Fig. 6.7 have a longer period and yet larger dips for the higher reflectivities.

In the same figure, it can be seen that the partially transmissive photon

number curves grow at a similar rate to the perfect mirror case until $t \approx 10$, but after this initial spurt, the mechanism described above leads to a difference in the photon number curves for different reflectivities.. This is not surprising considering that the photons have not had enough time to transfer amongst the two cavity halves and hence the resultant radiation pressure is negligible. These effects depend on the parametric driving, which is the same sinusoidal motion used throughout this chapter, and the other being the cavity frequency structure. We restrict mirror vibrations to be very close to the avoided crossing and hence the double cavity frequencies vary negligibly. Higher mirror displacement would require a higher cutoff frequency which would become very time-consuming to simulate. Furthermore, the reflectivities we consider are quite high, 91% ($\alpha = 1$) being the lowest. For higher reflectivites, the avoided crossing gap is much smaller and hence the diabatic frequencies are closer to the frequencies of the perfect single cavities. Thus, not only are the double cavity with the transmissive mirror frequencies very close to begin with, but also they vary negligibly as the mirror moves with small amplitude near the avoided crossing ($\epsilon = 0.001$). Consequently, it comes as no shock to find that before the tunelling mechanism causes the photon number curves to diverge in Fig. 6.7, the growth in photon number match very closely. Lastly, let us mention that as the central mirror reflectivity is lowered further, we expect the initial photon growth rate to go down. One can think of the case where the central mirror has zero reflectivity. In such a situation, the photon growth rate should be zero. Seeing how meagre the photon growth is due to the DCE even for a reflectivity of 91%, lower reflectivities which would yield even lower photon creation are not particularly interesting. A more promising candidate for numerical study would be to consider higher mirror displacement where the

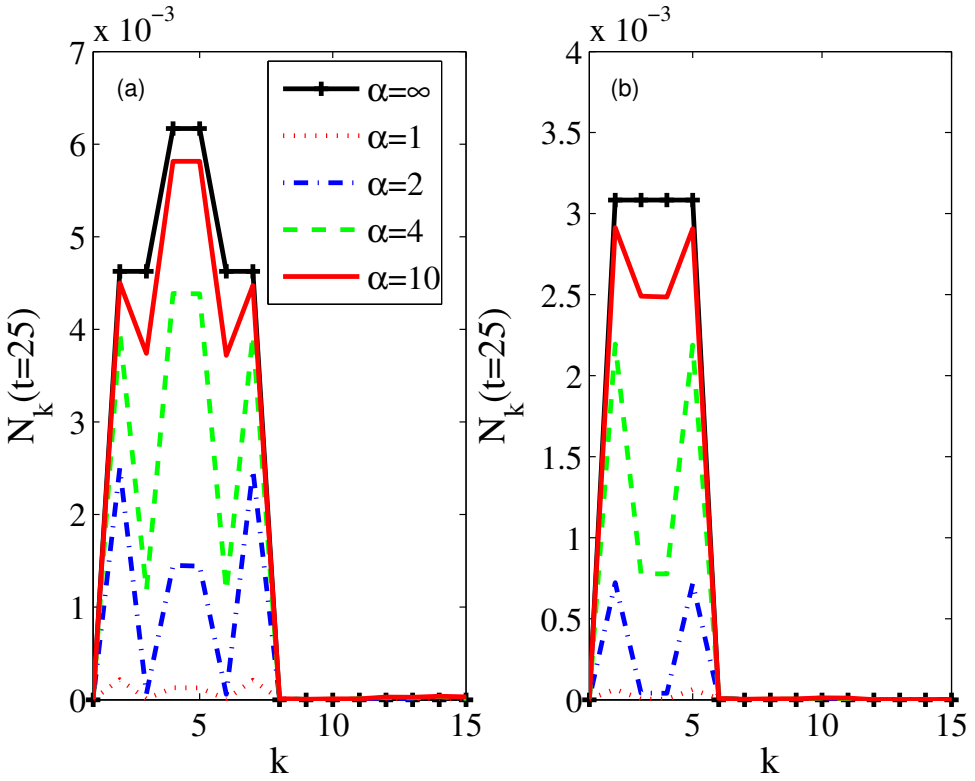

Figure 6.8: In this figure, we compare the number of photons created for each mode k for different central mirror reflectivities ($\alpha = 1, 2, 4, 10$) in the double cavity and compare it to the perfect central mirror case ($\alpha = \infty$). Figure (a) corresponds to a driving frequency of $\Omega_D = 4\pi$ while (b) is for $\Omega_D = 3\pi$. We see that the number of photons created for the perfect double cavity (i.e. two single cavities) is higher than the partially transmissive central mirror cases.

variation in the wavenumber structure due to various reflectivity parameters would be brought into play.

In Fig. 6.9, we plot the photon number per frequency mode number for the fixed time $t = 25$ and driving frequencies 4π in plot (a) and 3π in plot (b). For lower reflectivites of the driven central mirror, fewer photons are created in the double cavity. Apart from that, there is a qualitative difference in the mode populations between the perfect and the partially transmissive central mirror cases. In Fig. 6.9 (a), the $\alpha = \infty$ case exhibits equal population for modes 2 & 3, modes 4 & 5 and modes 6 & 7. This is because each of the mode pairs correspond to the diabatic modes of the uncoupled left and right cavity halves. Due to the uncoupled and symmetric nature of the two cavity halves, the photon creation in the diabatic mode pairs is equal. Also, note that mode 1 of the perfect central mirror case is an artificial construct, shown merely for the sake of comparison with the transmissive central mirror case where it is infact an eigenfrequency. However, from the figures we see that the parameters we use for the dynamical simulations yield a mode 1 population of either zero or very small. Going back to the qualitative difference discussion, we note that the finite reflectivity parameters plot (a) exhibits unequal population for modes 2 & 3 and modes 6 & 7. Instead, there are dips at modes 3 and 6. Similar qualitative features are also present in plot (b) for the off-resonance driving frequency. As the reflectivity approaches unity, these dips tend to flatten and approach the $\alpha = \infty$ case.

Fig. 2.3 shows the difference in frequency structure in the double cavity for the perfect and partially transmissive central mirror cases. The modes are denoted as the diabatic and adiabatic modes, respectively. When the mirror is exactly centered, the diabatic frequencies are degenerate, while the adiabatic

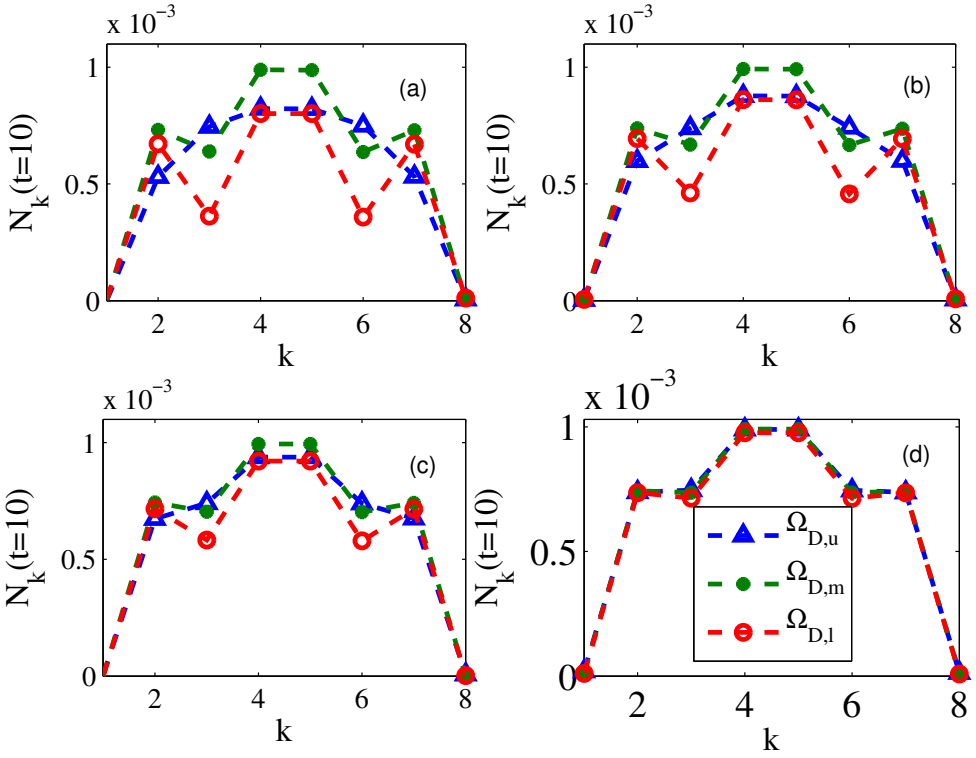

Figure 6.9: This figure shows the effect of varying the driving frequency of the central mirror in the double cavity so that it is resonant with the lower and upper wavenumber branches of an avoided crossing denoted by $\Omega_{D,l}$ and $\Omega_{D,u}$. $\Omega_{D,m}$ is the average of the upper and lower driving frequencies.We vary the central mirror reflectivity according to (a) $\alpha = 2$ (b) $\alpha = 2.5$ (c) $\alpha = 3.6$ (d) $\alpha = 10$ and plot the photon number per mode number. We find that not only do relatively small perturbations in the driving frequency influence the photon creation rate but this also has subtle influences on which modes are populated.

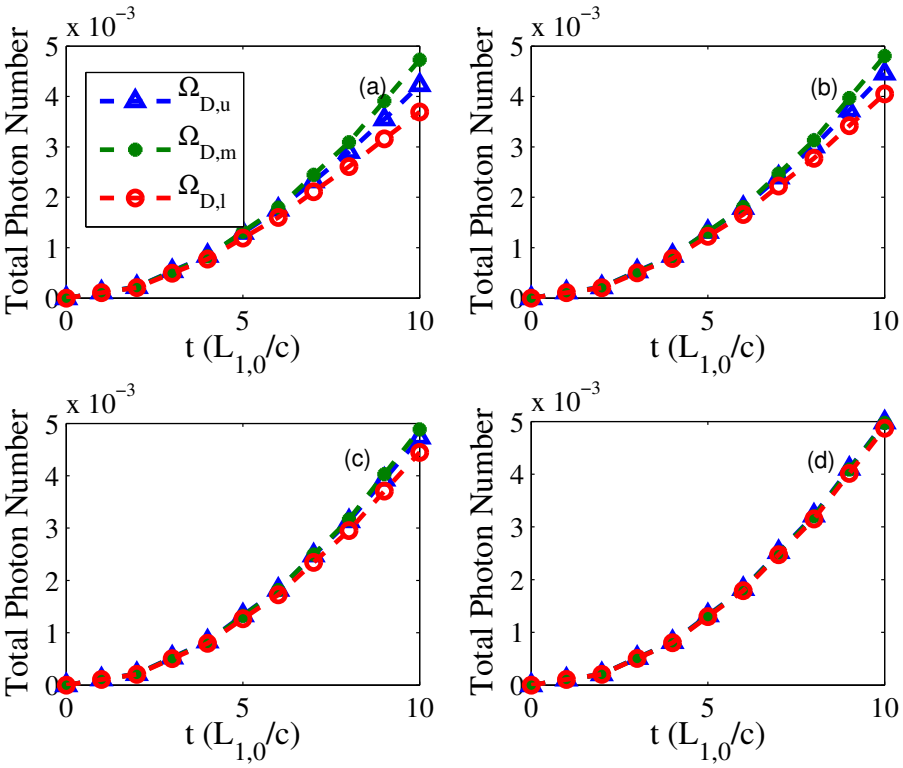

Figure 6.10: This figure shows the effect on total photon number of varying the driving frequency of the central mirror in the double cavity so that it is resonant with the lower and upper wavenumber branches of an avoided crossing denoted by $\Omega_{D,l}$ and $\Omega_{D,u}$. $\Omega_{D,m}$ is the average of the upper and lower driving frequencies.We vary the central mirror reflectivity according to (a) $\alpha = 2$ (b) $\alpha = 2.5$ (c) $\alpha = 3.6$ (d) $\alpha = 10$. We find that $\Omega_{D,m}$ leads to the greatest growth in total photon number followed by $\Omega_{D,u}$ and the $\Omega_{D,l}$. As the reflectivity is increased, the gap between the photon number curves close up while maintaining the same hierarchy.

frequencies have a gap of magnitude 2Δ. As we have discussed before, the gap vanishes as the mirror reflectivity approaches unity, i.e. $2\Delta \to 0$ as $\alpha \to \infty$. When we simulated the DCE previously, we picked driving frequencies resonant to the centered diabatic modes. For example, the driving frequency 4π is resonant with the degenerate centered diabatic modes 2π. Now, we wish to study the effect of a small perturbation to the driving frequency such that it is resonant with the lower or the upper branches. Let us refer to these cases as $\Omega_{D,l}$ and $\Omega_{D,u}$. In addition to that, we also simulate the DCE for the average of the two driving frequencies referred to as the middle driving frequency ($\Omega_{D,m}$). In Fig. 6.9 the photon number is plotted as a function of the frequency mode number. The reflectivity is changed in the plots (a) through (d). For each fixed reflectivity, we determine the driving frequency resonant to the lower and upper branch of the adiabatic modes near 2π. The reflectivities are (a) $R(\alpha = 2) = 97.5\%$, (b) $R(\alpha = 2.5) = 98.4\%$, (c) $R(\alpha = 3.6) = 99.2\%$ and (d) $R(\alpha = 10) = 99.9\%$. We find that the photon population dips that we observed in Fig. 6.7 are directly effected by the small perturbations in the driving frequency. We note that the dip for the middle driving frequency is smaller than the dip corresponding to the lower driving frequency. Meanwhile, the upper driving frequency result exhibits a monotonic decrease in photon number away from the central resonant modes. Lastly, it can be seen that increasing the reflectivity flattens out the photon population imbalances in modes 2 & 3 and modes 6 & 7. We see in Fig. 6.10 that the middle driving frequency leads to a highest total photon number curve, followed by the upper and lastly the lower driving frequency. As the central mirror reflectivity is increased, the three curves maintain the same hierarchy but close in towards each other while moving up.

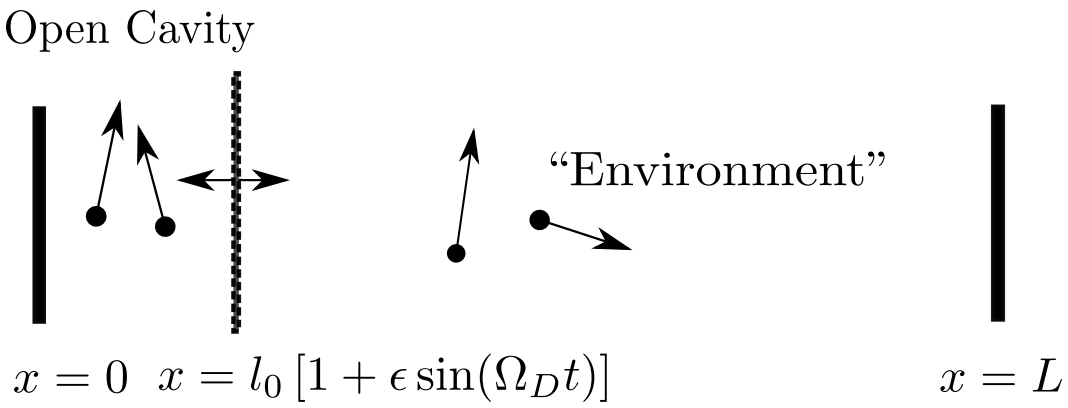

Figure 6.11: We model a semi-open single cavity by an asymmetric double cavity with a cavity with the dimensions of the open cavity of interest coupled to an extremely long cavity via a partially transmissive middle mirror. As the partially transmissive mirror is driven sinusoidally, photons are created in the open cavity. Furthermore, due to the open nature of the cavity, we see decay of photons as well.

6.4 Modelling a single cavity coupled to an environment via a Double Cavity

In this section, we study photon creation in an ideal semi-open cavity due to time-dependent boundary conditions. We define the ideal semi-open cavity as a semi-open cavity coupled to an infinite environment as opposed to the finite semi-open cavity forming a double cavity studied in the previous section. The ideal semi-open cavity is comprised of a perfect end mirror placed at $x = 0$ and a partially transmissive mirror at the variable position $x(t) = l_0\,[1 + \sin(\Omega_D t)]$. Hence, the cavity is coupled to a continuum of modes of the infinite environment via the partially transmissive mirror. Numerically, it is not possible to simulate the dynamics for a continuum of modes. We get around this problem, by modelling the infinite environment by another much larger cavity as shown in Fig. 6.4. Hence, we add an end mirror at the position $x = L$. Similar to the previous sections, we take the parameters $l_0 = 1$,

$\epsilon = 0.001$ and focus our attention on the driving frequency $\Omega_D = 4\pi$. The cavity used to model the environment, shown as the right cavity half in Fig. 6.4 is from here onwards referred to as the environment cavity, while the other half, the cavity of our main interest is referred to as the open cavity. One might also notice that the resultant cavity system forms a highly asymmetric double cavity. As the environment cavity length approaches infinity, the asymmetric double cavity approaches an ideal semi-open cavity. In order to study the convergence properties of the model, we vary the length of the environment cavity to be $L - l_0 = 3.1, 5.1, 7.1, 9.1$. Here, we have avoided environment cavity lengths of $3, 5, 7, 9$ $(\hbar/c\text{kg})$, to ensure that we are not studying the special case where the environment cavity length is an integer multiple length of the open cavity. In Fig. 6.12, we plot the eigenvalue structure corresponding to the parameters $\alpha = 4$, $L_1(t_0) = L_{1,0} = 1$ and $L_2(t_0) = L_{2,0} = 9.1$ $(\hbar/c\text{kg})$, which are the initial lengths of the open and environment cavity respectively. In addition, the diabatic modes (eigenmodes for $\alpha = \infty$) of the uncoupled cavities of initial lengths $L_{1,0}$ and $L_{2,0}$ are plotted for variable displacements of the central mirror from the initial position. The diabatic wavenumbers inside the smaller cavity of initial length $L_{1,0}$ change more significantly than the wavenumbers in the much larger cavity of initial length $L_{2,0}$. This is expected since for a perfect cavity the wavenumbers depend upon L and ΔL as

$$k_n(\Delta L) = \frac{n\pi}{L + \Delta L}. \tag{6.4}$$

For small perturbations in the length, which is the regime we operate in, $k_n(\Delta L) \approx \frac{n\pi}{L}\left(1 - \frac{\Delta L}{L}\right)$. Hence, for a mirror displacement of Δq, the change in diabatic frequencies inside the smaller cavity is given by $\Delta q / L_{1,0}^2$ and for

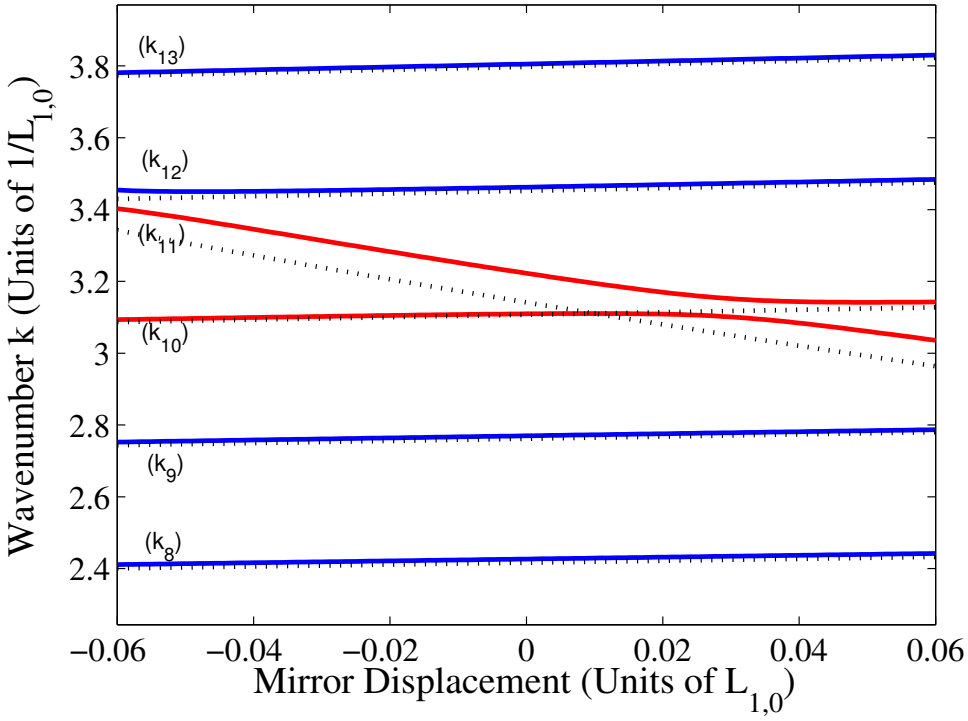

Figure 6.12: In this figure, we show the wavenumber structure for an asymmetric double cavity with a partially transmissive central mirror ($\alpha = 4$) and initial cavity half lengths of $L_1(t_0) = L_{1,0} = 1$ and $L_2(t_0) = L_{2,0} = 9.1$. The dotted curves represent the diabatic modes of the cavity, i.e. for $\alpha = \infty$ while the solid lines represent the adiabatic modes of the cavity. The blue solid lines represent modes that are strongly localized in the environment cavity. The red solid curves correspond to modes that are localized in the open cavity. When the length $L_{2,0} \to \infty$, the blue solid lines will become more dense and approach a continuum and the model approaches an ideal open cavity with a partially transmissive single cavity coupled to an infinitely large environment. Here, k_i represents the i-th wavenumber in the eigenspectrum.

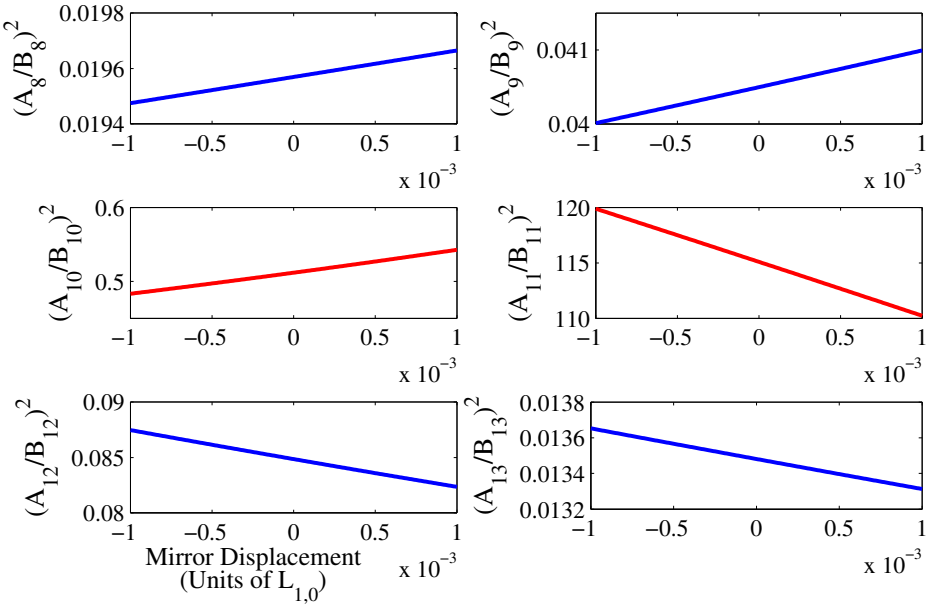

Figure 6.13: In this figure, we show the localization of the modes corresponding to the wavenumbers and parameters shown in Fig. 6.12 for various positioning of the driven mirror. A_m represent the amplitude of the corresponding eigenfunctions of k_m in the open cavity, while B_m represent the amplitude in the environment cavity. $(A_m/B_m)^2 \ll 1$ implies that the mode is strongly localized in the environment cavity.

the larger cavity is given by $\Delta q/L_{2,0}^2$. This can be seen in Fig. 6.12, where the diabatic modes (dotted curves) changing little correspond to the environment cavity while the diabatic mode changing significantly correspond to the open cavity. Near the intersection of the two sets of diabatic modes, the adiabatic modes of the asymmetric double cavity i.e. when the two cavities are coupled due to finite α, form an avoided crossing structure. In Fig. 6.12, these curves are shown in red, solid lines ($k_{10,11}$). Meanwhile, the blue, solid curves are the adiabatic modes located away from any intersection of diabatic modes. As the environment cavity length is increased , there will be a greater density of adiabatic modes that will approach a continuum for $L_{2,0} \to \infty$. Intuitively, since the blue, solid curves ($k_{8,9,12,13}$) closely follow the environment cavity diabtic modes, we expect it to be weakly localized in the semi-open cavity and vice-versa for the red, solid curves. In Fig. 6.13, we indeed see this to be true. In particular, we see that the light field of k_{11} is very strongly localized and k_{10} is somewhat localized in the open cavity. Meanwhile, for all other wavenumbers, the localization of light in the open cavity is very weak.

We begin our study of the DCE in the semi-open cavity by checking the convergence properties of the asymmetric double cavity (ADC) approximation of the ideal semi-open cavity as the length of the environment cavity is increased.. We fix the reflectivity parameter $\alpha = 1$ of the partially transmissive mirror for the environment cavity lengths $L_{2,0} = 3.1, 5.1, 7.1, 9.1$. The propagator for the quantum dynamics in this setup is numerically generated using the formalism setup in Sec. 5.4. In Fig. 6.14, total photon number in the semi-open cavity numerically generated employing the ADC model is plotted as a function of time. We consider a photon corresponding to a particular mode to be located in the semi-open cavity (as opposed to the environment cavity) if $\left(\frac{A_n}{b_n}\right)^2 > 1$

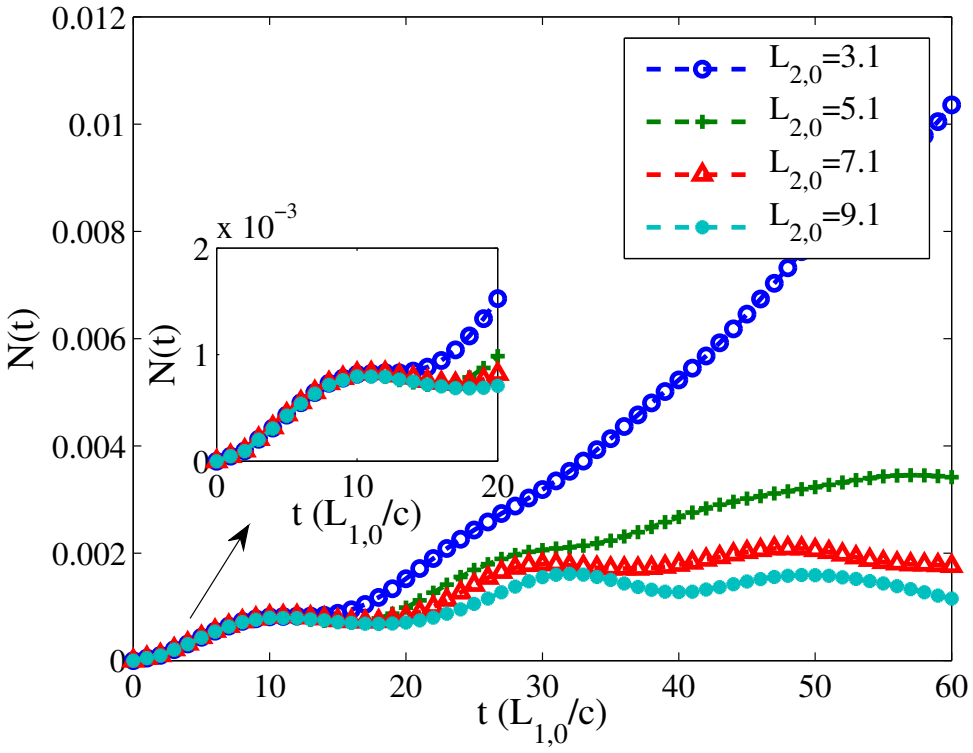

Figure 6.14: The total photon number in the semi-open cavity is plotted here as the length of the environment cavity is changed. The reflectivity parameter is $\alpha = 1$ throughout. For the shorter environment cavity length of $L_{2,0} = 3.1$, the light eigenmodes are not strongly localized in the open or environment cavity. Hence, the plotted total photon number for $L_{2,0} = 3.1$ is not particularly meaningful. For $L_{2,0} = 5.1, 7.1, 9.1$, the localization is much stronger and the total photon number in the open cavity become a meaningful quantity. We see that initially ($t \leq 15$), the growth in photon number agree for all the length values considered. Around $t \approx 15$, the growth in photon number reaches a local maximum. Moreover, we see a sloshing back and forth of the photon population in the form of some periodic micromodulation. This effect would be stronger for shorter environment lengths or lower reflectivities of the driven mirror. As the environment cavity length increases or the driven mirror reflectivity increases, we expect to see the sloshing of the photons go down.

as for the wavenumber k_{11} in Fig. 6.13. Total photon ($N(t)$) curves agree for all environment cavity lengths $L_{2,0} = 3.1, 5.1, 7.1, 9.1$ for $t \leq 12$. Furthermore, all of these curves exhibit a local maximum of photon number around $t \approx 10$, i.e. the photon growth rate in the semi-open cavity becomes zero. This sort of behaviour is not present in the perfect single cavity case where the photon number grow more or less monotonically as shown in Fig. 6.2. For $t > 15$, the $N(t)$ curves begin to diverge, a sign that the convergence of the ADC model is breaking down due to inadequate environment cavity length. The environment cavity length determines the time taken for the "decayed" light to slosh back into the semi-open cavity. In other words, as photons are being created in the semi-open cavity due to the moving mirror, it is constantly leaking out into the environment cavity since the driven mirror is transmissive. In an ideal semi-open cavity, this leaked light would never be reflected back into the semi-open cavity. Due to the approximation of the infinite environment by a large finite cavity for the sake of numerical simulations, the "decayed" photons eventually reflect back from the environment cavity end mirror and re-enters the semi-open cavity. Fig. 6.15 shows fixed time snapshots of photon population per mode localized in the semi-open cavity. At $t = 15$, the agreement between the $L_{2,0} = 7.1, 9.1$ is good which is expected since the corresponding $N(t)$ curves lie on top of each other for $t \leq 15$. At $t = 30$, it can be seen that the $N_k(t)$ curves begin separate due to the sloshing back of the decayed photons. From the convergence of the plots for $t \leq 15$ as the environment cavity length is increased, we conclude that the ADC model of the ideal semi-open cavity is a legitimate approximation in that time domain. Note that a lower reflectivity of the driven mirror would require higher environment cavity lengths to see convergence of the model to the ideal semi-open cavity case due to a faster

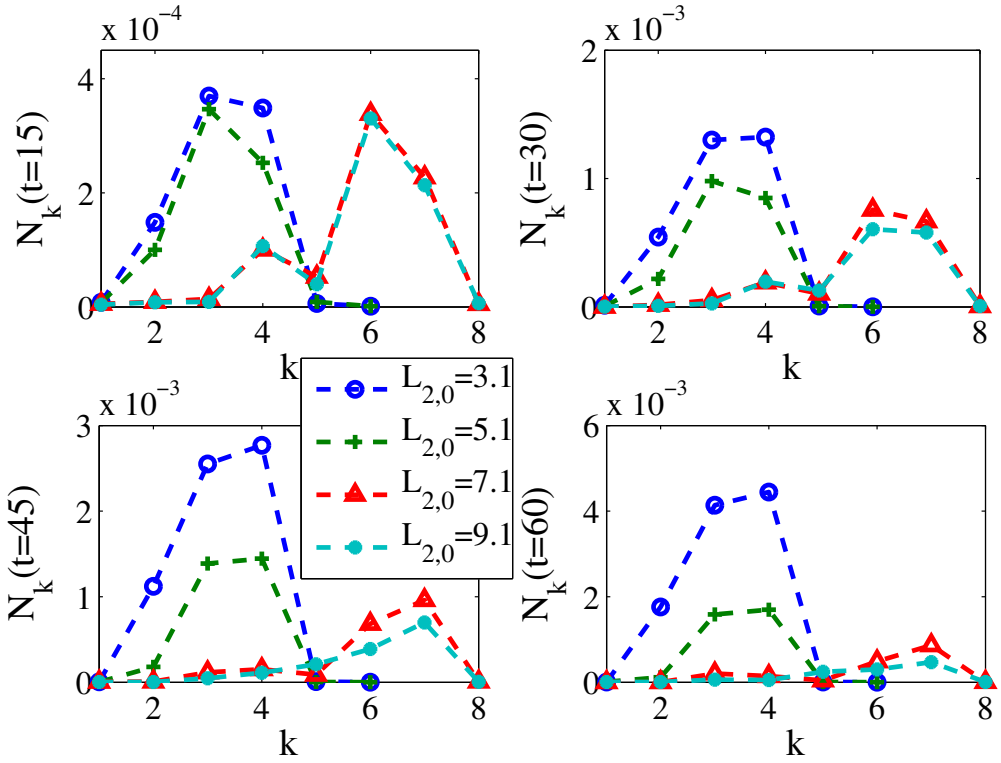

Figure 6.15: Here photon number for modes localized in the open cavity are plotted as a function of mode number while the environment cavity length is varied as $L_{2,0} = 3.1, 5.1, 7.1, 9.1$. The number of photons generated in the open cavity as a result of the partially transmissive ($\alpha = 1$) driven mirror as the environment cavity is lengthened converges showing that a model of the open cavity via an asymmetric double cavity is achieved. For short times $t \leq 15$, we see that the convergence is very good for $L_{2,0} = 9.1$, while, for $t \geq 15$, the convergence becomes worse with time implying that longer environment cavity is required to properly model the open cavity. Part of the reason for the lack of convergence for longer times is the finite size of the environment. Eventually, the photons created in the open cavity that had decayed into the environment slosh back into the open cavity.

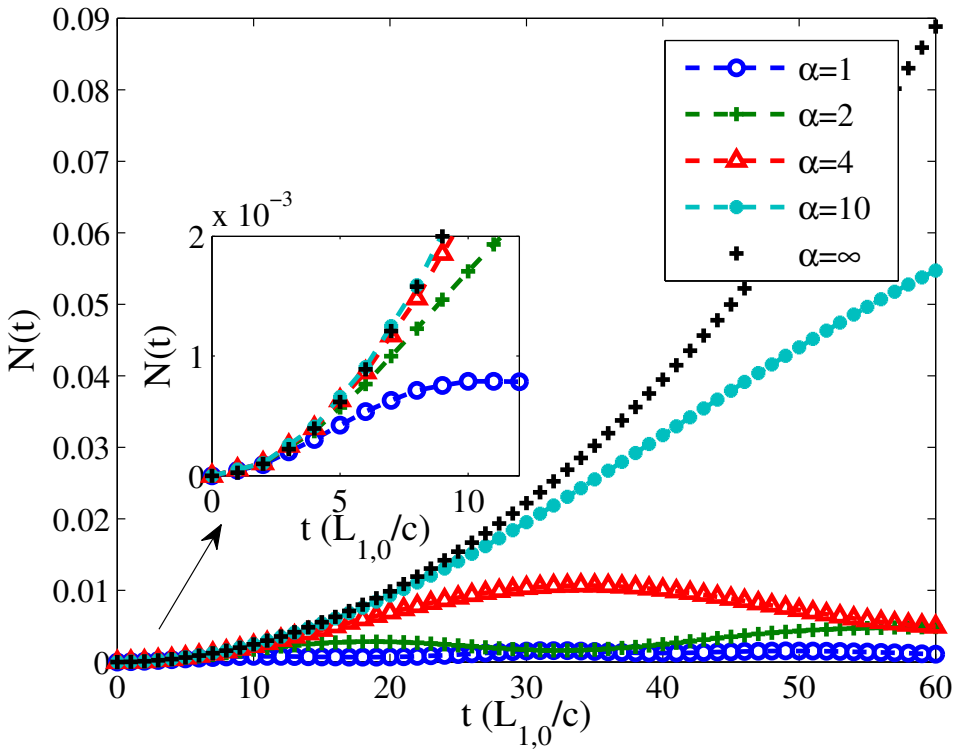

Figure 6.16: The number of photons in the semi-open cavity are plotted in this figure using the ADC model with an environment cavity length, $L_{2,0} = 9.1$. The semi-open cavity is taken to have the initial length of $L_{1,0} = 1$ and the driving frequency of the partially transmissive mirror is 4π. The reflectivity parameter of the driven mirror is varied and the corresponding photon number curves are compared against the perfect single cavity DCE represented by the $\alpha = \infty$ curve.

sloshing rate. Furthermore, for a more highly reflective driven mirror and fixed environment cavity length, the model is a valid approximation over a larger time domain compared to a driven mirror of lower reflectivity. In Fig. 6.16, we plot the results of the DCE in the semi-open cavity using the asymmetric double cavity (ADC) model. The growth of photon number in the semi-open cavity approaches the perfect single cavity curve as the mirror reflectivity is increased. The reflectivity parameter, $\alpha = 1$, is equivalent to a reflectivity of 91% for frequencies near 2π. We see in the figure that even for such a high

reflectivity, the resultant photon number growth is quite small compared to the perfect single cavity case. It is not surprising that the photon growth is drastically reduced since the static Casimir force for transmissive mirrors is weaker [69]. In experiments, the mirrors used would be partially transmissive and this result shows that only for very highly reflective mirrors would the results approach the perfect single cavity DCE results. Furthermore, the curves with $\alpha = 1, 2, 4$, show some oscillatory behaviour that can be attributed to the finite size approximation of the infinite environment leading to a sloshing back of the photons that had leaked out of the semi-open cavity. We do not see any such behaviour for the $\alpha = 10$ case, however, due to it is very high reflectivity, the sloshing time scale is much larger than the time domain of the simulated dynamics. In Fig. 6.17, the mode popuations of the ADC are plotted as a function of the mode numbers. In contrast to Fig. 6.15, where we only plot the mode numbers with strong localization in the semi-open cavity, here we plot all the modes regardless of the strength of localization in the semi-open or environment cavity. The spikes in the $N_k(t = 60)$ curve near $k = 10, 20, 30$ correspond to the photons created in the semi-open cavity. This plot shows us that the mode frequency cutoff number, $N = 54$, is adequate for our time domain of interest as the photon population beyond mode number 35 is negligible. Since we consider a driving frequency of 4π throughout this section, the growth of photons for frequency modes near 2π is resonantly enhanced. We denote the photon number curve for these resonant modes in both the perfect single cavity (PSC) and ADC systems as $N_r(t)$. Out of curiosity, we compare the growth of photons of the semi-open cavity using the ADC model against the PSC photon growth rate having factored in the decay of photons through the partially transmissive driven mirror. The resonant mode photon number

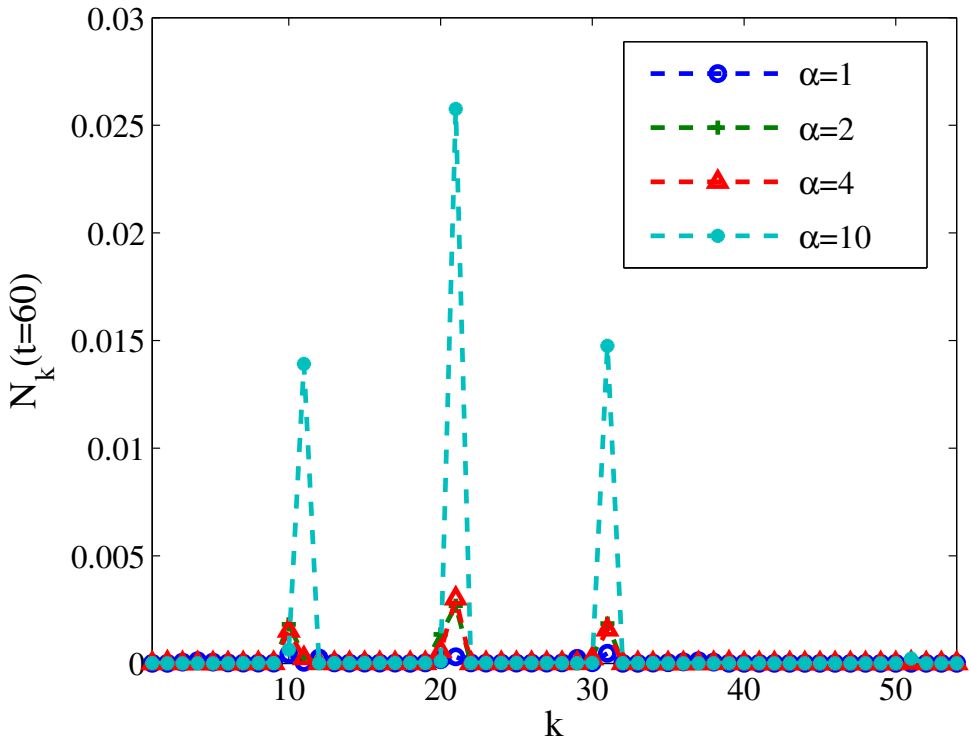

Figure 6.17: In this figure, we plot the photon number for each mode k for the semi-open cavity with the ADC model parameters, $L_{1,0} = 1$, $L_{2,0} = 9.1$, $\Omega_D = 4\pi$, and $\alpha = 1, 2, 4, 10$ at time $t = 60$. The photon population peaks at $k = 21$ since the mode is resonant with the driving frequency.

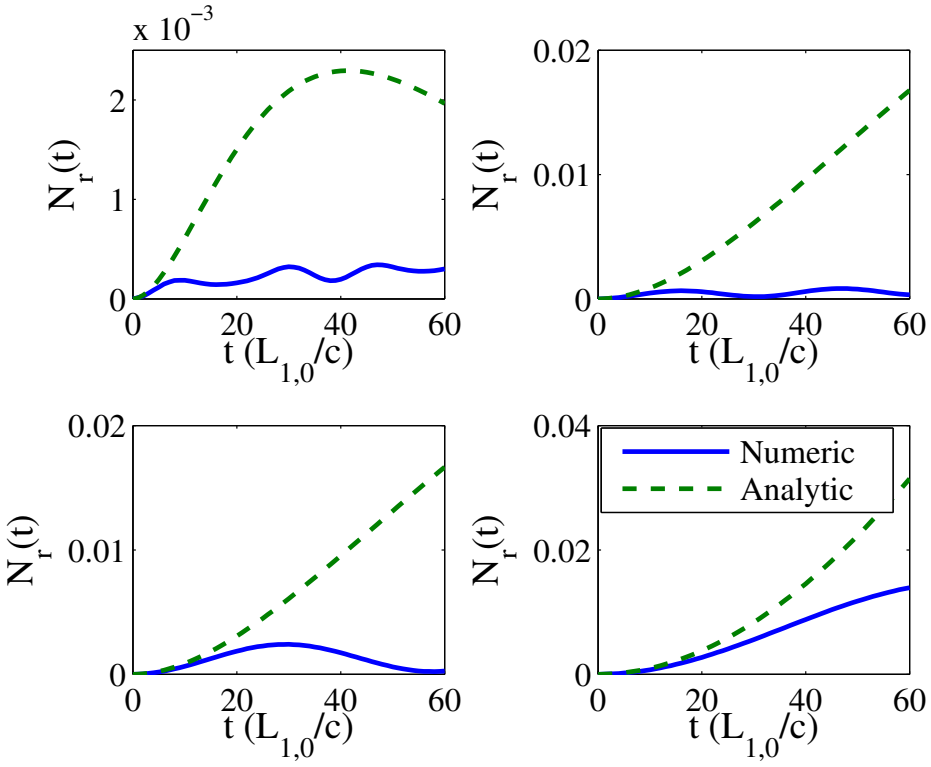

Figure 6.18: The numerical $N_r(t)$ curve denotes the growth of photons in the modes resonant to the driving frequency using the ADC model of the ideal semi-open cavity. The parameters for the ADC are $L_{1,0} = 1$, $L_{2,0} = 9.1$, $\Omega_D = 4\pi$ with variable reflectivity parameters across the panels of $\alpha = 1, 2, 4, 10$ m. It is compared to the analytic formula of the perfect single cavity growth multiplied by the decay factor in Eqn. 6.6.

for the semi-open cavity is given by

$$N_r(t) = N_{10}^{\mathrm{ADC}}(t) + N_{11}^{\mathrm{ADC}}(t) \tag{6.5}$$

and compared to the analytic result given by

$$N_r(t) = N_2^{\mathrm{PCS}} \exp\left(-\gamma t\right), \tag{6.6}$$

where, N_i^{PSC} and N_i^{ADC} are the photon number corresponding to the i^{th} mode in the perfect single cavity and the asymmetric double cavity model. The decay constant is given by [70]

$$\gamma = \frac{c}{L_{1,0}} \sqrt{\frac{1}{\sqrt{R}} + \sqrt{R} - 2}, \tag{6.7}$$

where R denotes the reflectivity of the partially transmissive, driven mirror. Note that the reflectivity is dependent on the wavenumber and that was taken into account as well. From Eqn. 6.3 and for short times, i.e. $t \leq 30$, we have that $N_2^{\mathrm{PCS}} = (10^{-3}\pi t)^2$. For $\alpha = 1$, we find the agreement between the analytic and the numeric curves to hold only for very short times ($t \leq 2$ or four mirror oscillation cycles). As the reflectivity parameter is increased, the time domain on which the two curves agree becomes larger. Hence, the semi-open cavity DCE cavity cannot by approximated as a perfect single cavity with decay introduced to it for longer time domains. The previous analytic formulae would perhaps best describe a semi-open cavity where the perfect end mirror is driven as in reference [66], where the theoretical calculations report that the effect of losses do not drastically change the photon growth. In reality, however, all mirrors are partially transmissive and our simulations

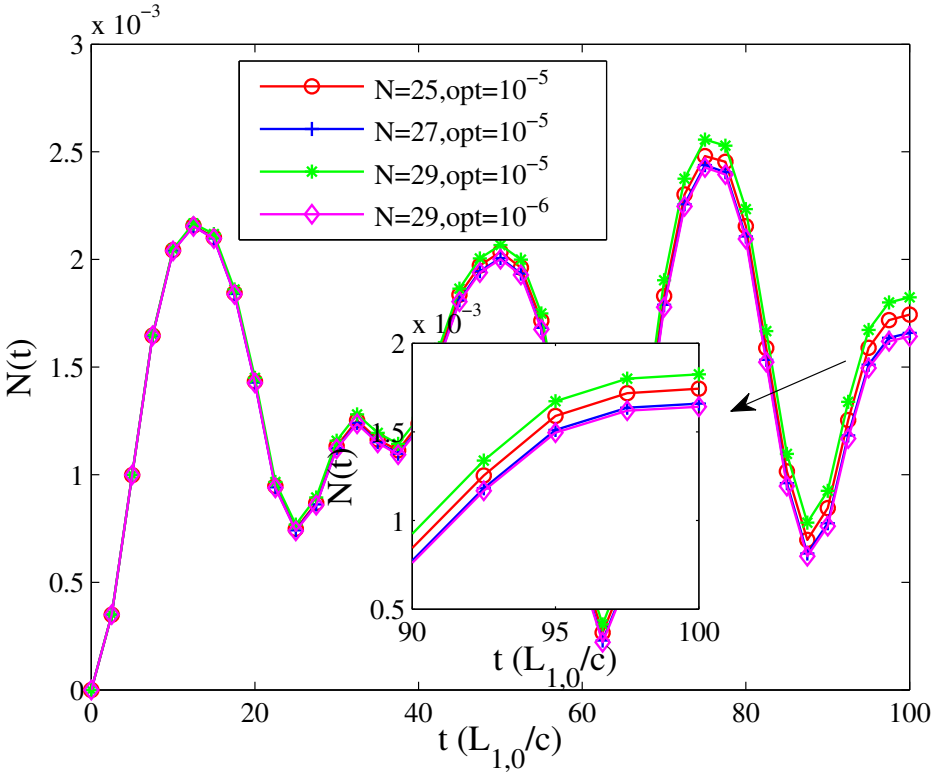

Figure 6.19: Here we plot the total photon number created in the double cavity for a central mirror with reflectivity parameter $\alpha = 1$, displacement of $0.001L_{1,0}$ and driven at frequency $\Omega_D = 4\pi$ generated via numerical simulations while varying the cutoff frequency mode number and the accuracy of the MATLAB ode solver denoted by *opt*. The initial length of the cavity halves are $L_{1,0} = L_{2,0} = 1$.

show that the DCE is strongly modified for such a scenario in comparison to the ideal perfect mirror case.

6.5 Regularization and Accuracy of Numerical Simulations

In this section we discuss the process by which determine the cutoff frequency for our simulations and the accuracy taken. There are two factors that can

be controlled to give a reliable photon number data, namely the maximum number of modes considered in the simulation (in principle we require an infinite number of modes, but that is not practical) and the accuracy used by the ODE solver. The accuracy of the MATLAB ode solver is denoted by *opt*. We use ode113 (Adams-Bashforth-Moulton PECE) and ode 45 (Runge-Kutta-Dormand-Prince) solver. The *opt* value sets the relative (RelTol in MATLAB) and absolute tolerance (AbsTol in MATLAB) of the solution. For example, $opt = 10^{-5}$ sets the relative and absolute tolerance, by the command "$opt = odeset('RelTol', 1e-5, 'AbsTol', 1e-5)$", to be 10^{-5} each. 'RelTol' is the measure of the error relative to the size of the solution and it controls the number of correct digits unless it is smaller than 'AbsTol'. 'AbsTol' sets the threshold below which the accuracy of the solution is unimportant. Moreover, it is used to determine the accuracy when the solution approaches zero and the ratio of the error to the solution blows up. At each time step, the error in the solution is less than the maximum of the two tolerances. The constraint for these types of numerical simulations are computation power and time. Fig. 6.19 shows the balance that needs to be achieved. As we can see, from the inset plot that $N = 25, 27$ and $opt = 10^{-5}$ curves agree quite well for short times and eventually for longer times the curves diverge a bit. We would expect that taking $N = 29$, $opt = 10^{-5}$ we would see some convergence in the three curves. However, simulations actually show the case to be different. The issue is that the order of magnitude of the extra terms now introduced is smaller than the accuracy of the ODE solver considered. Hence, adding more modes is actually adding greater error. Furthermore, we see in the figure that increasing the accuracy of the ODE solver to $opt = 10^{-6}$ for $N = 29$, we indeed do get a convergence of the three curves. Furthermore, we look at the

$N_k(t = t_f)$ vs k plot and check if the end mode populations are close to zero. This ensures that we have considered an adequate cutoff frequency.

Chapter 7

Conclusions and Outlook

In this thesis, we first studied the classical dynamics of light in the double cavity with a linearly driven, partially transmissive central mirror (chapters 2, 3 and 4). Following that we studied the dynamical Casimir effect inside the double cavity for a sinusoidally driven central mirror (chapters 5 and 6). Furthermore, we modelled a semi-open single cavity by an asymmetric double cavity (ADC) to get around the numerical simulation difficulties of dealing with a continuum of allowed cavity modes. Furthermore, a significant feature of our numerical study of the DCE is that we do not assume a *perfect* driven mirror which has difficulties associated with it according to author in references [5, 6]. In this chapter we summarize the main results in the thesis and discuss the future directions for this work.

7.1 Summary

We studied the classical dynamics of light in the double cavity using the Maxwell wave equation with time-dependent boundary conditions. Assuming that the motion of the central mirror is in a non-relativistic regime, i.e. mirror

speed is much smaller than the speed of light, we were able to approximately reduce the second order in time Maxwell wave eqation to a first order in time dynamics using a paraxial approximation in time. We went on to examine the validity of this first order in time reduction, referred to as the diabatic first order equation (DFOE), as the central mirror reflectivity, speed and the light frequency is varied. The DFOE is an exact reduction of the Maxwell wave equation only for the static double cavity case. The DFOE, which is a very good approximation for the optical frequency and mirror velocity to speed of light as high as $20,000$ ms^{-1}, diverges from the second order in time Maxwell wave equation when the central mirror reflectivity increases. However, this divergence is small and more importantly bounded as the central mirror reflectivity approaches unity. Furthermore, we found that the validity of the DFOE approximation improves for lower mirror speeds and higher frequencies of light in the cavity. In addition, the DFOE is unitary and hence predicts conserved field amplitudes even as the central mirror is driven, while the adiabatic second order equation (ASOE) which is the Maxwell wave equation written in the adiabatic basis correctly predicts non-conserved field amplitudes. In other words, the validity of DFOE as an approximation is equivalent to the extent of light energy non-conservation in the actual dynamics. All this was studied in chapter 3. In chapter 4, we confirmed that the non-conserved light energy in the double cavity with the driven mirror was due to the external driving source having to counteract the radiation pressure of the light field on the mirror. As a result, the external source ends up pumping energy into/out of the double cavity. This is a classical analog of the DCE which leads to photon creation due to the interaction of the vacuum field and the time-dependent boundary conditions. Lastly, we find that in the context of the double cavity,

moving the central mirror slowly enough ensures that the system will continue to remain in an instantaneous eigenstate and therefore achieving adiabaticity. But in contrast to the Schrödinger case, the amplitude of the eigenmode experiences a finite change while the changes in all the others vanish (the sum of the squares of all the amplitudes is not conserved).

After our in-depth study of the classical dynamics of light in the double cavity, we shifted our attention to the quantum dynamics. In particular, we focused on the DCE for a sinusoidally driven partially transmissive central mirror inside a double cavity. In chapter 5 we reviewed a very convenient reformulation of the Heisenberg equation of motion (due to reference [24]) in terms of auxillary variables that satisfy a first order in time differential equation and is less computationally intensive for light in the presence of a moving boundary. Moreover, this reformulation is general in the sense that it applies to the perfect single cavity and double cavity alike. In addition, the formalism can be easily adjusted to simulate DCE in analogous systems to a cavity with a moving mirror. For example, if the transmissivity (α in Eqn. (2.1)) or background dielectric constants in the cavity were to be varied, we would need to compute the instantaneous cavity frequencies and the corresponding electric field modes (Eqns. (2.9) and (2.6) for the moving mirror case) as a function of the parameter being varied. This in turn would modify the expressions in Eqns. (5.52) and (5.53), after which one can proceed with the numerical simulations of DCE analogs using Eqn. (5.52). Following references [3, 2] which numerically studies the DCE in a perfect single cavity (reviewed briefly in Sec. 6.2), we performed numerical simulations of the DCE in the more complex double cavity system. A novelty of our numerical study is that we assume that the driven mirror is partially transmissive as opposed to a completely re-

flective mirror which we find to be a significant idealization. We find that the photon creation in the double cavity approaches that of two perfect single cavities when the central mirror reflectivity approaches unity. However, even for reflectivities of 91%, the number of photons created is drastically lower compared to the perfect mirror case. When the reflectivity is taken very close to 100%, the photon creation asymptotically approaches that of the perfect mirror case. This implies that the experimental observation of the DCE for even highly reflective driven mirrors is much lower in comparison to the theoretical perfect cavity with completely reflective mirrors. Furthermore, in Sec. 6.3, we see effects analogous to parametric amplification, where a resonant driving frequency enhances the growth of photon number for particular modes (studied in Sec. 5.3). It is possible that the DCE can be greatly enhanced in the double cavity since the curvature of the avoided crossing structure which can be modified by fiddling with the cavity parameters might give us access to higher effective accelerations. Since the double cavity can be thought of as two semi-open cavities coupled to one another, it is natural to next consider a semi-open cavity coupled to an infinite environment. An infinite environment creates a difficulty in the implementation of the numerical simulation since the allowed eigenfrequencies in the cavity form a continuum. We get around this issue by modelling the environment by a large and finite cavity. This forms a highly asymmetric double cavity, but the allowed eigenmodes are discrete allowing us to numerically simulate the dynamics. In Sec. 6.4, we found that the ADC model is indeed well behaved and the photon numbers created in the semi-open cavity converge as the environment cavity becomes larger. For a fixed environment cavity length and reflectivity, as the photons leak out of the semi-open cavity, due to the finite size of the environment cavity length, it

eventually sloshes back into the semi-open cavity. The ADC model is accurate for time domains where a negligible amount of the leaked out photons have sloshed back. Lastly, we saw that factoring in decay to the photon production of a perfect single cavity is inadequate to explain the growth of photons in the semi-open cavity except for very highly reflective mirrors and even then for rather short times. Our study in chapter 6 shows that open cavities can behave quite differently than perfect cavities and creation of photons even for reflectivities as high as 91% is drastically reduced.

7.2 Future Directions

There are several interesting avenues beyond the scope of this thesis that open up following our numerical study of the quantum dynamics of light in the double cavity. The quantum dynamics of light in general coherent states in the double cavity relavant to optomechanical experiments could be simulated numerically to confirm theoretical and analytical results in the literature. The open cavity rather than the semi-open cavity coupled to an infinite environment could be modelled by a triple cavity and the resultant DCE compared to the analytical results due to [25, 26]. There are also a lot of subtle conceptual issues to be resolved in the DCE such as the implications of the periodicity of the off-diagonal Bogoliubov coefficients in Fig. 6.5 and their relation to the curious piecewise linear photon growth. Furthermore, one could ask how many of the photons pumped into the system in the DCE are only due to the external driving source having to counteract the static Casimir force for which we would need to know how the static Casimir force is modified for the double cavity. As the field of optomechanics progresses and the entanglement of the

optical and mechanical degrees are improved along with the advent of highly reflective mirrors, more elaborate versions of the numerical study done in this thesis might be used to understand the behaviour of light in such systems.

Appendices

Appendix A

Appendix to Chapter 3

A.1 Relativistic corrections to the Maxwell wave equation in a medium

According to [54], the approximate Maxwell wave equation in a moving dielectric correct to order v/c is given by

$$\frac{\partial^2 E}{\partial x^2} - \frac{n^2}{c^2}\frac{\partial^2 E}{\partial t^2} - v\frac{n^2-1}{c^2}\frac{\partial}{\partial x}\frac{\partial E}{\partial t} = 0. \tag{A.1}$$

The highest mirror velocity considered in this paper is $20,000$ ms^{-1}. The highest mirror reflectivity considered is 98% for cavity length 100μm and wavenumber 8.0425×10^6 m^{-1}. The Mirror width is taken to be 100nm. This approximately corresponds to an index of refraction of 4.

We can estimate the size of each term by substituting the ansatz $E(t,x) = \exp i\left[(kx - \omega t)\right]$ into equation (A.1). Order of magnitude of $\frac{\partial^2 E}{\partial x^2}$: k^2. Order of magnitude of $\frac{n^2}{c^2}\frac{\partial^2 E}{\partial t^2}$: $n^2k^2 = 16k^2$. Order of magnitutde of $v\frac{n^2-1}{c^2}\frac{\partial}{\partial x}\frac{\partial E}{\partial t}$: $\frac{v}{c}(n^2-1)k^2 = 0.001k^2$.

A.2 Changing optical lengths in cavities via index of refraction of background medium

Instead of the double cavity comprised of an optical cavity with a moveable central mirror, one can also implement a, equivalent system as two coupled waveguides with controllable refractive indices. Assume that each waveguide has length $L/2$ and has indices of refraction $n_{1/2}$. The lengths of the double

cavity halves can now be realized by making the substitution

$$L_{1/2} = n_{1/2}\frac{L}{2}. \tag{A.2}$$

In order to conserve the total optical length, the indices of refraction are varied as (for example, using the electro-optic effect)

$$\begin{aligned} n_1 &= n_0 + \eta \\ n_2 &= n_0 - \eta, \end{aligned} \tag{A.3}$$

where n_0 is the background dielectric material and η is the modulation. The modulation of the dielectric need only be small to change the optical length difference, $\Delta L = L_1 - L_2 = \eta L$. The transmission function of the central mirror in such a setup using the δ mirror model is given by

$$T = \frac{n_1^2}{\frac{(n_1+n_2)^2}{4} + \frac{k^2\alpha^2}{4}}. \tag{A.4}$$

In order to ensure that the wavenumber structure of the waveguide system with the controllable refractive index be equivalent to the double cavity with a moving central mirror, we need to make sure that the transmission function for the former agrees with the latter. This can indeed be ensures if we take that $\eta \ll n_0$ and we replace $\alpha k \to \alpha k/n_0$. By making these substitutions, most of the formulae derived for the double cavity with the moving mirror can be extended to the waveguide case.

Appendix B

Appendix to Chapter 5

B.1 Squeezed States

Coherent states, $|\alpha\rangle$ (α is a complex valued parameter), are states that satisfy the minimum uncertainty relation, $\Delta\hat{x}\Delta\hat{p} = \frac{\hbar}{2}$, where $\hat{x}$ and $\hat{p}$ are the position and momentum operators. In addition, the variances in the position and momentum co-ordinate of the coherent states are equal, i.e. $\Delta x = \Delta p$. Squeezed states are states that have unequal position and momentum variances ($\Delta x \neq \Delta p$) while satisfying the minimum uncertainty relation. Operator representation of a general squeezed coherent state, $|\alpha, \xi\rangle$, is given by

$$|\alpha, \xi\rangle = \hat{D}(\alpha)\hat{S}(\xi)|0\rangle \tag{B.1}$$

where

$$\hat{S}(\xi) = \exp\left\{\frac{1}{2}\left(\xi^*\hat{a}^2 - \xi(\hat{a}^\dagger)^2\right)\right\} \tag{B.2}$$

is the squeezing operator and

$$\hat{D}(\alpha) = \exp\left\{\alpha\hat{a}^\dagger - \alpha^*\hat{a}\right\} \tag{B.3}$$

is the displacement operator [64] and $\{\hat{a}, \hat{a}^\dagger\}$ are the creation/annihalation operators corresponding to the co-ordinates $\{\hat{x}, \hat{p}\}$. The squeezed mode above is referred to as a single squeezed mode. Meanwhile, two mode squeezed states are defined as

$$\hat{S}_2(\xi)|0\rangle = \exp\left\{\xi^*\hat{a}\hat{b} - \xi\hat{a}^\dagger\hat{b}^\dagger\right\}|0\rangle, \tag{B.4}$$

where $\hat{b}^\dagger$ and $\hat{b}$ are the creation/annihilation operators corresponding to some other mode in the system of interest.

Bibliography

[1] M. Aspelmeyer, T. J. Kippenberg, and F. Marquardt, Reviews of Modern Physics **86**, 1391 (2014).

[2] M. Ruser, Journal of Physics A: Mathematical and General **39**, 6711 (2006).

[3] M. Ruser, Journal of Optics B: Quantum and Semiclassical Optics **7**, S100 (2005).

[4] W. Naylor, S. Matsuki, T. Nishimura, and Y. Kido, Physical Review A **80**, 043835 (2009).

[5] G. T. Moore, Journal of Mathematical Physics **11** (1970).

[6] G. Barton and C. Eberlein, Annals of Physics **227**, 222 (1993).

[7] D. Lee, M. Underwood, D. Mason, A. Shkarin, S. Hoch, and J. Harris, Nature communications **6** (2015).

[8] A. Jayich, J. Sankey, B. Zwickl, C. Yang, J. Thompson, S. Girvin, A. Clerk, F. Marquardt, and J. Harris, New Journal of Physics **10**, 095008 (2008).

[9] G. Heinrich, J. Harris, and F. Marquardt, Physical Review A **81**, 011801 (2010).

[10] R. Lang, M. O. Scully, and W. E. Lamb Jr, Physical Review A **7**, 1788 (1973).

[11] D. Wilson, C. Regal, S. Papp, and H. Kimble, Physical review letters **103**, 207204 (2009).

[12] N. Miladinovic, F. Hasan, N. Chisholm, I. Linnington, E. Hinds, and D. O'Dell, Physical Review A **84**, 043822 (2011).

[13] L. O. Castaños and R. Weder, Physical Review A **89**, 063807 (2014).

[14] L. O. Castaños and R. Weder, Physica Scripta **90**, 068011 (2015).

[15] M. Born and V. Fock, Zeitschrift für Physik **51**, 165 (1928).

[16] C. K. Law, Phys. Rev. A **51**, 2537 (1995).

[17] H. Cheung and C. Law, Physical Review A **84**, 023812 (2011).

[18] H. B. Casimir, in *Proc. K. Ned. Akad. Wet*, Vol. 51 (1948) p. 150.

[19] M. Castagnino and R. Ferraro, Annals of Physics **154**, 1 (1984).

[20] S. Fulling and P. Davies, in *Proceedings of the Royal Society of London A: Mathematical, Physical and Engineering Sciences*, Vol. 348 (The Royal Society, 1976) pp. 393–414.

[21] P. Davies, Journal of Optics B: Quantum and Semiclassical Optics **7**, S40 (2005).

[22] V. V. Dodonov and A. B. Klimov, Physical Review A **53**, 2664 (1996).

[23] V. Dodonov, A. Klimov, and V. Man'ko, Physics Letters A **149**, 225 (1990).

[24] M. Razavy, Lettere al Nuovo Cimento (1971-1985) **37**, 449 (1983).

[25] F. Dezael and A. Lambrecht, EPL (Europhysics Letters) **89**, 14001 (2010).

[26] J. T. Mendonça, G. Brodin, and M. Marklund, Physics Letters A **375**, 2665 (2011).

[27] V. Dodonov, Physica Scripta **82**, 038105 (2010).

[28] J.-Y. Ji, H.-H. Jung, J.-W. Park, and K.-S. Soh, Phys. Rev. A **56**, 4440 (1997).

[29] R. Schützhold, G. Plunien, and G. Soff, Phys. Rev. A **57**, 2311 (1998).

[30] D. A. Dalvit and F. D. Mazzitelli, Physical Review A **57**, 2113 (1998).

[31] D. A. Dalvit and F. D. Mazzitelli, Physical Review A **59**, 3049 (1999).

[32] D. A. Dalvit, Nature **479**, 303 (2011).

[33] E. Yablonovitch, Physical Review Letters **62**, 1742 (1989).

[34] Y. E. Lozovik, V. Tsvetus, and E. Vinogradov, Physica Scripta **52**, 184 (1995).

[35] C. Wilson, G. Johansson, A. Pourkabirian, M. Simoen, J. Johansson, T. Duty, F. Nori, and P. Delsing, Nature **479**, 376 (2011).

[36] D. A. Dalvit, P. A. M. Neto, and F. D. Mazzitelli, in *Casimir Physics* (Springer, 2011) pp. 419–457.

[37] V. Dodonov, Physical Review A **58**, 4147 (1998).

[38] G. Schaller, R. Schützhold, G. Plunien, and G. Soff, Physical Review A **66**, 023812 (2002).

[39] A. Lambrecht, M.-T. Jaekel, and S. Reynaud, Physical review letters **77**, 615 (1996).

[40] M. T. Jaekel and S. Reynaud, Journal de Physique I **2**, 149 (1992).

[41] D. A. Dalvit and P. A. M. Neto, Physical review letters **84**, 798 (2000).

[42] I. Linington, *Quantum optics with dynamic environments*, Ph.D. thesis, University of Sussex (2007).

[43] I. Linington and B. Garraway, Physical Review A **77**, 033831 (2008).

[44] I. Linington and B. Garraway, Journal of Physics B: Atomic, Molecular and Optical Physics **39**, 3383 (2006).

[45] H. J. Kimble, Nature **453**, 1023 (2008).

[46] A. D. Boozer, A. Boca, R. Miller, T. E. Northup, and H. J. Kimble, Physical Review Letters **98**, 193601 (2007).

[47] T. Pellizzari, Physical Review Letters **79**, 5242 (1997).

[48] S. Van Enk, H. Kimble, J. Cirac, and P. Zoller, Physical Review A **59**, 2659 (1999).

[49] C. K. Law, Phys. Rev. A **49**, 433 (1994).

[50] S. Singh, G. Phelps, D. Goldbaum, E. Wright, and P. Meystre, Physical review letters **105**, 213602 (2010).

[51] R. Spreeuw, N. Van Druten, M. Beijersbergen, E. Eliel, and J. Woerdman, Physical review letters **65**, 2642 (1990).

[52] D. Bouwmeester, N. Dekker, F. v. Dorsselaer, C. Schrama, P. Visser, and J. Woerdman, Physical Review A **51**, 646 (1995).

[53] S. F. Preble, Q. Xu, and M. Lipson, Nature Photonics **1**, 293 (2007).

[54] U. Leonhardt and P. Piwnicki, Physical Review A **60**, 4301 (1999).

[55] C. Zener, in *Proceedings of the Royal Society of London A: Mathematical, Physical and Engineering Sciences*, Vol. 137 (The Royal Society, 1932) pp. 696–702.

[56] L. Landau, Physics of the Soviet Union **2**, 46 (1932).

[57] S. Friedberg, A. Insel, and L. Spence, "Linear algebra. 1997," .

[58] D. J. Griffiths, "Introduction to electrodynamics," (1999).

[59] L. Landau and E. Lifshitz, "Classical mechanics," (1960).

[60] U. Leonhardt, *Essential quantum optics: from quantum measurements to black holes* (Cambridge University Press, 2010).

[61] H. Goldstein, C. P. Poole, and J. L. Safko, *Classical Mechanics: Pearson New International Edition* (Pearson Higher Ed, 2014).

[62] K. Husimi, Progress of Theoretical Physics **9**, 381 (1953).

[63] R. J. Glauber, in *Quantum Measurements in Optics* (Springer, 1992) pp. 3–14.

[64] V. Dodonov, Journal of Optics B: Quantum and Semiclassical Optics **4**, R1 (2002).

[65] V. Dodonov, A. Klimov, and V. Man'Ko, Physics Letters A **149**, 225 (1990).

[66] G. Schaller, R. Schützhold, G. Plunien, and G. Soff, Physics Letters A **297**, 81 (2002).

[67] J. Mendonça and A. Guerreiro, Physical Review A **72**, 063805 (2005).

[68] J. T. Mendonca, G. Brodin, and M. Marklund, Physics Letters A **372**, 5621 (2008).

[69] D. Kupiszewska and J. Mostowski, Phys. Rev. A **41**, 4636 (1990).

[70] G. Grynberg, A. Aspect, and C. Fabre, *Introduction to quantum optics: from the semi-classical approach to quantized light* (Cambridge university press, 2010).